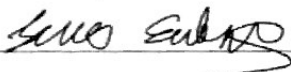
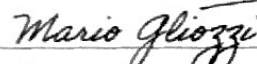
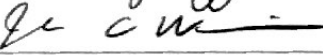
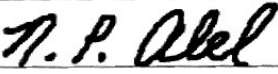
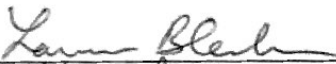
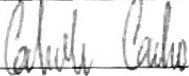

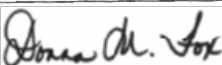
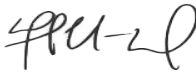


LOCAL RELICS: THE HUNT FOR INTERMEDIATE MASS BLACK HOLES

by

Jenna Cann
A Dissertation
Submitted to the
Graduate Faculty
of
George Mason University
in Partial Fulfillment of
The Requirements for the Degree
of
Doctor of Philosophy
Physics

Committee:

	Dr. Shobita Satyapal, Committee Chair
	Dr. Mario Gliozzi, Committee Member
	Dr. Joe Weingartner, Committee Member
	Dr. Nicholas Abel, Committee Member
	Dr. Laura Blecha, Committee Member
	Dr. Gabriela Canalizo, Committee Member
	Dr. Paul So, Department Chairperson
	Dr. Donna M. Fox, Associate Dean, Office of Student Affairs & Special Programs, College of Science
	Dr. Fernando Miralles-Wilhelm, Dean, College of Science

Date: 03/22/2021

Spring Semester 2021
George Mason University
Fairfax, VA

The Hunt for Intermediate Mass Black Holes

A dissertation submitted in partial fulfillment of the requirements for the degree of
Doctor of Philosophy at George Mason University

By

Jenna M. Cann
Bachelor of Science
George Mason University, 2017

Director: Dr. Shobita Satyapal, Professor
Department of Physics and Astronomy

Spring Semester 2021
George Mason University
Fairfax, VA

Copyright © 2021 by Jenna M. Cann
All Rights Reserved

Dedication

I dedicate this work to my parents, Marie Catherine Cann, Theresa Marie Cann, and William Arthur Cann, and my grandmothers, Joan Alice Cann and Marie Catherine Thomas.

Živjeli!

Acknowledgments

There were many sources of guidance and support that I received during this research. I received support from the National Science Foundation (NSF) Graduate Research Fellowship Program (GRFP), as well as from a Mason 4-VA Innovation Grant.

I would first like to thank the faculty and staff members in the Department of Physics at GMU, especially those who served on my committee: Shobita Satyapal, Joe Weingartner, and Mario Gliozzi.

I would like to thank the members of my committee. Nick Abel was the first collaborator I worked with in the summer before grad school taught me everything I know about running Cloudy. Laura Blecha was a coauthor on all of my papers, and provided insight on all of the projects from a theorist's perspective. Mario Gliozzi helped with all X-ray components, theoretical and observed, throughout my projects, and patiently listened to my practice talks way more than anyone should have had to. Gaby Canalizo and her students taught me how to observe and reduce Keck data, and how to snorkel.

While I have a large committee, it was not large enough to fit everyone I wanted to acknowledge. Barry Rothberg and R.T. Gatto provided invaluable assistance in the data collection and reduction processes, as well as technical and moral support throughout many proposal cycles. Nathan Secrest provided mentorship throughout my degree - you were a fantastic role model to look up to as I progressed through the program. I did not meet Rita Sambruna until late in my degree, but she has already been such an inspiration to me, and I look forward to hopefully working more closely throughout my postdoc.

I would also like to thank all of my coauthors who helped me throughout the process of publishing the papers highlighted in this work.

Special thanks goes to all of the student and postdoc collaborators - Ryan Pfeifle, Thomas Bohn (UC Riverside), Rem Sexton (UC Riverside, USNO), Christina Manzano-King (UC Riverside), William Matzko, and Lara Kamal. I had so much fun working with all of you and hope we have many more opportunities to collaborate in the future!

Thanks also to Ana, Molly, Allie, and Scarlett - you always knew how to make me smile even when I was stressed. Vector - I didn't think I would like to have a cat, but we are on the same wavelength.

Thanks to the Black Hole Galaxy Connection Group for providing a supportive community to learn more about our Universe. Ryan Pfeifle - I am so glad we started our PhD's together and that I had a partner on this journey.

Thank you to the grad students and alumni who helped create a research environment that I could flourish in and made sure that even the most stressful experiences of grad school never outweighed the fun - Ryan Pfeifle, Luis Fernandez, Kat Fernandez, Kevin Collins, Joe Renaud, Prabal Saxena, Adam Jacobs, Phil Hess, and Tiffany Lewis.

I was lucky enough to become friends with a group of phenomenal women who continually inspire me: Natasha Latouf, Kat Fernandez, Carly Solis, Sami Collins, Lara Kamal, Nishat Sultana, and Melissa Bierschenk - I hope to have more stemminist happy hours with

you and I am so excited to celebrate all of your future achievements. To my Spectrum co-founders, Carly, Kat, & Natasha, I really needed that community, and I am so proud of us for setting it up for future generations of students. I would also like to thank the faculty and staff of the faculty mentoring committee for helping ensure that our work will help generations of students, even after we all graduate: Joe Weingartner, Karen Sauer, Brooke Vaughn, Erhai Zhao, and Fernando Camelli, as well as Paul So and Faith Gaile.

Special thanks goes to Carly - I am so grateful that we met outside of Joe's office struggling on the same homework problem in our first semester at GMU. You have been an irreplaceable part of my support system and I cannot wait to eventually travel into space (and Antarctica, and Iceland, and Egypt) with you.

Alex - Thank you for being my biggest cheerleader. You are the first person I go to with all my new, half-baked ideas, and you are the one who supports me as I try (sometimes successfully) to turn them into reality. You make sure that I take time to laugh, no matter how stressed or busy I am, and much of my resilience these past years can be attributed to you.

Joe - I've said it many times, but it is still true. There were so many times that your kindness and dedication to helping students was a huge factor in ensuring I completed my Bachelor's, let alone my PhD. I have learned so much in your classes, as your LA, and through the way you work with students and colleagues. Thank you for your unwavering support throughout my time at GMU.

Shobita - There is nothing I can do to ever pay back everything you have done for me. You dragged confidence out of me when I felt I did not belong in this program, you taught me how to stand up for myself effectively and professionally, and you provided innumerable opportunities for me. Your commitment to kindness over everything in science is a model that I will take with me as I continue my career. You have been an advisor, a mentor, and a friend, and I look forward to continuing to work with you.

Table of Contents

	Page
List of Tables	viii
List of Figures	ix
Abstract	xiv
1 Introduction	1
1.1 Motivation	1
1.2 The Seed Models of SMBHs	2
1.3 Previous Studies	5
1.4 Research Statement	8
2 The Limitations of Optical Spectroscopic Diagnostics in Identifying AGNs in the Low Mass Regime	9
2.1 Introduction	9
2.2 Methods	11
2.2.1 The AGN Continuum	11
2.2.2 Geometrical Distribution of the Gas	14
2.2.3 Physical State of the Gas and Dust	16
2.2.4 Parameter Space	16
2.3 Modeling Results	16
2.4 Implications	21
2.4.1 Detectability with Current Facilities	22
2.4.2 Additional Considerations and Caveats	23
3 The Diagnostic Potential of Infrared Coronal Lines	26
3.1 Introduction	26
3.1.1 Methods	27
3.1.2 Results	28
3.1.3 Implications	30
4 Multi-wavelength observations of SDSS J105621.45+313822.1, a broad-line, low- metallicity AGN	41
4.1 Methodology	45
4.1.1 NIR Observations and Data Reduction	45

4.1.2	Optical Observations and Analysis	46
4.1.3	X-ray Observations and Data Reduction	46
4.2	Results	47
4.2.1	Near-infrared and Optical Spectra of J1056+31	47
4.2.2	X-ray Results	50
4.2.3	Black Hole Mass and Luminosity Estimates	55
4.3	Discussion	55
4.3.1	Coronal Lines	55
4.3.2	Metallicity Estimates	57
4.3.3	Implications	58
4.4	Conclusions	59
5	Future Work	61
5.1	Chapter Overview	61
5.2	Model Validation using Gemini	61
5.3	The Hunt for Intermediate Mass Black Holes in Low Metallicity Dwarf Galaxies	62
5.3.1	Ground-based	62
5.3.2	JWST	63
5.4	XMM	64
	Bibliography	66

List of Tables

Table	Page
3.1 Brightest Coronal Lines in the 1 – 30 μm Range	35
4.1 Near-IR (Keck NIRSPEC) emission line fluxes. Broad lines are identified by “br.”	48
4.2 Optical SDSS emission line fluxes. Broad lines are identified by “br.”	52
5.1 CLOUDY Parameters	65

List of Figures

Figure		Page
1.1	Figure from Inayoshi et al. [2020] plotting high- z quasars ($z > 6$) and their reported masses.	4
2.1	Accretion disk SEDs from black holes with masses that span $10^2 - 10^8 M_{\odot}$ accreting at $0.1 \dot{m}_{Edd}$. The units of the vertical axis are set for illustrative purposes by assuming a distance of 30 Mpc. We have labeled the location of the ionization potentials of several coronal lines accessible by <i>JWST</i> by the dotted vertical lines. As can be seen, the shift in disk temperature for the range of black hole masses explored in this work significantly moves the location of the "Big Blue Bump" relative to the ionization energies of key coronal lines observable by <i>JWST</i>	12
2.2	SED from black hole of mass $10^7 M_{\odot}$ with soft excess and power law components. The units of the vertical axis are set by assuming a distance of 30 Mpc. We have labeled the location of the ionization potentials of several coronal lines accessible by <i>JWST</i> by the dotted vertical line. As can be seen, several coronal lines have an ionization potential that could be greatly affected by the presence of a soft excess component.	15

2.3	<p>BPT diagram for our photoionization models for a range of black hole masses from $10^3 - 10^8 M_\odot$ at constant $\log U = -2$, $n_H = 300 \text{ cm}^{-3}$, and $\dot{m}/\dot{m}_{Edd} = 0.1$ at Solar (left) and 0.1-Solar (right) metallicities. The red and blue lines correspond to demarcations separating star-forming galaxies from AGNs from Kauffmann et al. [2003] (red) and Kewley et al. [2001] (blue), respectively. For black hole masses $< 1000 M_\odot$ in the top panel, the line ratios fall outside the plotted region shown in the figure. We also show the observed BPT line ratios of RGG118 (black 'x') reported by Baldassare et al. [2017], POX 52 (red 'x') reported by Barth et al. [2004], and NGC 4395 (blue 'x') reported by Kraemer et al. [1999]. Note our models do not include star formation. The arrows denote the direction that model points would move in the presence of star formation (red) and higher electron densities (black).</p>	17
2.4	<p>Fraction of total flux in X-ray photons with energies greater than 20 Ryd striking the illuminated face of the cloud per second compared to total photon flux per second as a function of black hole mass for a range of Eddington ratios. As can be seen, in low mass black holes, a large fraction of radiation emitted is over 20 Ryd.</p>	19
2.5	<p>Contour plots showing the changes of the BPT line ratios over a range of BH mass from $100 - 10^8 M_\odot$ and ionization parameter from $\log U = -1$ to -4 for $\dot{m}/\dot{m}_{Edd} = 0.1$ and $\log n_H = 300 \text{ cm}^{-3}$.</p>	20
2.6	<p>BPT plots for $\dot{m}/\dot{m}_{Edd} = 1$ (left) and 0.01 (right) with $\log U = -2.5$ and $n_H = 300 \text{ cm}^{-3}$. Note that masses not pictured here fall outside the plotted region shown in the figure, below the non-AGN demarcation. Red and blue lines are as denoted in Figure 2.3. The presence of star formation would move the model points in the direction of the red arrow in Figure 2.3. Note that as you lower the Eddington ratio, the temperature of the accretion disk decreases such that for the most massive black holes, the resulting softening of the SED of the accretion disk causes a net decrease in the $[\text{OIII}]/\text{H}\beta$, as seen in the lowest panel above.</p>	20

2.7	Additional BPT diagrams using the [S II]/H α (top) and [O I]/H α (bottom) line ratios for the $n_H = 300 \text{ cm}^{-3}$, $\dot{m}/\dot{m}_{Edd} = 0.1$, solar metallicity, $\log U = -2$ model. The blue and red lines correspond to the demarcations separating AGN and star-forming galaxies (blue) and AGN from LINERS (red). Masses below $10^3 M_\odot$ in the top panel and below $10^{3.5} M_\odot$ in the lower panel are outside the range plotted, in the star-forming region.	21
2.8	Luminosity of [O III] as a function of black hole mass for the $n_H = 300 \text{ cm}^{-3}$, solar metallicity, $\log U = -3$ model, for a range of Eddington ratios. Also plotted are the median [O III] luminosity of SDSS star forming dwarf galaxies (black dotted line), the aperture-reduced [O III] luminosity from star formation detected in a 0.2" IFU spaxel (green dotted line), and the [O III] luminosity corresponding to a detection threshold of 10^{-17} s^{-1} (red dot-dashed line). Note that the horizontal luminosity thresholds displayed correspond to a distance of 10 Mpc and even the lowest black hole masses could be detected in closer sources using an IFU.	24
3.1	Simulated spectra between $1 - 30 \mu\text{m}$ for black holes of mass $10^2 M_\odot$, $10^5 M_\odot$, and $10^8 M_\odot$ for a standard gas density of $n_H = 300 \text{ cm}^{-3}$ and an ionization parameter of $\log U = -1.0$. Key emission lines are labeled in the figure.	29
3.2	Infrared CL ratios as a function of black hole mass for our $n_H = 300 \text{ cm}^{-3}$ and $\log U = -1.0$ models (top) and $\log U = -2.0$ (middle and bottom). Note that these diagrams are not meant to be compared to observations.	36
3.3	Contour plots showing the dependence on mass and U at $n_H = 300 \text{ cm}^{-3}$ for various predictive line ratios. While high ratios generally are indicative of a definitive mass range, lower ratios can correspond to many possibilities. The highest ratio in each plot is normalized to one.	37
3.4	Contour plots showing the dependence on mass and U at $n_H = 300 \text{ cm}^{-3}$ for a selection of line ratios more sensitive to U than black hole mass. As can be seen, these CL ratios vary more significantly with U than with black hole mass over the range of parameter space explored in our models. The highest ratios in each plot is normalized to one.	38

3.5	Observed [Si VI] $1.962\mu\text{m}$ /[Si X] $1.430\mu\text{m}$ line flux ratios from Lamperti et al. [2017], Mason et al. [2015], Riffel et al. [2006], Rodríguez-Ardila et al. [2011], Mould et al. [2012], Alonso-Herrero et al. [2000], Rhee and Larkin [2005], Müller-Sánchez et al. [2018]	39
3.6	Predicted [Si VI] $1.962\mu\text{m}$ /[Si X] $1.430\mu\text{m}$ line flux ratios as a function of black hole mass for a gas density of $n_H = 300 \text{ cm}^{-3}$ and an ionization parameter of $\log U = -2.0$. The line ratio has been normalized to 1.0 at its peak.	40
4.1	BPT diagram comparing J1056+31 (red ‘x’) with the BASS sample [Koss et al., 2017], with the AGN [Kewley et al., 2001] and composite [Kauffmann et al., 2003] demarcation regions in blue and orange respectively. Also plotted are NGC 4395 [blue ‘x’; Filippenko and Ho, 2003] and Pox 52 [green ‘x’; Barth et al., 2004]. Note that J1056+31 is the only target that meets our metallicity selection criteria and displays star-forming ratios.	43
4.2	Mid-infrared color-color diagram showing the placement of low metallicity galaxies with comparable $\log[\text{N II}]/\text{H}\alpha$ to J1056+3138, as defined by $\log[\text{N II}]/\text{H}\alpha \leq -1.3$ using emission line fluxes from the MPA catalog. The box corresponds to the Jarrett et al. [2011] demarcation region.	44
4.3	K-band spectra from Keck NIRSPEC of J1056+3138. Note that this galaxy displays a prominent broad Pa α line and the [Si VI] coronal line, as well as Br δ and H $_2$ lines. An SDSS <i>gri</i> color composite image is also displayed, showing its compact morphology.	47
4.4	Upper Right: The detected [Si VI] emission line, as well as nearby Br δ and H $_2$ lines. Lower Left: A heat map showing the output of the <i>emcee</i> fits for the amplitude and width of the Gaussian for the [Si VI] detection in J1056+3138. The contour levels show the σ intervals up to 3σ , and the histograms (upper left and lower right) show the distribution of potential fits for the width (upper left) and amplitude (lower right) of the Gaussian. As can be seen, the solution converged very well, proving a robust detection.	49
4.5	Optical spectra from SDSS of J1056+3138. The top panel displays the fits for the [Ne V] $\lambda 3345, 3425$ coronal lines. The center panel displays the fit for the [Fe VII] $\lambda 5722, 6085$ coronal lines. The bottom panel displays the fit for the broad H α	51

4.6 L_X/L_{W2} compared with metallicity diagnostic $[\text{N II}]/\text{H}\alpha$ for galaxies in the MPA-JHU catalog (DR8) that show mid-infrared colors suggestive of AGN activity based on three color cuts: $W1-W2 > 0.5$ (blue), $W1-W2 > 0.8$ (purple), and the Jarrett et al. [2011] cut (orange). Galaxies with optical broad lines and $[\text{N II}]/\text{H}\alpha$ ratios that fall below the low metallicity cut-off ($\log([\text{N II}]/\text{H}\alpha) < -1.0$) are shown as green squares, and J1056+3138 is shown as a red 'X'. Note that J1056+3138 has the lowest L_X/L_{W2} ratio when compared to similar galaxies. 54

Abstract

THE HUNT FOR INTERMEDIATE MASS BLACK HOLES

Jenna M. Cann, PhD

George Mason University, 2021

Dissertation Director: Dr. Shobita Satyapal

While supermassive black holes (SMBHs) up to a billion times the mass of the Sun are found in the centers of all massive galaxies and stellar mass black holes of ~ 10 solar masses (M_{\odot}) are formed from supernovae, there is currently no direct evidence for intermediate mass black holes (IMBHs) with masses between $\approx 100 - 10^4 M_{\odot}$. Black holes in this “mass desert” are of significant astrophysical interest, because they could provide insight into SMBH “seeds”, formed at high redshift and observationally undetectable. With the discovery of over 200 SMBHs with masses more a billion times the mass of our Sun found when the Universe was less than a billion years old, there has been increased interest in determining the origins of these mysterious giants. As SMBHs have been found much earlier in cosmic time than previously believed possible given radiation pressure limits on the growth rate of stellar mass black holes, this requires new thought as to their initial formation. Were they formed from the end products of massive primordial stars, resulting in numerous black hole seeds of mass $\approx 100 M_{\odot}$? Or were they formed from the direct collapse of massive clouds of gas that may have formed in the low angular momentum, metal-free environment of the early universe, forming rarer seeds up to $10^4 M_{\odot}$ in size?

Finding a population of IMBHs in dwarf galaxies, which have not undergone significant

growth and evolution over cosmic history, as indicated by their low stellar masses and metallicities, can provide insight into which path is more likely to have occurred. While there is now a growing number of black holes found with masses between $10^5 - 10^6 M_{\odot}$, very little is known about the existence, properties, host galaxy demographics, and scaling relations of black holes with masses less than $\approx 10^5 M_{\odot}$. Determining the mass function and occupation fraction of this elusive population will prove pivotally important to disentangling the history of these objects.

Most searches for IMBHs have been done using traditional optical spectroscopic, X-ray, and radio diagnostics, however, these diagnostics fail in the low mass and low metallicity regimes, causing a large population of IMBHs to remain elusive. The work of this thesis focuses on theoretically determining, and observationally validating, the most effective ways to search for IMBHs in these significant environments. In this thesis, I highlight the deficiencies of traditional optical diagnostics in finding IMBHs and provide an alternative solution using infrared coronal lines, fine structure emission lines with ionization potentials greater than 60 eV. These emission lines are particularly significant as stars do not produce enough high energy radiation to excite these ions, meaning that the detection of a coronal line can provide robust evidence for the presence of an AGN. As the emission structure of a black hole is dependent on its mass, these coronal lines could also provide a diagnostic to estimate the mass of the black hole. In order to test the efficacy of coronal lines in finding AGNs in low metallicity galaxies, a multi-wavelength study was done on J1056+3138, showing the power of infrared diagnostics in the search for black holes in extreme environments.

Chapter 1: Introduction

1.1 Motivation

Black holes with masses from a million to up to a billion times the mass of the sun are now known to be ubiquitous in the centers of galaxies, and their masses appear to correlate with properties of the host in which they reside [e.g., Magorrian et al., 1998, Gebhardt et al., 2000, Gültekin et al., 2009, McConnell and Ma, 2013]. There is now a growing number of black holes found with masses between $10^5 - 10^6 M_{\odot}$ [Greene and Ho, 2004, 2007, Greene et al., 2010, Jiang et al., 2011, Xiao et al., 2011, Dong et al., 2012b, Reines et al., 2013, Baldassare et al., 2015]. However, very little is known about the existence, properties, host galaxy demographics, and scaling relations of black holes with masses less than $\approx 10^5 M_{\odot}$. In fact, there is currently no *direct* evidence for black holes with masses between $\approx 150 M_{\odot}$ and $\approx 10^4 M_{\odot}$. Black holes in this “mass desert” in the local universe are of significant astrophysical interest. This is because they are potential analogs of the original seed black holes formed at redshifts $z > 15$. The mass function and occupation fraction of these “intermediate mass black holes (IMBHs)” in the local universe hold vital clues into the origins of supermassive black holes (SMBHs), potentially allowing us to discriminate between lower mass seeds formed from stellar remnants or massive seeds formed directly out of the collapse of dense gas [Volonteri and Natarajan, 2009, Volonteri and Begelman, 2010, van Wassenhove et al., 2010, Greene, 2012, Reines and Comastri, 2016, Mezcua, 2017]. Furthermore, the study of IMBHs can help us understand the black hole-galaxy co-evolution in the low mass regime. Moreover, mergers between black holes in this mass range are one of the most promising sources of gravitational waves (GWs) detectable with the Laser Interferometer Space Antenna [LISA; Amaro-Seoane et al., 2013], yet black hole

pairs in this mass range in the local universe have not yet been identified and their merger rate is unknown. Apart from their importance in understanding the origin of SMBHs and their connection to their host galaxies, IMBHs are of intrinsic interest in studying the physics of accretion in the low-mass regime, where some of the fundamental signposts of accretion activity, such as the broad line region [Elitzur and Ho, 2009, Chakravorty et al., 2014] and the torus [Krolik and Begelman, 1988] may disappear. Finding a population of IMBHs, measuring their masses, determining their merger rates, and understanding their connection to their host galaxies is therefore of fundamental astrophysical importance.

1.2 The Seed Models of SMBHs

With the discovery of over 200 SMBHs with masses more than a billion times the mass of our Sun found when the Universe was less than a billion years old [e.g. Dietrich and Hamann, 2004, Fan et al., 2006, Jiang et al., 2007, Kurk et al., 2007, Maiolino et al., 2007, Shields et al., 2008, Riechers et al., 2009, Wang et al., 2010, Mortlock et al., 2011, Wu et al., 2015, Bañados et al., 2016, Matsuoka et al., 2018, Wang et al., 2018, Li et al., 2020], there has been increased interest in determining the origins of these mysterious giants. As SMBHs have been found much earlier in cosmic time than previously believed possible given radiation pressure limits on the growth rate of stellar mass black holes, this requires new thought as to their initial formation. A recent review paper by [Inayoshi et al., 2020] reports a compilation of quasars discovered at $z > 6$ and their masses (see Figure 1.1)

There are three main schools of thought behind the origins of SMBH seeds, each with different estimates for the occupation fraction and mass function of SMBHs in dwarf galaxies at low redshift [see Inayoshi et al., 2020, for review]. Determining the population statistics of black holes in local dwarf galaxies that have not undergone dramatic evolution since their formation will provide insight as to the most likely seed model to form these giants.

The first formation model is through the supernova of massive primordial (Pop III) stars formed out of metal-free gas. These supernova remnants will result in black holes

$\approx 100M_{\odot}$ in mass, and, as they are a natural end to the stellar life cycle, are likely to be very common [Volonteri and Begelman, 2010]. There is considerable uncertainty in the mass function of these stars, however, so the actual black hole masses may be much lower [Woods et al., 2019]. Therefore, if this is the most probable seed model, we would expect to see a high occupation fraction of IMBHs in local dwarf galaxies, however their masses will be relatively low. As black holes have a canonical limit to their accretion rates, defined by the balance of gravitational and radiation pressures (the Eddington limit), there is a theoretical limit to the growth of a black hole over a given amount of time. This limit is particularly notable when compared to the masses $> 10^9 M_{\odot}$ discovered at high redshifts. This rate of growth would require sustained periods of accretion faster than the Eddington limit, known as super-Eddington accretion [Volonteri, 2010]. There have been several hypotheses proposed as to how this could be possible, including accretion off of a dense stellar cluster or non-isotropic radiation through jets [see Volonteri and Rees, 2005, Natarajan, 2021, and references therein], though typical environments would only allow short periods of sub-Eddington growth [Alvarez et al., 2009].

The second model involves a black hole formed by the runaway mergers of massive stars in a dense nuclear star cluster [Ebisuzaki et al., 2001, Freitag et al., 2006, Tagawa et al., 2016, Ryu et al., 2016, Stone et al., 2017]. While this model provides higher mass seeds than the Pop III model, this method requires stars to form very efficiently in the core of the protogalaxy and for the merger process to happen quickly before the stars evolve off of the main sequence [Ebisuzaki et al., 2001, Begelman and Rees, 1978].

The final model theorizes the formation of black hole seeds through the direct collapse of massive clouds of gas that may have formed in the low angular momentum, metal-free environment of the early universe. To form a direct collapse black hole (DCBH), the environment must have specific conditions. The primary goal behind these conditions is to ensure that the gas cloud does not cool down and fragment to form stars. First, the gas cloud must be metal-free to avoid efficient metal-cooling. Furthermore the hydrogen in the gas cloud must be ionized with Lyman-Werner radiation to further prevent efficient cooling

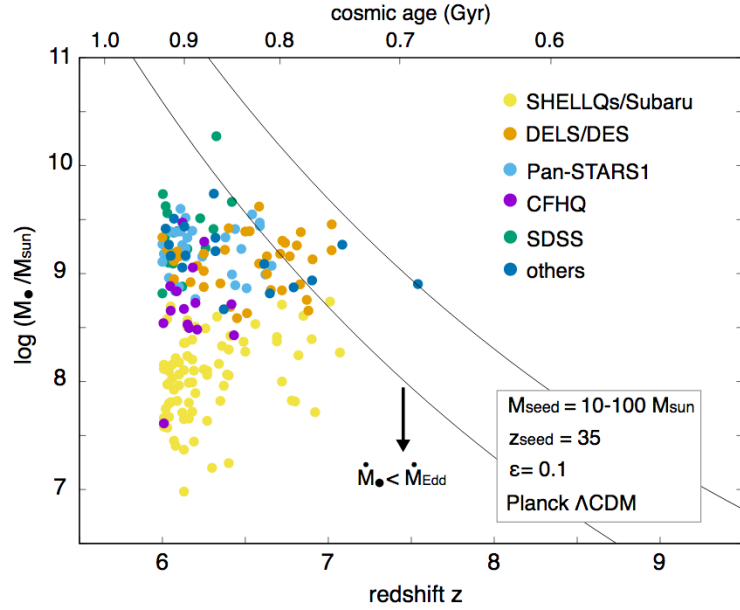


Figure 1.1: Figure from Inayoshi et al. [2020] plotting high- z quasars ($z > 6$) and their reported masses.

[Haehnelt and Rees, 1993, Bromm and Loeb, 2003, Latif and Ferrara, 2016, Wolcott-Green et al., 2017, Regan et al., 2017, e.g.]. This pathway would result in more massive seeds, up to $\approx 10^4 M_{\odot}$ in mass, but much rarer in number due to the stringent environmental conditions required [Greene, 2012, Natarajan, 2011, Agarwal et al., 2013, Natarajan, 2014, Inayoshi et al., 2014, Van Borm et al., 2014]. Observational evidence of a low occupation fraction of more massive IMBHs in dwarf galaxies would suggest this is more probable seed model.

As can be seen, determining the mass function and occupation fraction of IMBHs in local dwarf galaxies can provide insight to the formation pathway of their supermassive counterparts. Therefore, a dedicated and complete study on the presence of IMBHs in dwarf galaxies is of vital astrophysical importance.

1.3 Previous Studies

Unfortunately, finding and studying the properties of IMBHs is challenging since the sphere of influence, the region in which we would see stars orbiting the central black hole, of even a $10^5 M_\odot$ black hole at a distance of 10 Mpc is only approximately $0.01''$. Detecting a population of IMBHs through resolved kinematics is therefore currently observationally impossible. A significant sample of IMBHs can therefore only be detected if they are accreting. However, accretion activity for such low mass black holes is also challenging to detect. This is because accreting IMBHs are likely to be found in the centers of low-mass galaxies, where star formation in the host galaxy can dominate the optical spectrum [Trump et al., 2015] and gas and dust can obscure the central engine at optical, and even X-ray, wavelengths. Indeed, recent *NuSTAR* observations are revealing a growing number of nearby low luminosity active galactic nuclei (AGNs) that are Compton thick [e.g., Annuar et al., 2015, 2017, Ricci et al., 2016]. Moreover, even if highly accreting and unobscured, AGNs powered by IMBHs will have low luminosities. For example, a $10^3 M_\odot$ black hole radiating at its Eddington rate will have a bolometric luminosity of only 10^{41} erg s $^{-1}$. The X-ray luminosities of these low luminosity AGNs will be low and can be comparable to, and therefore indistinguishable from, a population of high mass X-ray binaries in the host galaxy. This problem is exacerbated in low mass galaxies which have lower metallicities, where X-ray emission from high mass X-ray binaries is enhanced [e.g., Mapelli et al., 2009, Fragos et al., 2013]. Likewise, the radio emission from a potential AGN in a low mass galaxy can be comparable to, and indistinguishable from, a compact nuclear starburst [Condon et al., 1991], making it impossible to uniquely identify accretion around IMBHs with radio observations alone. While mid-infrared color-selection is a powerful tool in uncovering obscured AGNs [e.g., Lacy et al., 2004, Stern et al., 2005, Donley et al., 2012, Stern et al., 2012, Assef et al., 2013, Mateos et al., 2012, Satyapal et al., 2018], it is well-known that this method fails in galaxies where the luminosity of the stellar emission from the host galaxy is comparable to, or exceeds, that from the AGN. Young starbursts can

also mimic the mid-infrared colors of luminous AGNs [Hainline et al., 2016], although only under extreme conditions [Satyapal et al., 2018]. Even broad emission lines in the optical spectrum, usually a hallmark signature of an AGN powered by a massive black hole, are associated with supernova activity for the majority of cases in dwarf galaxies [Baldassare et al., 2016], further emphasizing the limitations of optical studies in the hunt for IMBHs in the local universe, although these sources have narrow emission lines consistent with star forming galaxies. Finally, even the standard optical emission lines used to classify galaxies dominated by AGNs using the Baldwin-Phillips-Terlevich (BPT) diagram [Baldwin et al., 1981] has been established only for higher mass black holes and are also affected by the presence of shocks [e.g., Kewley et al., 2001, Kauffmann et al., 2003]. It is not yet known whether these diagnostic diagrams are robust AGN indicators in the IMBH mass range.

Given the challenges associated with finding IMBHs, current searches have yielded relatively small numbers of candidates. There are several candidate IMBHs reported in globular clusters, where some firm upper limits on the black hole masses have been obtained [e.g., Maccarone et al., 2005, 2007, Strader et al., 2012, Lützgendorf et al., 2012, 2013, Wrobel et al., 2016, Kızıltan et al., 2017, Perera et al., 2017]. Searches for AGNs in low mass galaxies have yielded a small but slowly growing sample of candidate active IMBHs [e.g., Filippenko and Ho, 2003, Barth et al., 2004, Satyapal et al., 2007, Greene and Ho, 2007, Satyapal et al., 2008, 2009, Dewangan et al., 2008, Shields et al., 2008, Ghosh et al., 2008, Izotov and Thuan, 2008, Desroches and Ho, 2009, Gliozzi et al., 2009, McAlpine et al., 2011, Jiang et al., 2011, Reines et al., 2011, Secrest et al., 2012, Ho et al., 2012, Dong et al., 2012b, Araya Salvo et al., 2012, Secrest et al., 2013, Simmons et al., 2013, Reines et al., 2013, Coelho et al., 2013, Schramm et al., 2013, Bizzocchi et al., 2014, Reines et al., 2014, Maksym et al., 2014, Moran et al., 2014, Yuan et al., 2014, Secrest et al., 2015, Miller et al., 2015, Mezcuca et al., 2016, Lemons et al., 2015, Baldassare et al., 2015, Pardo et al., 2016, Baldassare et al., 2017, Chen et al., 2017, Chilingarian et al., 2018] using a variety of multi-wavelength tools. Optical searches, like those published in [Reines et al., 2013, Chilingarian et al., 2018, e.g.,] take advantage of diagnostics such as the Baldwin-Phillips-Terlevich (BPT)

diagram [Baldwin et al., 1981, Kewley et al., 2001, Kauffmann et al., 2003], in which optical narrow line emission separates galaxies between AGNs and star-forming dominated regions. Accreting IMBHs, however, are likely to be found in the centers of low-mass galaxies, where star formation in the host galaxy can dominate the optical spectrum [Trump et al., 2015] and gas and dust can obscure the central engine.

This obscuration can also affect the effectiveness of X-ray searches for IMBHs. While several recent studies have had success in unearthing low mass SMBHs [Dong et al., 2012b, Mezcua et al., 2018, Birchall et al., 2020, e.g.], recent *NuSTAR* observations are revealing a growing number of nearby low luminosity active galactic nuclei (AGNs) that are Compton thick [e.g., Annuar et al., 2015, 2017, Ricci et al., 2016]. Moreover, even if highly accreting and unobscured, AGNs powered by IMBHs will have low luminosities. For example, a $10^3 M_{\odot}$ black hole radiating at its Eddington rate will have a bolometric luminosity of only 10^{41} erg s $^{-1}$. The X-ray luminosities of these low luminosity AGNs will be low and can be comparable to, and therefore indistinguishable from, a population of high mass X-ray binaries in the host galaxy. This problem is exacerbated in low mass galaxies which have lower metallicities, where X-ray emission from high mass X-ray binaries is enhanced [e.g., Mapelli et al., 2009, Fragos et al., 2013]. Likewise, the radio emission from a potential AGN in a low mass galaxy can be comparable to, and indistinguishable from, a compact nuclear starburst [Condon et al., 1991], making it impossible to uniquely identify accretion around IMBHs with radio observations alone.

While mid-infrared color-selection is a powerful tool in uncovering obscured AGNs [e.g., Lacy et al., 2004, Stern et al., 2005, Donley et al., 2012, Stern et al., 2012, Assef et al., 2013, Mateos et al., 2012, Satyapal et al. in press], it is well-known that this method fails in galaxies where the luminosity of the stellar emission from the host galaxy is comparable to, or exceeds, that from the AGN. Young starbursts can also mimic the mid-infrared colors of luminous AGNs [Hainline et al., 2016], although only under extreme conditions [Satyapal et al., 2018]. Even broad emission lines in the optical spectrum, usually a hallmark signature of an AGN powered by a massive black hole, are associated with supernova activity for

the majority of cases in dwarf galaxies [Baldassare et al., 2016], further emphasizing the limitations of optical studies in the hunt for IMBHs in the local universe, although these sources have narrow emission lines consistent with star forming galaxies.

Recently, optical variability surveys have uncovered AGN candidates in dwarf and low mass galaxies [Baldassare et al., 2018, 2020, Martínez-Palomera et al., 2020], however detection of the lowest mass IMBHs will require high cadence due to short variability timescales [Martínez-Palomera et al., 2020]. Despite the growing number of these discoveries, the fraction of low mass galaxies with evidence of accretion identified through these techniques is extremely small and the mass range probed is still above $\approx 10^4 M_{\odot}$.

1.4 Research Statement

In this study, the diagnostic potential of various methods to detect the presence of an IMBH will be tested, both through theoretical models and observations. We have undertaken three studies that develop and test the tools necessary to make the most of *JWST* at its launch.

The first project tests the efficacy of current optical diagnostics in the intermediate mass regime. While these are commonly used tools to identify AGNs, to date there have been no studies of the efficacy of these diagnostics in the low mass regime.

The second project focuses on modeling for the first time the dependence of infrared emission lines on the mass of the central black hole.

The third project tests the use of infrared coronal lines as a diagnostic in finding intermediate mass black holes in local analogs of primitive galaxies.

Future work to further investigate these questions is detailed in Chapter 5.

Chapter 2: The Limitations of Optical Spectroscopic Diagnostics in Identifying AGNs in the Low Mass Regime

2.1 Introduction

The most widely used diagnostic diagram uses the $[\text{O III}]/\text{H}\beta$ versus the $[\text{N II}]/\text{H}\alpha$ emission line ratios (commonly referred to as the Baldwin-Phillips-Terlevich, BPT, diagram), in which most known AGNs exhibit higher line ratios than star-forming galaxies [Kewley et al., 2001]. Using these diagnostics, there have been a growing number of AGNs discovered in low mass galaxies or galaxies lacking classical bulges [e.g., Reines et al., 2013]. However, despite the vast amount of optical spectroscopic data available from the Sloan Digital Sky Survey, to date, there exist only a small fraction of dwarf galaxies optically classified as hosting AGNs. Indeed, a key and striking result based on optical spectroscopic studies, is that the fraction of galaxies with signs of accretion activity drops dramatically at stellar masses $\log M_*/M_\odot < 10$ [e.g. Kauffmann et al., 2003]. In fact, for a sample of dwarf galaxies with stellar masses $\log M_*/M_\odot < 9.5$ and high quality optical emission line measurements, only 0.1% of galaxies are unambiguously identified as AGNs based on their emission line ratios [Reines et al., 2013], compared to $> 80\%$ of galaxies with $\log M/M_\odot > 11$ [Kauffmann et al., 2003]. While this suggests AGN activity is less prevalent in low mass galaxies, the effectiveness of optical emission line ratios in identifying accreting *low mass* black holes has not been established.

It is well known that optical spectroscopic diagnostics can fail at identifying AGNs in galaxies with active star formation, where photoionization from stars and starburst-driven winds can dominate the optical spectrum, and gas and dust can obscure the central engine [e.g. Goulding and Alexander, 2009, Kewley et al., 2013, Trump et al., 2015]. However, it is

not known how these emission line ratios depend on the mass of the black hole. This is of prime importance for high spatial resolution follow-up observations, where it has generally been assumed that if contamination from surrounding star formation is reduced, the AGN can be identified. Indeed, follow-up optical spectroscopic observations using high spatial resolution integral field units (IFUs) are currently the gold standard to confirm or refute an AGN candidate identified through multiwavelength studies. Many more AGN candidates are expected to be identified at X-ray wavelengths with the launch of eRosita in 2019 [Singh et al., 2017]. Recent work by Agostino & Salim [Agostino and Salim, 2019] demonstrates that there is a significant population of X-ray identified AGN that have BPT line ratios consistent with star-forming galaxies. With a limiting flux of $\approx 10^{-13} \text{ erg/cm}^2/\text{s}$ in the 2-10 keV band, the detection of black holes with masses as low as $1000M_{\odot}$ is possible within 10 Mpc. As the SDSS catalog has observations of ≈ 3000 dwarf galaxies with masses less than 10^8M_{\odot} and high S/N, and ≈ 1200 with masses less than 10^7M_{\odot} , there will be a large sample available in which optical spectra can be used to constrain X-ray contribution from stellar processes. Reliance on optical spectroscopic confirmation could therefore severely bias conclusions about the black hole occupation fraction. As the optical spectroscopic diagnostic diagrams have been established based on semi-empirical classification schemes using galaxy samples with black hole masses in excess of 10^6M_{\odot} [Kewley et al., 2001, Kauffmann et al., 2003] and photoionization models using a stellar ionizing continuum and a single power law to model the ionizing radiation field of the AGN [Veilleux and Osterbrock, 1987, Kewley et al., 2001], these models do not take into account the effect of black hole mass on the ionizing radiation field, which in turn would impact the predicted emission line spectrum and potentially the currently employed optical BPT AGN classification schemes for IMBHs. As the black hole mass decreases, the Schwarzschild radius decreases, and in response, the temperature of the surrounding accretion disk increases. The shape of the ionizing radiation field therefore changes with black hole mass, which in turn will impact the emission line spectrum at optical wavelengths, potentially affecting the location on the BPT diagram.

2.2 Methods

In order to model the emission line spectrum of gas ionized by an AGN, we used version c17 of the spectral synthesis code CLOUDY [Ferland et al., 2017]. The emission line spectrum depends on several factors, including the shape of the ionizing radiation field, the geometrical distribution of the gas, the chemical composition and grain properties, the gas properties, and the equation of state.

2.2.1 The AGN Continuum

We assume that the AGN continuum consists of three components: an accretion disk, Comptonized X-ray radiation in the form of a power law, and an additional component seen in the X-ray spectrum of most AGNs, often referred to as the "soft excess component".

Multiwavelength observations of quasars suggest that the continuum emission from AGNs peaks in the ultraviolet part of the electromagnetic spectrum [e.g., Shields, 1978, Elvis et al., 1986, Laor, 1990]. This emission, often referred to as the "Big Blue Bump" (BBB) is attributed to the emission from the accretion disk around the black hole. In our models, we assume that the accretion disk is a simple geometrically thin, optically thick disk [Shakura and Sunyaev, 1973], where the emission from the disk is approximated by the superposition of blackbodies at temperatures corresponding to the different disk annuli at radius R , with the temperature as a function of radius R given by Peterson [1997], Frank et al. [2002]:

$$T = 6.3 \times 10^5 \left(\frac{\dot{m}}{\dot{m}_{Edd}} \right)^{1/4} \left(\frac{M_{BH}}{10^8 M_\odot} \right)^{-1/4} \left(\frac{R}{R_s} \right)^{-3/4} K \quad (2.1)$$

where \dot{m}_{Edd} and \dot{m} are the Eddington and actual accretion rates, respectively, M_{BH} is the mass of the black hole, and R_s is the Schwarzschild radius.

In most observed SMBHs, where masses range from 10^6 - $10^9 M_\odot$, this temperature change is not significant. Indeed, the inner temperature of the accretion disk changes

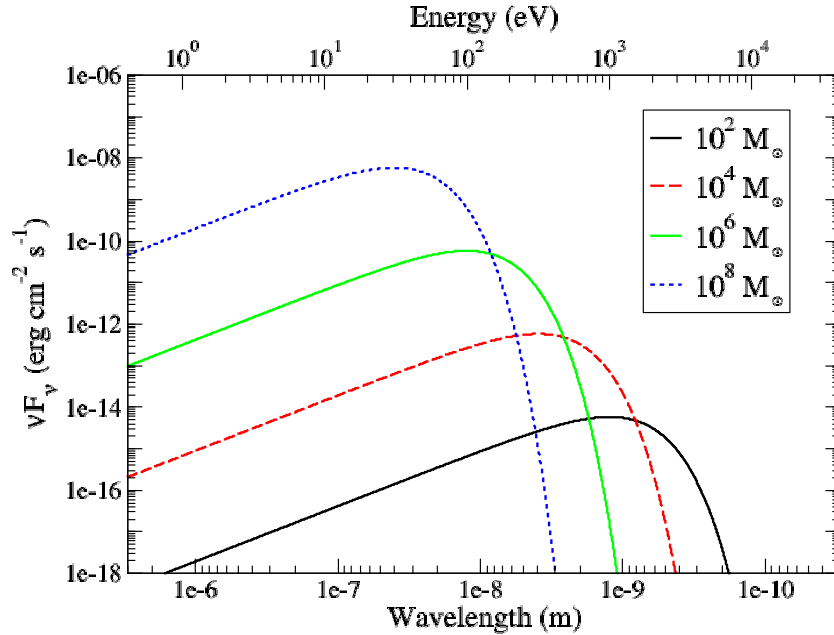


Figure 2.1: Accretion disk SEDs from black holes with masses that span $10^2 - 10^8 M_{\odot}$ accreting at $0.1 \dot{m}_{Edd}$. The units of the vertical axis are set for illustrative purposes by assuming a distance of 30 Mpc. We have labeled the location of the ionization potentials of several coronal lines accessible by *JWST* by the dotted vertical lines. As can be seen, the shift in disk temperature for the range of black hole masses explored in this work significantly moves the location of the "Big Blue Bump" relative to the ionization energies of key coronal lines observable by *JWST*.

by only a factor of 2 when the black hole mass changes by three orders of magnitude. Because of this, most studies do not take temperature-dependent changes in the accretion disk SED shape into account. When looking at wider range of black hole masses, however, this temperature difference can cause the peak of the accretion disk spectrum to move dramatically (Figure 2.1). Moreover, because the ionization potentials of the coronal lines fall at energies very close to the peak of the BBB, changes in black hole mass will strongly affect the coronal line emission spectrum emitted by the surrounding gas, potentially providing a diagnostic of the black hole mass.

In this study, the accretion disk spectrum was modeled using the DISKBB model [Mitsuda et al., 1984, Makishima et al., 1986] of XSpec v12.9.0¹ [Arnaud, 1996]. To set the temperature at the inner disk radius, we used Equation 2.1 and varied the black hole mass from $10^2 - 10^8 M_{\odot}$ and assumed that the black hole is accreting at $0.1 \dot{m}_{Edd}$. The accretion disk SED from this model is shown in Figure 2.1. Over the range of black hole mass explored in this work the peak of the BBB varies from 13 eV to 424 eV.

Observations of AGN spectra show a high energy component that can be well-approximated by a power law, believed to be caused by Comptonization of seed photons produced by the disk [Svensson, 1999] by energetic electrons in a hot corona [Krolik, 1999]. In this study, we adopt a spectral index of 0.8 [e.g., Wilkes and Elvis, 1987, Grupe et al., 2006] and an α_{OX} ratio of 1.2 [Netzer, 1993] for this power law component. We assume a high energy cutoff of 100 keV. As the emission lines we are analyzing have ionization potentials of less than or equal to 500 eV, the detailed shape of the AGN SED at the highest energies will not play a significant role in our calculations.

An additional component to the AGN has been observed as excess radiation between 100 to 300 eV that cannot be explained by simply extending the power law to lower energies. This emission, referred to as the "soft excess", has been detected in over 50% of Seyfert 1 galaxies [Halpern, 1984, Turner and Pounds, 1989], though recent studies of local Seyfert 1s suggest that the fraction can reach up to 70-90% [e.g., Piconcelli et al., 2005, Bianchi et al., 2009, Scott et al., 2012, Boissay et al., 2016]. The origin of this emission is still a topic of debate, with three primary schools of thought being: a Comptonized disk [Czerny and Elvis, 1987, Done et al., 2012, Jin et al., 2017], blurred ionized reflection [Fabian et al., 2005, Crummy et al., 2006], or relativistic smeared absorption [Gierliński and Done, 2004, Middleton et al., 2007].

While the origin of the soft excess is not clear, this spectral component is remarkably well fit with a blackbody with a roughly constant temperature of $\approx 100 - 200$ eV [e.g., Gierliński and Done, 2004, Ricci et al., 2017]. In this work, we model the soft excess

¹<http://www.heasarc.gsfc.nasa.gov/docs/xanadu/xspec>

phenomenologically as a blackbody with a temperature of 150 eV (1.7×10^6 K). We assume that the ratio of the luminosity of the soft-excess component to the luminosity of the power law component is constant with respect to black hole mass and adopt a ratio consistent with what is typically observed (1) [Vignali et al., 2004, Piconcelli et al., 2005, Chakravorty et al., 2012]. Little variation in the soft excess emission with respect to mass is seen [Gierliński and Done, 2004, Boissay et al., 2016], but only a small range of black hole masses have been explored. In Figure 2, we plot the incident continuum, including all three components, for our $10^7 M_\odot$ model. For black holes with mass $< 10^3 M_\odot$, the emission from the disk shifts into the soft X-rays and dominates over the soft excess. Note that because the ionization potentials of the coronal lines extend into the soft X-rays, it is important to include this component into our AGN continuum. We emphasize that we have not attempted to present a model finely tuned to match the properties of any one particular AGN. The strength and shape of the continuum in the 100 – 400 eV range is important in replicating observed CL line ratios. The generic AGN model adopted in this work predicts the relative behavior of the CL ratios as a function of BH mass, and demonstrates which line ratios are the most sensitive to BH mass. A sample SED for the $10^7 M_\odot$ black hole can be found in Figure 2.2.

2.2.2 Geometrical Distribution of the Gas

We assume a one-dimensional spherical model with a closed geometry, where the cloud is between the observer and the continuum source, and the ionization parameter and gas density are allowed to vary. The ionization parameter, U , is defined as the dimensionless ratio of the incident ionizing photon density to the hydrogen density:

$$U = \frac{\phi_H}{n_H c} = \frac{Q(H)}{4\pi R^2 n_H c} \quad (2.2)$$

where ϕ_H is the flux of hydrogen-ionizing photons striking the illuminated face of the cloud per second, n_H is the hydrogen density, c is the speed of light, and $Q(H)$ is the number of hydrogen ionizing photons striking the illuminated face per second. In our calculations,

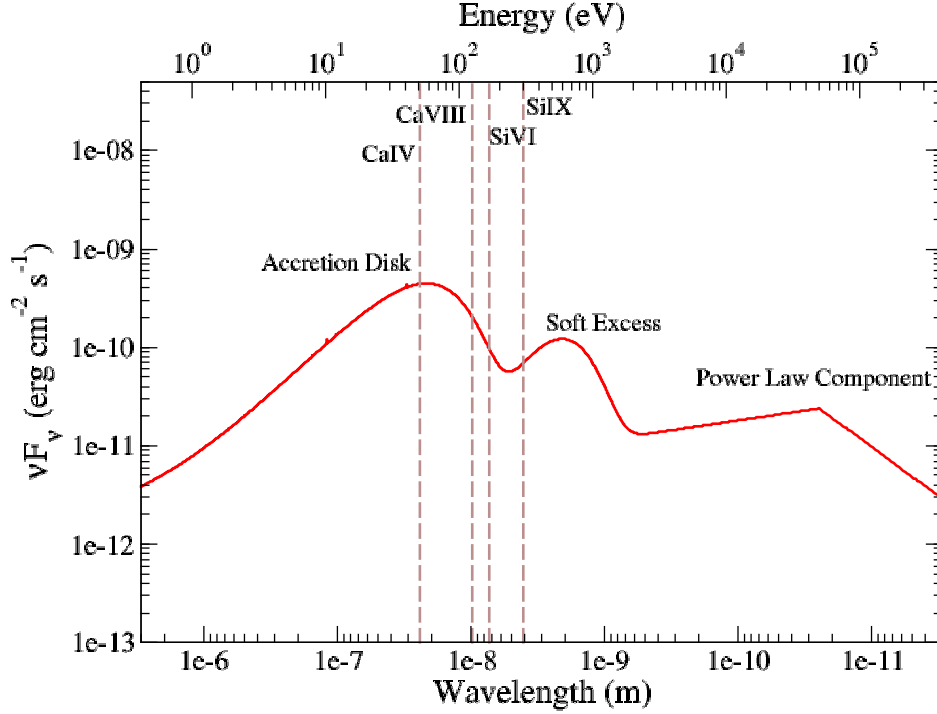


Figure 2.2: SED from black hole of mass $10^7 M_{\odot}$ with soft excess and power law components. The units of the vertical axis are set by assuming a distance of 30 Mpc. We have labeled the location of the ionization potentials of several coronal lines accessible by *JWST* by the dotted vertical line. As can be seen, several coronal lines have an ionization potential that could be greatly affected by the presence of a soft excess component.

U is allowed to vary from 10^{-4} to 10^{-1} . On average, U is $\sim 10^{-3}$ based on observations of the optical emission lines in local galaxies and HII regions [Dopita et al., 2000, Moustakas et al., 2010], but can be higher in ULIRGS [Abel et al., 2009] or high-redshift galaxies [Pettini et al., 2001, Brinchmann et al., 2008, Maiolino et al., 2008, Hainline et al., 2009, Erb et al., 2010], and in the CL region. We therefore explored a large dynamic range of ionization parameters in this project.

2.2.3 Physical State of the Gas and Dust

We chose the gas and dust abundances in our calculations to be consistent with the local interstellar medium (ISM). The effects of variations in metallicity on the computed spectrum will be explored in future work. We assume constant density, and vary the hydrogen density of the gas from $\log(n_H/cm^3) = 1.5 - 3.5$, in units of 1.0 dex. We include thermal, radiation, and turbulent pressure in our models with the turbulent velocity set to 5.0 km s^{-1} . Our calculations extend only to the Hydrogen ionization front, defined as the point when the hydrogen ionization fraction drops below 0.01, since all of the lines are produced in the ionized region of the cloud.

2.2.4 Parameter Space

We computed a total of 5,070 models, where ionization parameter was varied between $\log U = -1$ to $\log U = -4$ in increments of 0.25 dex, the hydrogen gas density between $\log n_H/cm^{-3} = 1.5$ to 3.5 in increments of 1.0 dex, the Eddington ratio between $10^{-4} - 1$ in increments of 1.0 dex, and mass between $100 - 10^8 M_\odot$ in increments of 0.5 dex.

2.3 Modeling Results

In Figure 2.3, we show the optical BPT diagram as a function of black hole mass for the $\dot{m} = 0.1$, $n_H = 300 \text{ cm}^{-3}$, $\log U = -2.0$ model. Note that, typically, U is $\sim 10^{-3}$ based on observations of optical emission lines in star-forming galaxies and HII regions [Dopita et al., 2000, Moustakas et al., 2010], but values as high as $\log U = -2.0$ are found in regions such as ULIRGs [Abel et al., 2009] or high redshift galaxies [e.g., Brinchmann et al., 2008, Erb et al., 2010]. For illustrative purposes, we plot in Figure 2.3 the higher ionization parameter case, which may be more typical in dwarf galaxies [Izotov et al., 2001]. The effect of ionization parameter on the line ratios is shown in Figure 2.5. We also plot the widely adopted AGN demarcation lines used in the literature to identify AGNs, and the location of RGG118 [Baldassare et al., 2017], a dwarf galaxy recently found to host

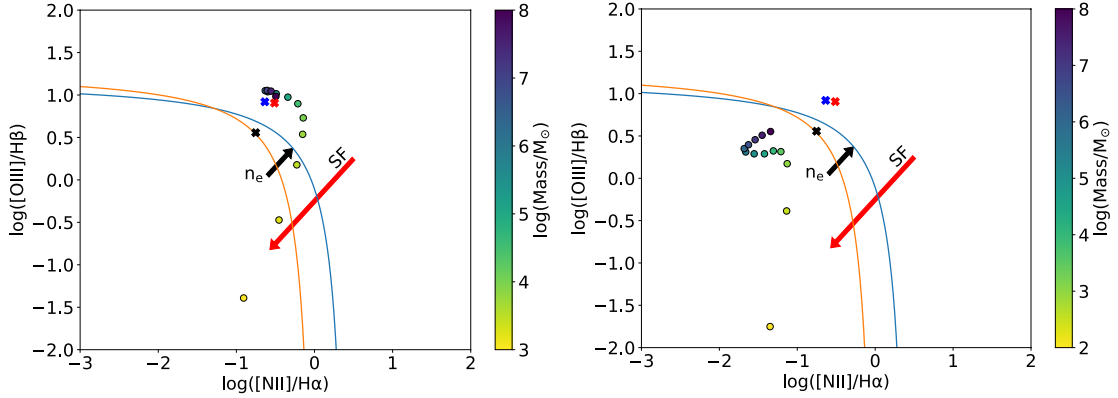


Figure 2.3: BPT diagram for our photoionization models for a range of black hole masses from $10^3 - 10^8 M_\odot$ at constant $\log U = -2$, $n_H = 300 \text{ cm}^{-3}$, and $\dot{m}/\dot{m}_{Edd} = 0.1$ at Solar (left) and 0.1-Solar (right) metallicities. The red and blue lines correspond to demarcations separating star-forming galaxies from AGNs from Kauffmann et al. [2003] (red) and Kewley et al. [2001] (blue), respectively. For black hole masses $< 1000 M_\odot$ in the top panel, the line ratios fall outside the plotted region shown in the figure. We also show the observed BPT line ratios of RGG118 (black 'x') reported by Baldassare et al. [2017], POX 52 (red 'x') reported by Barth et al. [2004], and NGC 4395 (blue 'x') reported by Kraemer et al. [1999]. Note our models do not include star formation. The arrows denote the direction that model points would move in the presence of star formation (red) and higher electron densities (black).

a $50,000 M_\odot$ black hole, the lowest mass SMBH currently known. As can be seen, our model predicts that as black hole mass decreases, the line ratios fall outside the widely used AGN and composite demarcation regions of the diagram, and that the transition mass is at approximately $10,000 M_\odot$. Interestingly, the line ratios of RGG118 fall right on the edge of the star-forming/composite demarcation line, consistent with the predictions of our models given its black hole mass. We also show the effects of changes in gas density, metallicity, and adding a contribution from star formation. Note that both lowering the metallicity and increasing the contribution from star formation, both of which likely accompany IMBH hosts, results in line ratios that move further into the star-forming region of the diagram.

The observed behavior of the line ratios with black hole mass is a consequence of two main factors. As the black hole mass decreases, the resulting hardening of the AGN spectral

energy distribution (SED) changes the ionization structure of the nebula. For massive black holes in the $10^7 - 10^8 M_\odot$ range, the dominant ionization states of oxygen are O^+ and O^{2+} , but as the black hole mass decreases, and the ionizing radiation field shifts to higher energies, some of the O is found in higher ionization states, extending even up to O^{8+} for the lowest masses modeled. In addition, as the black hole mass decreases, the enhanced X-ray emission from the accretion disk penetrates further into the cloud, resulting in a significantly extended partially ionized zone where H^+ is produced but O^{2+} is not. This effect results in a net decrease in the predicted $[O\ III]/H\beta$ emission line ratio. The fraction of Nitrogen in N^+ , on the other hand, is relatively constant as a function of black hole mass over the range explored in our models. However, the extended partially ionized zone results in an overall decrease in the $[N\ II]/H\alpha$ emission line ratio. Note it is well known that AGNs in general produce a much more extended partially ionized zone in which collisionally excited forbidden lines can be produced than is seen in HII regions around massive young stars. This is because the ionizing radiation field produced by a stellar continuum produces very few X-ray photons, resulting in a much sharper ionization front. The fraction of X-ray photon flux relative to the total flux as a function of black hole mass is shown in Figure 2.4. As can be seen, there is a steep increase in the fraction of X-ray photons when the black hole mass falls below $10^5 M_\odot$.

We note that we have shown the effect of black hole mass on the BPT diagram for typical ISM conditions and a single Eddington ratio. The line ratios are of course a strong function of the ionization parameter, since the ionization parameter affects the ionization structure of the nebula. The size of the H^+ region and the dominant stage of ionization increases with increasing ionization parameter. In Figure 2.5, we show the effect of both black hole mass and ionization parameter on the BPT line ratios. For typical ionization parameters, which are between $-3.2 < \log U < -2.9$ for local HII regions [Dopita et al., 2000] and local star-forming galaxies [Moustakas et al., 2010], both the $[OIII]/H\beta$ and the $[NII]/H\alpha$ emission line ratios are lower for IMBHs compared with black holes above $10^6 M_\odot$, and never make it into the AGN demarcation for black hole masses below $10^3 M_\odot$. Lower

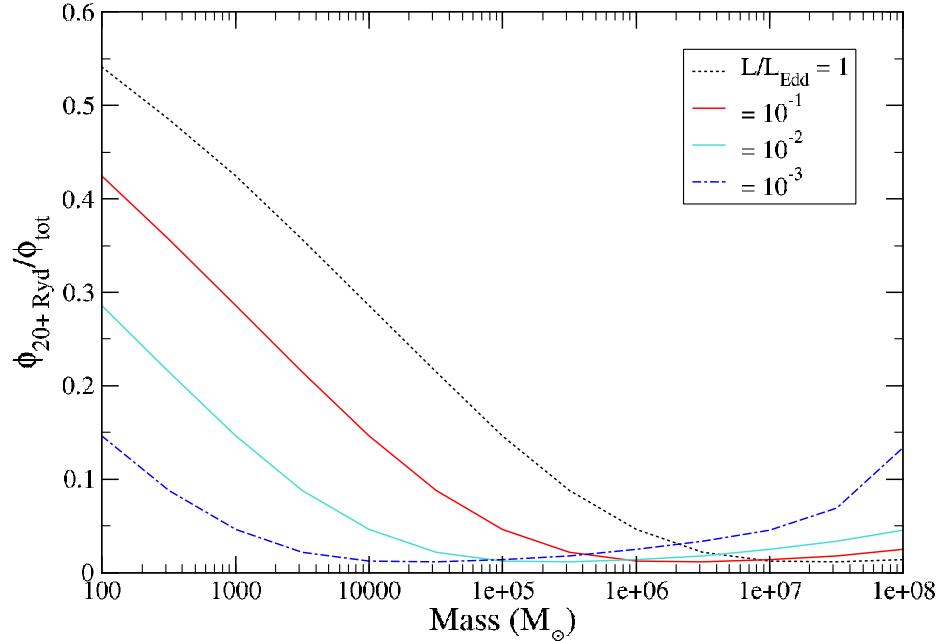


Figure 2.4: Fraction of total flux in X-ray photons with energies greater than 20 Ryd striking the illuminated face of the cloud per second compared to total photon flux per second as a function of black hole mass for a range of Eddington ratios. As can be seen, in low mass black holes, a large fraction of radiation emitted is over 20 Ryd.

ionization parameter models show a wider range of black hole masses emitting in the AGN regime, but photoionization from star formation will result in line ratios that shift toward the star-forming region of the diagram. Note the models we have shown here are for a fixed Eddington ratio. The shape of the AGN continuum will change as a function of the Eddington ratio, which in turn will impact the line ratios as seen in Figure 2.6. As can be seen, the low mass black holes radiating at higher Eddington ratios fall below the AGN demarcation region, but if the Eddington rate is reduced, they move to the traditional AGN regime.

There are additional optical diagnostics used to confirm and identify AGN, using the

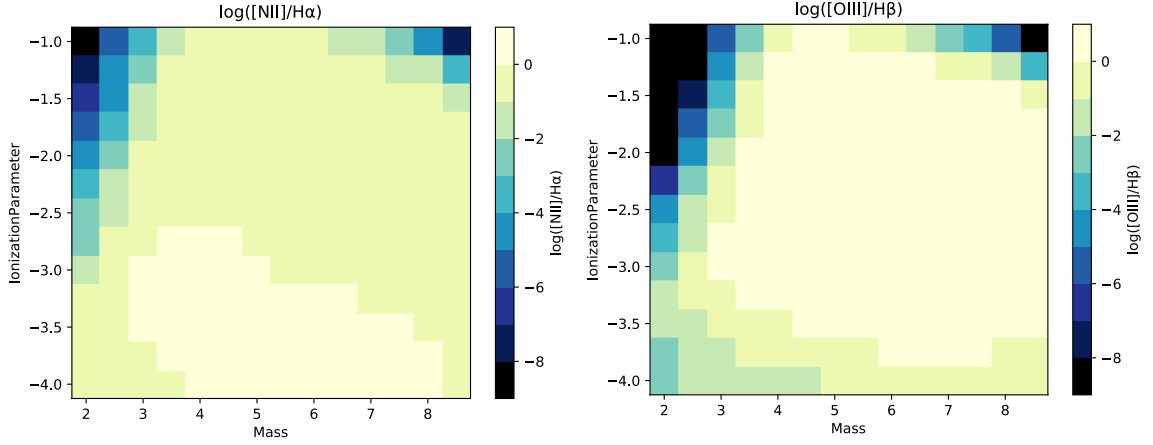


Figure 2.5: Contour plots showing the changes of the BPT line ratios over a range of BH mass from $100 - 10^8 M_{\odot}$ and ionization parameter from $\log U = -1$ to -4 for $\dot{m}/\dot{m}_{Edd} = 0.1$ and $\log n_H = 300 \text{ cm}^{-3}$.

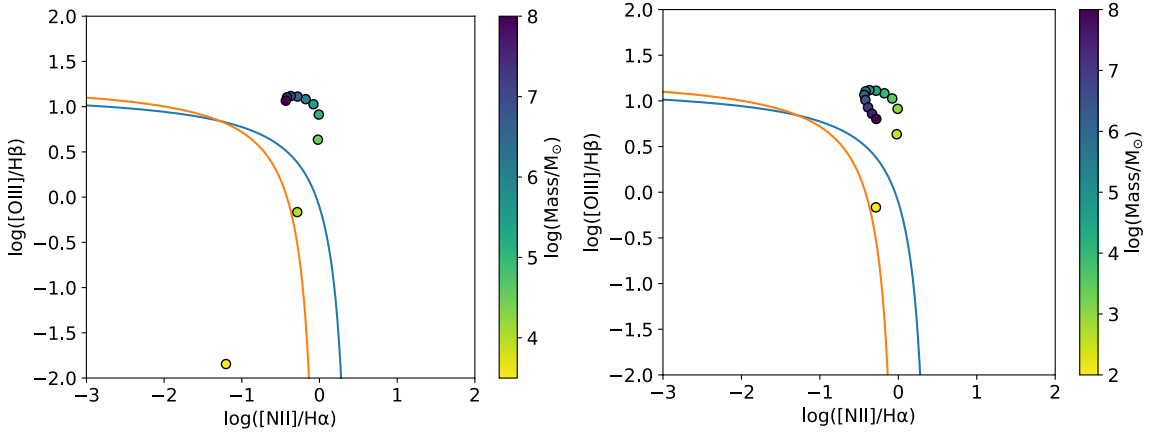


Figure 2.6: BPT plots for $\dot{m}/\dot{m}_{Edd} = 1$ (left) and 0.01 (right) with $\log U = -2.5$ and $n_H = 300 \text{ cm}^{-3}$. Note that masses not pictured here fall outside the plotted region shown in the figure, below the non-AGN demarcation. Red and blue lines are as denoted in Figure 2.3. The presence of star formation would move the model points in the direction of the red arrow in Figure 2.3. Note that as you lower the Eddington ratio, the temperature of the accretion disk decreases such that for the most massive black holes, the resulting softening of the SED of the accretion disk causes a net decrease in the $[OIII]/H\beta$, as seen in the lowest panel above.

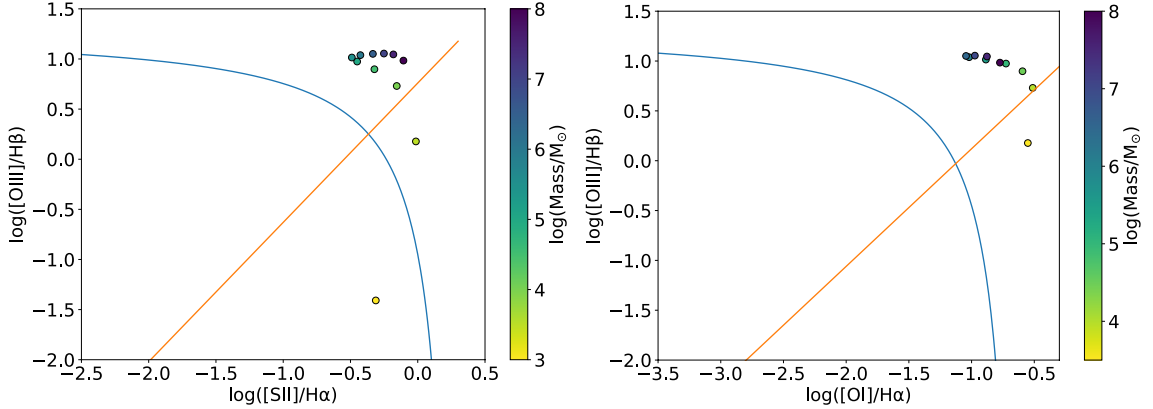


Figure 2.7: Additional BPT diagrams using the [S II]/H α (top) and [O I]/H α (bottom) line ratios for the $n_H = 300 \text{ cm}^{-3}$, $\dot{m}/\dot{m}_{Edd} = 0.1$, solar metallicity, $\log U = -2$ model. The blue and red lines correspond to the demarcations separating AGN and star-forming galaxies (blue) and AGN from LINERS (red). Masses below $10^3 M_\odot$ in the top panel and below $10^{3.5} M_\odot$ in the lower panel are outside the range plotted, in the star-forming region.

[S II]/H α and [O I]/H α line ratios. The dependence of these ratios on black hole mass was also tested, with the results shown in Figure 2.7. As can be seen, a larger range of black hole masses have line ratios that fall in the AGN regime of the graph, however, the line ratios dramatically change and fall into the star-forming region of the plot when black hole mass falls below $10^3 - 10^{3.5} M_\odot$. If optical diagnostics are to be taken for a candidate IMBH, it is recommended that all BPT line ratios be observed and considered to increase the possibility of an accurate identification, though the lack of AGN colors is still not enough to disregard a strong candidate for the lowest masses.

2.4 Implications

The models presented in this work call into question the completeness of optical BPT diagrams in confirming the presence of AGNs powered by IMBHs. For a non-negligible region in parameter space, our models predict that low mass AGNs do not produce optical emission line ratios occupied by higher mass black holes. In fact, a $10,000 M_\odot$ black hole will

always be classified as a star-forming galaxy at an ionization parameter of $\log U = -2$ unless the Eddington ratio falls below 0.1, even without including the effects of photoionization from stars. At Eddington ratios below 0.1, the AGN will be less luminous and the line ratios will likely be dominated by photoionization from star formation, suggesting that accreting black holes in this mass range may rarely be detected as AGNs using this standard optical diagnostic diagram. As Greene and Ho [2007] find a typical Eddington ratio for low mass black holes of 0.4, our results leave open the possibility that the use of these diagnostics to confirm IMBH candidates below $\approx 10^4 M_\odot$ could severely bias the inferred low-mass black hole occupation fraction. We note that apart from the limitations of these narrow line region diagnostics, Chakravorty et al. [2014] have shown that such low mass black holes may not even show a broad line region and Baldassare et al. [2016] have shown that, in low mass galaxies, broad lines can actually be due to supernovae, further emphasizing the shortcomings of optical diagnostics in finding AGNs powered by IMBHs.

2.4.1 Detectability with Current Facilities

Our results have important consequences for high spatial resolution optical spectroscopic follow-up studies of accreting IMBH candidates. While it is well-known that dilution from circumnuclear star formation significantly limits the diagnostic power of optical spectroscopy in identifying AGNs in low mass galaxies using large aperture surveys such as SDSS, it has been assumed that if contamination from star formation is reduced using high spatial resolution optical spectroscopy, the AGN can be revealed. To illustrate this point, the typical [O III] luminosities of star forming dwarf galaxies within the 3" SDSS fiber is about 10^{39} erg/s [Reines et al., 2013], which corresponds approximately to the Eddington limit for a $1000 M_\odot$ black hole, given a conversion between L_{bol} and $L_{[O III]}$ of about 100 for low luminosities [e.g., Lamastra et al., 2009]. Star formation would therefore dominate over the AGN emission from a $10^3 - 10^4 M_\odot$ black hole for all but the most highly accreting systems. However, assuming that the star formation rate is reasonably uniform within the 3" aperture, star formation within the 0.2" spaxels of an IFU with AO would only

contribute about 10^{36} *erg/s* to the [O III] emission, allowing an accreting IMBH as low as $100-1000M_{\odot}$ to be detected, *if* they exhibited line ratios similar to higher mass black holes. Our results demonstrate that such follow-up optical spectroscopic studies will misidentify accreting IMBHs, which will masquerade as star forming galaxies, *even when the effects of contamination from surrounding star formation are removed.*

Using our black hole mass dependent models, we plot in Figure 2.8 the [O III] luminosity as a function of black hole mass for a wide range of Eddington ratios. While [N II] is generally the weaker line, and the limiting factor in identifying an AGN, we have chosen to show [O III] luminosity, as the [O III]/H β line ratio showed a wider range of values across our models. We also show the median [O III] luminosity of star forming dwarf galaxies ($\log M_{*} < 9.5$) from the SDSS 3" fiber (black dotted line), the aperture-reduced [O III] luminosity from star formation in a 0.2" IFU spaxel (green dotted line), and the [O III] line luminosity assuming a detection threshold of 10^{-17} *erg/cm²/s* assuming a 10 Mpc distance. As can be seen, using our mass dependent models and assuming a distance of 10 Mpc, the [O III] luminosity of black holes with masses down to 10^3M_{\odot} could be identified. However, our work shows that such IMBHs would typically not be identified as AGN using the widely-used BPT classifications for higher mass black holes.

2.4.2 Additional Considerations and Caveats

Our goal in this project is to examine the first order effects of black hole mass on the widely used BPT line ratios. We have chosen a simple accretion disk, together with a power law and soft excess component, to model the AGN continuum. The predicted line ratios will change with more complex models. However, the purpose of this investigation is to explore the dependence of predicted emission line strengths on the SED of the accretion disk as black hole mass varies.

We note emission line strengths can also be affected by many other physical processes not included in this initial study. This model does not include the effects of shocks generated by AGN outflows or starburst driven winds, which can alter the emission line spectrum [Allen

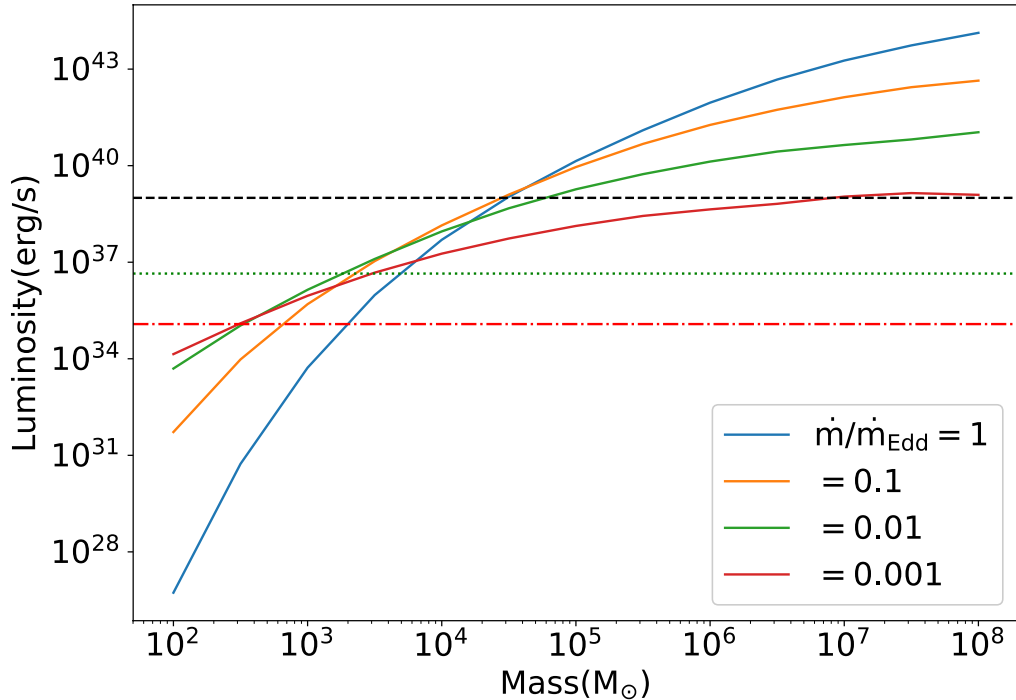


Figure 2.8: Luminosity of [O III] as a function of black hole mass for the $n_H = 300 \text{ cm}^{-3}$, solar metallicity, $\log U = -3$ model, for a range of Eddington ratios. Also plotted are the median [O III] luminosity of SDSS star forming dwarf galaxies (black dotted line), the aperture-reduced [O III] luminosity from star formation detected in a $0.2''$ IFU spaxel (green dotted line), and the [O III] luminosity corresponding to a detection threshold of 10^{-17} s^{-1} (red dot-dashed line). Note that the horizontal luminosity thresholds displayed correspond to a distance of 10 Mpc and even the lowest black hole masses could be detected in closer sources using an IFU.

et al., 2008, Kewley et al., 2013], and can even generate emission lines consistent with star-forming galaxies in pure AGN models [Molina et al., 2018]. Our model also takes into account ionizing radiation from the AGN only, however, as discussed in the introduction, dilution from star formation only exacerbates the effects discussed here. The limitations of optical diagnostics are even more severe in low metallicity galaxies at all black hole masses [Groves et al., 2006].

In addition, our models have assumed a simple geometrically thin, optically thick disk.

This assumes the accretion is radiatively efficient, and viscous heating is balanced by radiative cooling. When the mass accretion rate falls below $0.01 \dot{m}/\dot{m}_{Edd}$, the accretion flow is predicted to be advection-dominated and radiatively inefficient (RIAF) [Narayan et al., 1998, Ho, 2008, Yuan and Narayan, 2014], producing a significantly different SED that may lack a standard big blue bump with much of the emission arising in the IR [Quataert and Gruzinov, 2000]. We also note that we do not take into account the effect of black hole spin, which would affect the innermost stable orbit, and therefore the temperature of the accretion disk, which in turn would affect the shape of the emergent SED. Our model also does not take into account radiative transfer through the atmosphere of the disk.

Chapter 3: The Diagnostic Potential of Infrared Coronal Lines

3.1 Introduction

Observations of the infrared fine structure lines offer us one of the only definitive tools to discover buried AGNs in dusty galaxies. As has been shown in previous works, AGNs show prominent high-excitation fine structure line emission, whereas starburst and normal galaxies are characterized by a lower excitation spectra characteristic of HII regions ionized by young stars [e.g., Genzel et al., 1998, Sturm et al., 2002, Satyapal et al., 2004]. Fine structure lines from ions with ionization potentials greater than ≈ 70 eV [Abel and Satyapal, 2008, Satyapal et al., 2021], the so-called "coronal" lines (CLs), cannot be easily produced in HII regions surrounding young stars, the dominant energy source in starburst galaxies, since even hot massive stars emit very few photons with energy sufficient for the production of these ions. The power of these diagnostics in finding buried AGN has been strikingly demonstrated by the *Spitzer* mission through the discovery of a population of AGNs in galaxies that display optically "normal" nuclear spectra [e.g., Lutz et al., 1999, Satyapal et al., 2007, 2008, 2009, Goulding and Alexander, 2009]. Given that AGNs powered by IMBHs will be low luminosity, reside in low mass galaxies with potentially enhanced star formation [Trump et al., 2015], and may have enhanced obscuration [Geha et al., 2006] compared with AGNs in higher mass galaxies, an IR *spectroscopic* study is crucial to provide unambiguous proof of an AGN and study its properties in this class of objects.

With the advent of the *JWST*, infrared spectroscopic observations with unprecedented sensitivity will be possible. These observations can potentially uncover IMBHs in large samples of galaxies, possibly revolutionizing our understanding of this class of objects. Not

only can infrared CLs uniquely identify accretion activity from low-luminosity AGNs residing in dusty star forming hosts, but since the ionization potentials of the associated ions are in the ultraviolet to soft X-ray regime, at wavelengths that are not directly observable due to Galactic absorption, the infrared CLs can potentially be used to indirectly reconstruct the shape of the spectral energy distribution (SED) of the AGN at wavelengths where the emission from the accretion disk is expected to peak [e.g., Lynden-Bell, 1969, Shakura and Sunyaev, 1973, Netzer, 1985], potentially allowing us to gain insight into the accretion properties of the black hole and its mass. As the black hole mass decreases, the Schwarzschild radius decreases, and in response, the temperature of the surrounding accretion disk increases. The shape of the ionizing radiation field therefore changes with black hole mass, which in turn will impact the emission line spectrum at both optical and infrared wavelengths. Not only do infrared fine structure lines carry the advantage of being less sensitive to dust extinction, the excitation energies corresponding to the transitions are small compared to the ambient nebular temperature, and so the infrared line ratios of two different stages of ionization produced by the same element are only weakly dependent on the electron temperature of the gas in which they are produced. They are therefore the ideal tool to study the nature of the ionizing radiation field in the dust enshrouded nuclear regions of galaxies.

3.1.1 Methods

The models used in this project are the same as those used in Project 1. As part of the pilot study, we only included models with $\dot{m}/\dot{m}_{Edd} = 0.1$ and Solar metallicity. As seen by Equation 2.1, accretion rate and black hole mass have equal and opposite effects to the temperature of the accretion disk. A more highly accreting black hole will have the same temperature as a lower mass black hole with a slower accretion rate. All other parameters spanned the full range as in Project 1. Given the full set of black hole masses, ionization parameters, and gas densities, we computed a total of 507 simulations. For each model, we computed the emergent spectrum of all emission lines with ionization potentials in excess

of 70 eV that are within $1 - 30 \mu\text{m}$. We explored the behavior of only the most prominent lines that can potentially be detected by *JWST*, the brightest of which are listed in Table 3.1.

3.1.2 Results

The predicted infrared emission line spectrum in our simulations is strongly dependent on the shape of the ionizing radiation field incident on the gas and hence the black hole mass. In Figure 3.1, we show the transmitted continuum in the $1 - 30 \mu\text{m}$ range for the $10^2 M_\odot$ and $10^8 M_\odot$ AGN models for a standard gas density of $n_H = 300 \text{ cm}^{-3}$ and an ionization parameter of $\log U = -1.0$. As can be seen, the strength of the emission lines in this wavelength range changes significantly with black hole mass, with the CLs with the highest ionization potentials being more prominent in the lower black hole mass model (see Table 3.1). In Figure 3.2, we show the mass dependence of a selection of key abundance-insensitive line ratios as a function of black hole mass, again for $n_H = 300 \text{ cm}^{-3}$ and $\log U = -1.0$. As can be seen, for a given ionization parameter and gas density, line ratios involving ions with different ionization potentials vary dramatically with black hole mass in response to changes in the shape of the AGN ionizing continuum with black hole mass. The CLs with the highest ionization potentials ($\gtrsim 300 \text{ eV}$) peak at the lowest black hole masses, and the line ratios can vary by over six orders of magnitude between $10^2 M_\odot$ and $10^6 M_\odot$. We also find a series of line ratios that peak in the intermediate mass range ($10^4 - 10^5 M_\odot$), demonstrating that the suite of line ratios is sensitive to different mass ranges explored in our models.

The CL ratios vary with both the shape of the ionizing continuum and the ionization parameter adopted in our models. As the ionization parameter increases, the ratio of photon flux to gas density increases, which in turn increases the ionization rate while keeping the recombination rate relatively constant for our constant density models. The combination of the hardness of the radiation field, which depends on the black hole mass, and the ionization stage of a particular element determines the CL ratio for a given gas density. In Figure

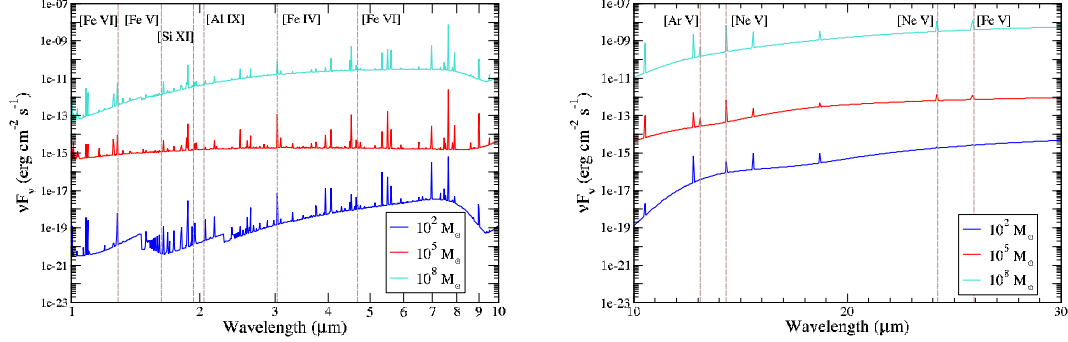


Figure 3.1: Simulated spectra between 1 – 30 μm for black holes of mass $10^2 M_\odot$, $10^5 M_\odot$, and $10^8 M_\odot$ for a standard gas density of $n_H = 300 \text{ cm}^{-3}$ and an ionization parameter of $\log U = -1.0$. Key emission lines are labeled in the figure.

3.3, we show the dependence of a selection of key CL ratios with both black hole mass and ionization parameter to illustrate this point. As can be seen, the line ratios are sensitive to both the black hole mass and the ionization parameter since both parameters affect the dominant ionization stage of a given species and the ionization structure of the nebula. However, CLs associated with the highest ionization potentials are most prominent only in models with the smallest black hole masses and high ionization parameters, indicating that extremely high observed ratios will be associated only with low mass black holes. For intermediate ratios, our models demonstrate that there are degeneracies between U and black hole mass. In such cases, a large set of CL observations can be used to constrain the black hole mass and the ionization parameter. Based on our models, we identify line ratios that display much larger variations with ionization parameter than with mass as can be seen from Figure 3.4. This ratio stays nearly constant across the lower mass range, but spans a wide range of values in ionization parameter, and so could be a potential diagnostic for determining ionization parameter in an AGN.

3.1.3 Implications

Based on our photoionization models, we have demonstrated that the infrared CLs are potentially a powerful probe of the black hole mass in AGNs. In particular, emission lines associated with ions with the highest ionization potentials, such as Si XI, Si X, and Fe XIII are predicted to be far stronger in the smallest black hole mass models. Our models suggest that the following line ratios will be higher for AGNs powered by IMBHs with masses $< 10^6 M_{\odot}$:

- $[\text{Si XI}]1.934\mu\text{m}/[\text{Si X}]1.430\mu\text{m}$
- $[\text{Si XI}]1.934\mu\text{m}/[\text{Si VI}]1.962\mu\text{m}$
- $[\text{Si IX}]3.928\mu\text{m}/[\text{Si VI}]1.962\mu\text{m}$
- $[\text{Si VII}]6.512\mu\text{m}/[\text{Si VI}]1.962\mu\text{m}$
- $[\text{Fe XIII}]1.074\mu\text{m}/[\text{Fe VI}]1.010\mu\text{m}$

which are most prominent for the lowest mass IMBHs ($< 10^4 M_{\odot}$), and the

- $[\text{Al IX}]2.044\mu\text{m}/[\text{Al VI}]9.113\mu\text{m}$
- $[\text{Al IX}]2.044\mu\text{m}/[\text{Al VI}]3.659\mu\text{m}$
- $[\text{Al IX}]2.044\mu\text{m}/[\text{Al V}]2.904\mu\text{m}$
- $[\text{Ca VIII}]2.321\mu\text{m}/[\text{Ca IV}]3.206\mu\text{m}$
- $[\text{Ca VIII}]2.321\mu\text{m}/[\text{Ca V}]4.157\mu\text{m}$
- $[\text{Mg VII}]9.006\mu\text{m}/[\text{Mg IV}]4.487\mu\text{m}$

which peak for IMBHs in the $10^4 M_{\odot} - 10^6 M_{\odot}$ range.

These line ratios are predicted to vary by many orders of magnitude with black hole mass and can thus help inform future AGN studies with *JWST*.

Based on existing observations of AGNs, the number of CLs detected decreases with increasing ionization potential [Rodríguez-Ardila et al., 2006]. Indeed, in the entire sample of 838 nearby powerful AGNs from the *Swift*/*BAT* survey, not a single [Si XI] and [S XI] line is detected in the 102 observed in the near-IR [Lamperti et al., 2017]. We searched the literature for all CL studies of nearby AGNs and found that the most frequently detected CL is the [Si VI]1.962 μm line, which is detected in a total of 76 AGNs [Lamperti et al., 2017, Mason et al., 2015, Riffel et al., 2006, Rodríguez-Ardila et al., 2011, Mould et al., 2012, Alonso-Herrero et al., 2000, Rhee and Larkin, 2005, Müller-Sánchez et al., 2018]. In contrast, we could only find a total of 3 detections of the [Si XI] 1.932 μm line reported in the literature. Given that the mean mass of the active black holes observed in the literature, measured either through broad lines or the velocity dispersion of the Ca II triplet or the CO band-heads, is $\approx 10^7 M_\odot$ with a very narrow spread in mass, it is possible that this observational fact is caused by a powerful selection effect: we are observing lines that are predicted to be the strongest precisely for the black hole masses probed by our observations. The CLs associated with higher ionization potentials may be weak because we have not yet observed a significant sample of AGNs powered by lower mass black holes. It is possible that these CLs will be enhanced relative to the lower ionization potential CLs in AGNs with lower mass black holes that will be observed with *JWST*.

We have shown that several key diagnostic CL line ratios (see Figure 3.2) vary by many orders of magnitude over the mass range explored in this work. The observed ratios of detected CLs in the literature thus far do not show this range of variation. In Figure 3.5, we show the distribution of [Si VI]1.962/[Si X]1.430 line flux ratios from the literature. As can be seen the variation in this line ratio is less than an order of magnitude for the relatively small sample of objects observed thus far, suggesting similar black hole masses, ionization parameters and physical properties of the gas. In contrast, this ratio can vary by over seven orders of magnitude over the mass range explored in our calculations as can be seen from Figure 3.6. Moreover, the ratio is expected to peak precisely at the black hole masses probed by current observations, suggesting that the predominance of the [Si VI]1.962

CL relative to the higher ionization potential lines may be a selection effect caused by the range of black hole masses thus far explored.

Additional Considerations and Caveats

Our goal in this project is to explore the first order effects of varying black hole mass on the coronal line spectrum of gas ionized by an AGN. We emphasize that we have not attempted to present a model finely tuned to match the properties of any one particular AGN. The strength and shape of the continuum in the 100-400 eV range is important in replicating observed CL line ratios. The generic AGN model adopted in this work predicts the *relative* behavior of the CL ratios as a function of BH mass, and demonstrates which line ratios are the most sensitive to BH mass. The absolute line ratios are not meant to replicate observed line ratios in any particular AGN. In particular, the AGN continuum model we have adopted does not produce sufficient photons in the EUV or soft X-rays to generate the observed CL strengths seen in nearby AGNs. This has been also found in several other studies which show that photoionization models with a similar AGN continuum as that adopted in this work fail to produce the observed strengths of the HeII edge in quasars [Korista et al., 1997] and the CL spectrum in Circinus [Oliva et al., 1994], unless a harder radiation field is introduced. Moreover, the observed emission line spectrum will likely originate from multiple clouds with differing physical parameters. Indeed, the variation in line width with ionization potential and the blueshifts observed in many CLs [Grandi, 1978, Marconi et al., 1996, Mazzalay and Rodríguez-Ardila, 2007, Rodríguez-Ardila et al., 2006, 2011, Müller-Sánchez et al., 2011] suggest stratification in the photoionized region producing the CLs and the presence of outflows. Simple photoionization models of a single cloud will therefore not likely replicate observed line ratios.

We note that this first exploratory study of the CL emission line spectrum as a function of black hole mass was carried out assuming an accretion rate of $0.1\dot{m}_{Edd}$. Note that the SED from the accretion disk is a function of the accretion rate adopted. While changes in the accretion rate will affect the predicted CL spectrum, a $10^8 M_{\odot}$ black hole would need

to accrete at $10^5 \dot{m}_{Edd}$ to produce an accretion disk of the same temperature as a $100 M_{\odot}$ black hole radiating at $0.1 \dot{m}_{Edd}$. Therefore, the line ratios that uniquely identify low mass black holes as seen in Figure 3.2 are likely to still have diagnostic potential.

The strengths of the emission lines and their ratios can also be affected by other physical processes that we have not included in this preliminary exploration. For example, we have not included the effects of shocks in our calculations, which can result in collisional ionization as well as photoionization effects. Outflows from the AGN or winds driven by star formation in the surrounding gas can produce shock fronts that ionize the gas and affect the observed emission line spectrum [Allen et al., 2008, Kewley et al., 2013]. The presence of blue-shifted line profiles in many CLs is indeed consistent with the presence of outflows [e.g., Marconi et al., 1996, Mazzalay and Rodríguez-Ardila, 2007, Rodríguez-Ardila et al., 2006, 2011, Müller-Sánchez et al., 2011]. For fast shocks, the ionizing radiation generated by the cooling of the hot gas behind the shock front can generate ionizing radiation that can even extend into the soft X-rays, causing significant photoionization effects for the coronal line spectrum [Allen et al., 2008]. Several studies suggest, however, that the main driver of the CL emission is photoionization by the AGN continuum [e.g., Oliva et al., 1994, Korista et al., 1997, Marconi et al., 1996], and there is some question on whether shocks can produce the required energetics to produce the observed CL line luminosities [Wilson et al., 1997], although some contribution from shocks cannot be ruled out [Rodríguez-Ardila et al., 2006, Geballe et al., 2009]. Note that the strength and shape of the ionizing radiation field produced by shocks is a strong function of the shock velocity. A significant contribution from shocks would be accompanied by high shock velocities which would result in other distinguishing features in the emission line spectrum [Allen et al., 2008, Kewley et al., 2013].

The physics of the dust can also affect the observed CL spectrum. In addition to being a source of heating and depletion of refractory elements, grains will absorb the ionizing radiation, thereby affecting the ionization structure of the nebula. We considered models that did not include the presence of grains, as well as models that varied the grain abundance

with distance from the ionizing source in order to simulate the effect of grain destruction due to sublimation from the hard radiation field. These variations only effected the observed CL ratios by less than an order of magnitude, significantly less than the effect of black hole mass.

In addition, our models have assumed a simple geometrically thin optically thick disk. This assumes that the accretion is radiatively efficient, and viscous heating is balanced by radiative cooling. In some instances, the accretion can be advection-dominated and radiatively inefficient [Yuan and Narayan, 2014], producing a significantly different SED in the range of the ionization potentials of the coronal lines studied in this work. We also note that we do not take into account the effect of black hole spin, which would affect the inner radius of the accretion disk, and hence its temperature, and therefore the shape of the emergent ionizing SED from the disk. Our model also does not take into account radiative transfer through the atmosphere of the disk.

Finally, we should note that the AGN continuum we have adopted is based on observations of the reprocessed radiation. There is significant uncertainty in the actual ionizing radiation field incident on the gas. We have added an ad hoc soft excess component in our calculations. Recent work suggests that there is no dependence of soft excess with black hole mass and a positive correlation with accretion rate [Gliozzi and Williams, 2020, e.g.], though these studies have been focused on high mass AGNs. Indeed, because this component contributes significantly to the ionization of the coronal lines, this could prove to be a significant source of uncertainty. While parameters other than black hole mass will have some effect on the observed CL ratios, we have demonstrated that variations in the black hole mass are predicted to cause variations by many orders of magnitude in key CL ratios which we have identified in Figures 3.2 and 3.3. The fact that the observed CL ratios of the current suite of observations which probe a very narrow range in black hole mass show little variation (see Figure 3.5) may suggest that the physical conditions of the gas are not likely to vary significantly in AGNs.

Table 3.1: Brightest Coronal Lines in the 1 – 30 μm Range

Line	Transition	Wavelength (μm)	Ionization Potential (eV)	Critical Density (cm^{-3})
[Fe VI]	$^4\text{P}_{1/2} - ^2\text{D}_{3/2}$	1.01089	75	1.070×10^7
[Fe XIII]	$^3\text{P}_0 - ^3\text{P}_1$	1.07462	331	6.498×10^8
[Si X]	$^2\text{P}_{1/2} - ^2\text{P}_{3/2}$	1.43008	351	1.300×10^8
[Si XI]	$^3\text{P}_1 - ^3\text{P}_2$	1.93446	523	1.129×10^8
[Si VI]	$^2\text{P}_{1/2} - ^2\text{P}_{3/2}$	1.96247	167	3.022×10^8
[Al IX]	$^2\text{P}_{1/2} - ^2\text{P}_{3/2}$	2.04444	285	9.806×10^7
[Ca VIII]	$^2\text{P}_{1/2} - ^2\text{P}_{3/2}$	2.32117	127	5.012×10^6
[Si VII]	$^3\text{P}_2 - ^3\text{P}_1$	2.48071	205	1.101×10^8
[Al V]	$^2\text{P}_{1/2} - ^2\text{P}_{3/2}$	2.90450	120	1.067×10^8
[Ca IV]	$^2\text{P}_{1/2} - ^2\text{P}_{3/2}$	3.20610	51	1.259×10^7
[Al VI]	$^3\text{P}_1 - ^3\text{P}_2$	3.65932	154	3.400×10^6
[Si IX]	$^3\text{P}_1 - ^3\text{P}_0$	3.92820	304	1.114×10^7
[Mg IV]	$^2\text{P}_{1/2} - ^2\text{P}_{3/2}$	4.48712	80	1.285×10^7
[Ar VI]	$^2\text{P}_{1/2} - ^2\text{P}_{3/2}$	4.52800	75	7.621×10^5
[Mg VII]	$^3\text{P}_1 - ^3\text{P}_2$	5.50177	187	4.580×10^6
[Mg V]	$^3\text{P}_2 - ^3\text{P}_1$	5.60700	109	5.741×10^6
[Si VII]	$^3\text{P}_1 - ^3\text{P}_0$	6.51288	205	1.254×10^7
[Ne VI]	$^2\text{P}_{1/2} - ^2\text{P}_{3/2}$	7.64318	126	3.573×10^5
[Fe VII]	$^3\text{F}_3 - ^3\text{F}_4$	7.81037	99	1.733×10^6
[Ar V]	$^3\text{P}_1 - ^3\text{P}_2$	7.89971	60	2.025×10^5
[Mg VII]	$^3\text{P}_1 - ^3\text{P}_0$	9.00655	187	2.742×10^6
[Na IV]	$^3\text{P}_2 - ^3\text{P}_1$	9.03098	72	1.313×10^6
[Fe VII]	$^3\text{F}_2 - ^3\text{F}_3$	9.50763	99	1.858×10^8
[Fe VI]	$^4\text{F}_{7/2} - ^4\text{F}_{9/2}$	12.3074	75	3.020×10^5
[Ar V]	$^3\text{P}_0 - ^3\text{P}_1$	13.0985	60	9.516×10^4
[Ne V]	$^3\text{P}_1 - ^3\text{P}_2$	14.3228	97	4.792×10^4
[Fe VI]	$^4\text{F}_{5/2} - ^4\text{F}_{7/2}$	14.7670	75	2.996×10^5
[Fe VI]	$^4\text{F}_{3/2} - ^4\text{F}_{5/2}$	19.5527	75	1.456×10^5
[Ne V]	$^3\text{P}_0 - ^3\text{P}_1$	24.2065	97	2.656×10^4

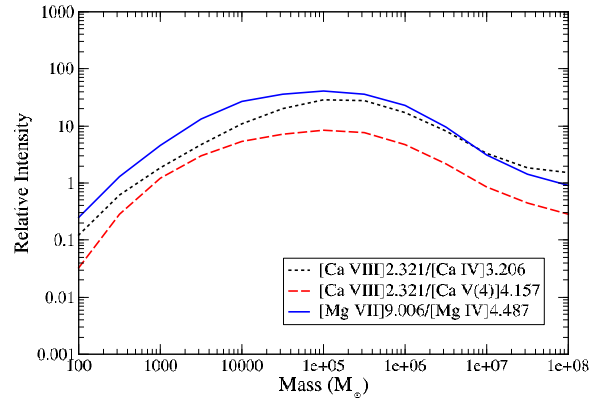
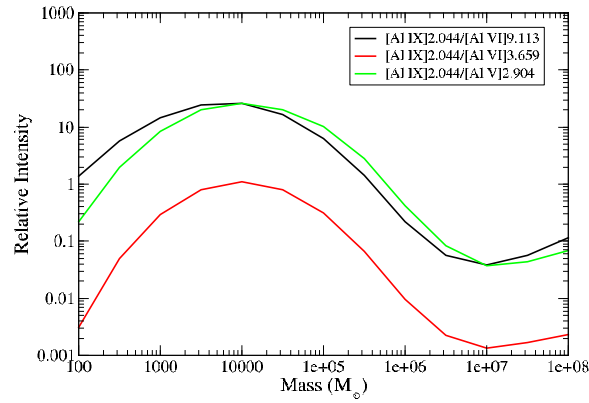
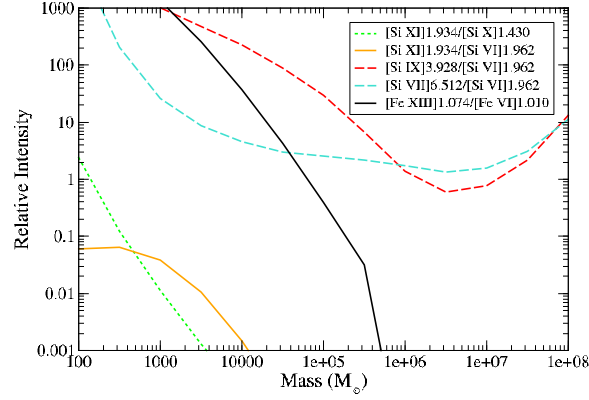


Figure 3.2: Infrared CL ratios as a function of black hole mass for our $n_H = 300 \text{ cm}^{-3}$ and $\log U = -1.0$ models (top) and $\log U = -2.0$ (middle and bottom). Note that these diagrams are not meant to be compared to observations.

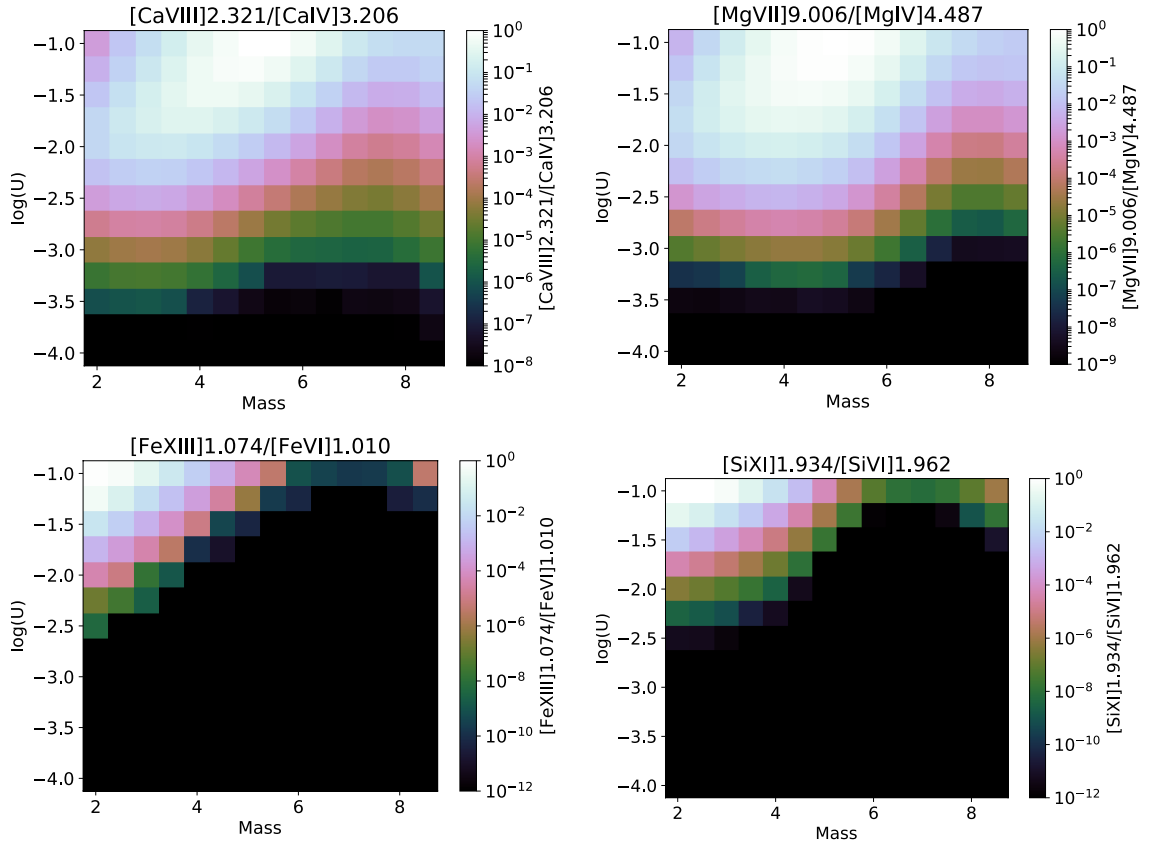


Figure 3.3: Contour plots showing the dependence on mass and U at $n_H = 300 \text{ cm}^{-3}$ for various predictive line ratios. While high ratios generally are indicative of a definitive mass range, lower ratios can correspond to many possibilities. The highest ratio in each plot is normalized to one.

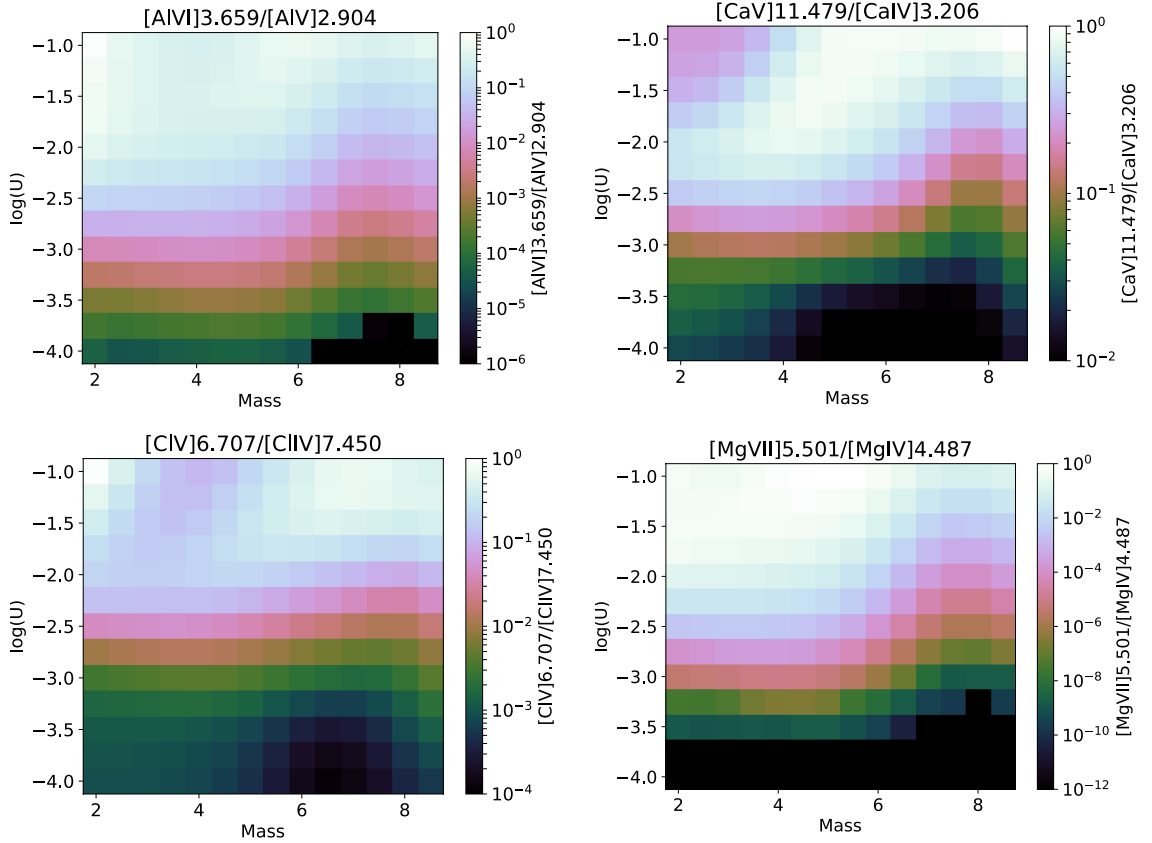


Figure 3.4: Contour plots showing the dependence on mass and U at $n_H = 300 \text{ cm}^{-3}$ for a selection of line ratios more sensitive to U than black hole mass. As can be seen, these CL ratios vary more significantly with U than with black hole mass over the range of parameter space explored in our models. The highest ratios in each plot is normalized to one.

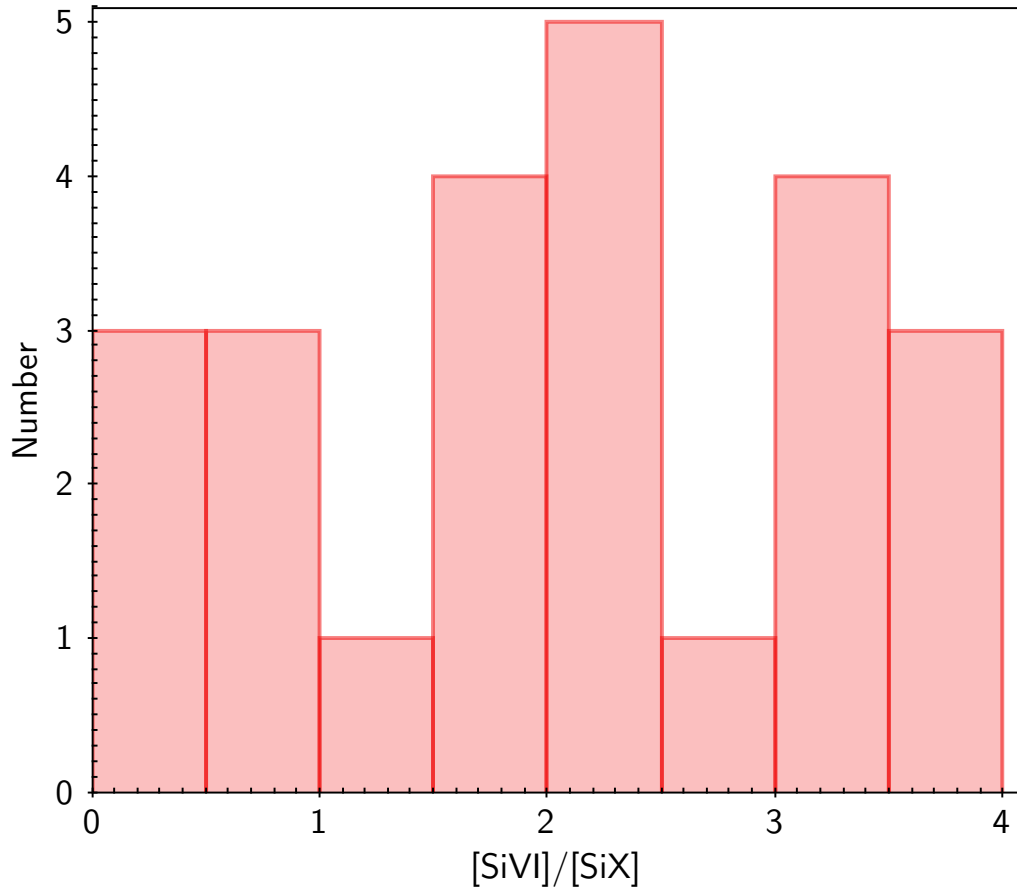


Figure 3.5: Observed [Si VI]1.962μm/[Si X]1.430μm line flux ratios from Lamperti et al. [2017], Mason et al. [2015], Riffel et al. [2006], Rodríguez-Ardila et al. [2011], Mould et al. [2012], Alonso-Herrero et al. [2000], Rhee and Larkin [2005], Müller-Sánchez et al. [2018]

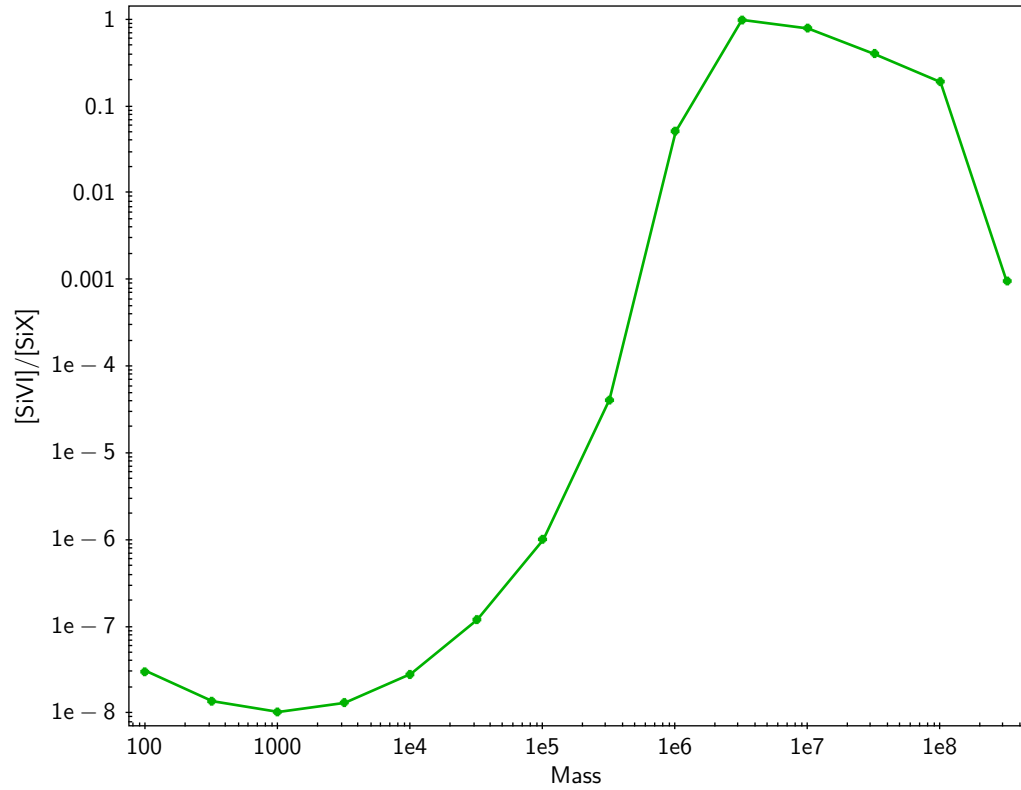


Figure 3.6: Predicted $[\text{Si VI}]_{1.962\mu\text{m}}/[\text{Si X}]_{1.430\mu\text{m}}$ line flux ratios as a function of black hole mass for a gas density of $n_H = 300 \text{ cm}^{-3}$ and an ionization parameter of $\log U = -2.0$. The line ratio has been normalized to 1.0 at its peak.

Chapter 4: Multi-wavelength observations of SDSS J105621.45+313822.1, a broad-line, low-metallicity AGN

The vast majority of active galactic nuclei (AGNs) are found in massive bulge dominated galaxies with gas phase metallicities that are typically super solar [e.g., Storchi-Bergmann et al., 1998, Hamann et al., 2002]. Since the gas phase metallicity is strongly correlated with the galaxy’s stellar mass, low metallicity AGNs are likely to reside in low mass galaxies. The hunt for AGNs in dwarf galaxies has been an active field of research in recent years, since the black hole occupation fraction and mass distribution in the low mass regime place important constraints on models of supermassive black hole (SMBH) seed formation [e.g., Volonteri and Natarajan, 2009, Volonteri and Begelman, 2010, van Wassenhove et al., 2010, Greene, 2012]. However, searches for AGNs in low mass galaxies have yielded only a small fraction of AGNs, all with solar or only slightly sub-solar metallicities. This is a severe limitation, since the premise behind the use of dwarf galaxies to probe seed black holes rests on the assumption that they have had a quiescent cosmic history, free of external factors such as merging or tidal stirring, both of which would drive gas to the center, fueling star formation, enriching the gas, growing a bulge, and potentially fueling the SMBH. For example, in an extensive search of type 2 AGNs using the Sloan Digital Sky Survey (SDSS) Groves et al. [2006] and Barth et al. [2008] found only a small fraction of AGNs residing in low mass hosts, all with either Solar or only slightly sub-Solar metallicities. Similarly, in the recent optical survey of dwarf galaxies by Reines et al. [2013], nearly all of the dwarf galaxies with narrow emission line ratios consistent with AGNs have at least Solar metallicities, consistent with the high metallicity range found for the low mass broad line AGNs identified by Greene and Ho [2007]. While extremely rare, there have been a few low metallicity AGNs reported in the literature. Izotov et al. [2007], Izotov and Thuan [2008], and Izotov et al. [2010] found

evidence for extremely luminous broad line emission consistent with AGNs in a handful of low metallicity dwarf galaxies, most with optical narrow line ratios typical of HII regions, and Schramm et al. [2013] found X-ray evidence for an AGN in several low mass galaxies, one of which is metal deficient, suggesting that low metallicity AGNs do exist. Of these few low metallicity AGNs, extensive multiwavelength observations are thus far lacking in the literature.

Here we present a multi-wavelength study of a low metallicity, broad line AGN, SDSS J105621.45+313822.1 (hereafter J1056+3138), a galaxy which is identified as a QSO broad line object by SDSS DR12, and in past catalogs has been classified as a broad line QSO [D’Abrusco et al., 2009, Richards et al., 2009, Souchay et al., 2012, 2015, Richards et al., 2015] or broad line AGN [Toba et al., 2014, Rakshit et al., 2017]. Based on the MPA/JHU catalog, the galaxy has a redshift of $z=0.161$ and a stellar mass of $10^{9.89} M_{\odot}$, roughly $2.5\times$ the mass of the Large Magellanic Cloud. In Figure 4.1, we plot the location of J1056+3138 on the Baldwin-Phillips-Terlevich (BPT) diagram [Baldwin et al., 1981]. As can be seen, it has one of the lowest $[\text{N II}]/\text{H}\alpha$ emission line ratios, a robust indicator of gas phase metallicity regardless of ionizing radiation field and ionization parameter [Groves et al., 2006], compared to the entire sample of *Swift*/BAT AGNs from the 70 month catalog [Baumgartner et al., 2013], which comprise the most complete sample of hard X-ray (14 to 195 keV) selected AGNs in the local universe. Note that the well known dwarf galaxies with AGNs, NGC 4395 [Filippenko and Ho, 2003] and POX 52 [Barth et al., 2004], both have at least $2 - 10\times$ higher gas metallicities than our target as suggested by their $[\text{N II}]/\text{H}\alpha$ ratios shown in Figure 4.1.

In addition to the identification of broad lines, J1056+3138 displays mid-infrared colors suggestive of an AGN using the all-sky *Wide-field Infrared Sky Explorer (WISE)* and the 3-band demarcation from Jarrett et al. [2011]. In general, low metallicity galaxies tend to be bluer, with relatively few displaying mid-infrared colors $[3.4\mu\text{m}]-[4.6\mu\text{m}]$ (hereafter $W1 - W2$) > 1.0 [Griffith et al., 2011, Izotov et al., 2011]. Those that do show red *WISE* colors tend to reside to the left of region that typically signifies dominant AGNs when

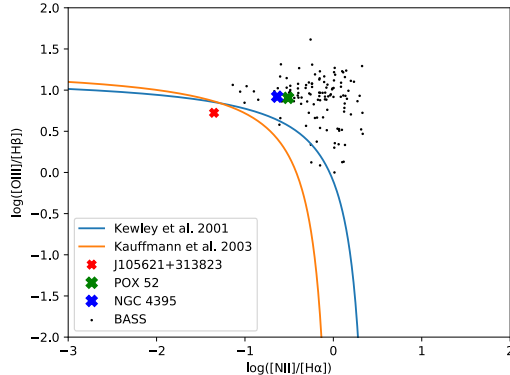


Figure 4.1: BPT diagram comparing J1056+31 (red ‘x’) with the BASS sample [Koss et al., 2017], with the AGN [Kewley et al., 2001] and composite [Kauffmann et al., 2003] demarcation regions in blue and orange respectively. Also plotted are NGC 4395 [blue ‘x’; Filippenko and Ho, 2003] and Pox 52 [green ‘x’; Barth et al., 2004]. Note that J1056+31 is the only target that meets our metallicity selection criteria and displays star-forming ratios.

plotted in $W1 - W2$ vs. $[4.6\mu\text{m}]-[12\mu\text{m}]$ (hereafter $W2 - W3$) space [Jarrett et al., 2011]. As can be seen in Figure 4.2, only $\approx 0.7\%$ of galaxies with similar metallicity to J1056+3138 display mid-infrared colors characteristic of an AGN, further emphasizing the unique nature of this object.

Broad line AGNs with optical narrow line diagnostics consistent with star forming galaxies such as J1056+3138 constitute an extremely rare population. There are only $\approx 5\%$ of broad line AGNs falling in the star-forming region of the BPT diagram according to a recent study by Stern and Laor [2013]. Using the full Max Planck Institut für Astrophysik/Johns Hopkins University (MPA/JHU) catalog of derived galaxy properties for the SDSS data release 8 (DR8), approximately 4% of broad line galaxies have comparable comparable or lower $[N II]/H\alpha$ emission line ratios indicating low gas phase metallicities. Only 1.5% of all broad line AGNs have $\log([N II]/H\alpha)$ ratios less than -1.3, the value for J1056+3138.

This paper is organized as follows. In Section 2, we describe our near-infrared and X-ray observations and data analysis, followed by a description of our results in Section 3. In

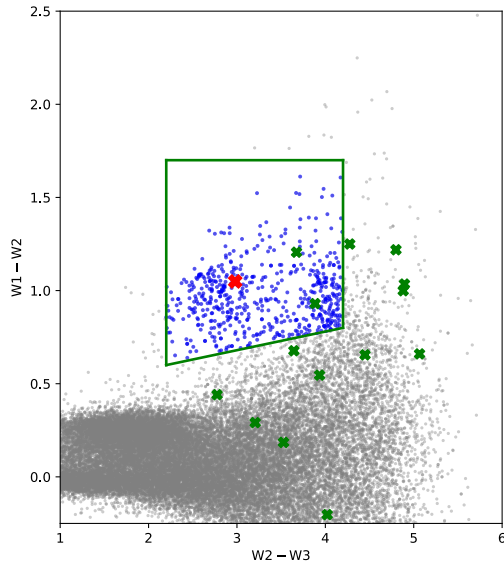


Figure 4.2: Mid-infrared color-color diagram showing the placement of low metallicity galaxies with comparable $\log[\text{N II}]/\text{H}\alpha$ to J1056+3138, as defined by $\log[\text{N II}]/\text{H}\alpha \leq -1.3$ using emission line fluxes from the MPA catalog. The box corresponds to the Jarrett et al. [2011] demarcation region.

Grey points correspond to galaxies that would not be identified as potential AGN using the strict Jarrett et al. [2011] color cut, and blue points denote galaxies that would be characterized as potential AGN. The location of J1056+3138 is marked with a red ‘X’ and locations of other published low metallicity galaxies are marked with green ‘X’s [Thuan and Izotov, 2005, Izotov et al., 2007, Izotov and Thuan, 2008, Izotov et al., 2012].

Section 4, we discuss our results, and summarize our findings in Section 5.

We adopt a standard Λ CDM cosmology with $H_0 = 70 \text{ km s}^{-1} \text{ Mpc}^{-1}$, $\Omega_M = 0.3$, and $\Omega_\Lambda = 0.7$.

4.1 Methodology

4.1.1 NIR Observations and Data Reduction

We obtained near-infrared observations of J1056+3138 using the Near-Infrared Spectrograph [NIRSPEC; McLean et al., 1998] on the Keck II telescope on 2018 March 5, with a total exposure time of 32 minutes. These observations were carried out using the low resolution mode with a slit width of $0.76''$ and a slit length of $42''$ to provide a resolution of $R \approx 1400$. We used the filter NIRSPEC-7 for a wavelength coverage of $1.839 - 2.630 \mu\text{m}$. Observations were done using an ABBA pattern, nodding along the slit. This target was observed under clear weather conditions, with $\sim 0.''5$ seeing. A telluric standard (A0V) was observed immediately after at similar air mass.

The data reduction was carried out using a modified version of LONGSLIT_REDUCE¹ for Keck NIRSPEC, and REDSPEC². These packages followed the standard steps for IR spectral data reduction, including flat fielding, sky subtraction, wavelength calibration, spectral extraction, and telluric correction. Flux calibration was done in Python by estimating the flux of the telluric A0V star through its K-band magnitude and scaling the spectrum by this flux. A small corrective factor ($< 5\%$) was included due to the wavelength difference between the center of K-band and that of the wavelength coverage used. Line fluxes and uncertainties were determined from best-fit Gaussian models to the emission lines using a custom Bayesian maximum-likelihood code implemented in Python using the affine-invariant Markov Chain Monte Carlo (MCMC) ensemble sampler *emcee* [Foreman-Mackey et al., 2013].

¹http://www.astro.caltech.edu/~gdb/nirspec_reduce/nirspec_reduce.tar.gz

²<https://www2.keck.hawaii.edu/inst/nirspec/redspec.html>

4.1.2 Optical Observations and Analysis

This object was observed twice by SDSS, once on 2004 May 12 with the SDSS spectrograph and once on 2013 March 18 with the BOSS spectrograph [Dawson et al., 2013]. Aside from the emergence of a [Fe VII]5722 emission line in the 2013 that was not visible in 2004, these two spectra are nearly equivalent, with consistent broad and narrow line fluxes within photometric uncertainties, so the remainder of the paper will analyze the 2013 spectrum as it has the higher signal-to-noise. We analyzed this spectrum in order to compare broad line fluxes and widths to our near-IR observations. Optical spectral decomposition was performed on the SDSS spectrum using *emcee* [Foreman-Mackey et al., 2013] as done by Sexton et al. [2019]. For the $H\beta/[O\ III]$ region, we fit the region from restframe 4400 - 5800Å, which includes the Mg 1b region used to estimate stellar velocity dispersion. All emission lines are modeled using Gaussians, with narrow-line FWHM and velocity offsets tied during the fitting process. For the $H\alpha/[N\ II]$ region, we fit the region from restframe 6200 - 7000Å. The lack of prominent stellar absorption features in this region prevents us from using stellar template fitting, and thus the continuum is fit using only the power-law component, with amplitude and power-law index as free parameters. As with the near-IR data, line fluxes and uncertainties were determined using best-fit Gaussian models.

4.1.3 X-ray Observations and Data Reduction

Chandra observations of this target were taken on 20 October 2019 in Cycle 19. Data was taken with the ACIS-S instrument, with an exposure time of 16 ks, and pointed with the target centered at the aimpoint of the S3 chip. The data was reduced and analyzed using the *Chandra* Interactive Analysis of Observations (CIAO) data package v4.11 and the Chandra Calibration Database v4.8.2 (CALDB). After reprocessing and filtering the event file into full (0.3 – 8 keV), soft (0.3 – 2 keV), and hard (2 – 8 keV) energy bands, we used the DMEXTRACT module to extract the source counts from a 1.5'' radius aperture centered on the source position. Background counts were extracted from a 25'' radius aperture in

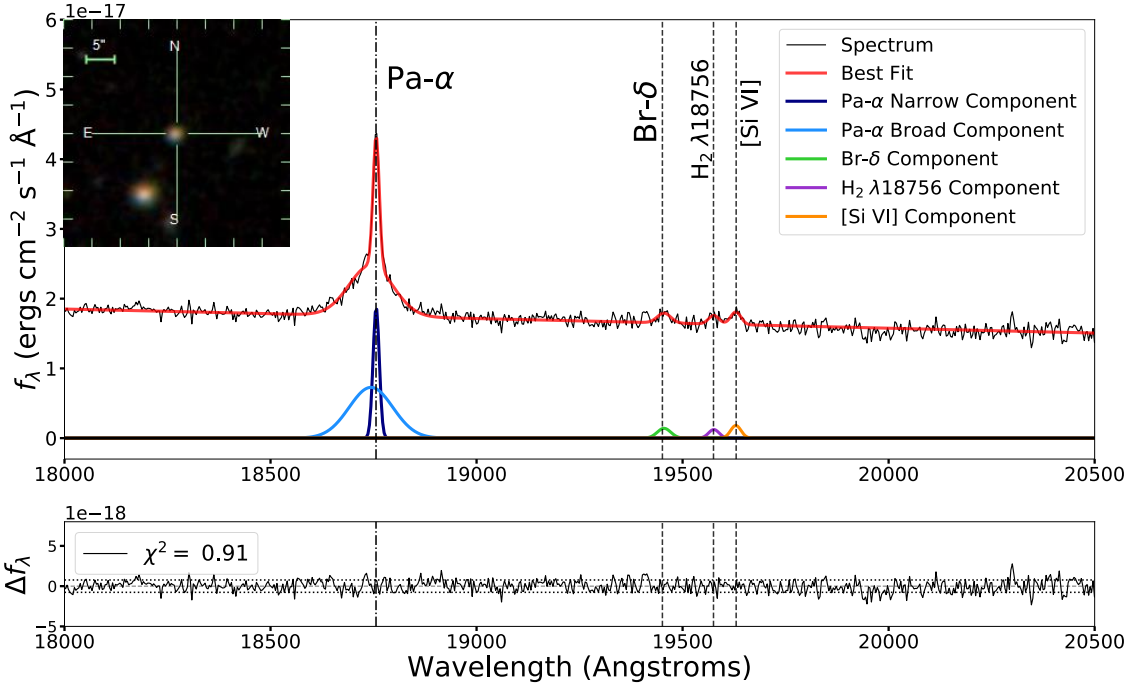


Figure 4.3: K-band spectra from Keck NIRSPEC of J1056+3138. Note that this galaxy displays a prominent broad Pa α line and the [Si VI] coronal line, as well as Br δ and H $_2$ lines. An SDSS *gri* color composite image is also displayed, showing its compact morphology.

the vicinity of the source and in an area free of other sources. Due to the low count nature of this source, we use binomial statistics, using the Gehrels [1986] approximation to account for the error in the source counts, where the upper bound is given by $1 + \sqrt{x + 0.75}$, the lower bound by $\sqrt{x - 0.25}$, and x is the number of counts detected. All X-ray fluxes and luminosities quoted hereafter are derived from background-subtracted counts.

4.2 Results

4.2.1 Near-infrared and Optical Spectra of J1056+31

The near-infrared *K*-band spectrum of J1056+31 can be found in Figure 4.3. Most notably, this target contains a 3.3σ [Si VI] detection, with a flux of $(5.69 \pm 1.75) \times 10^{-17}$ erg cm $^{-2}$ s $^{-1}$

Table 4.1: Near-IR (Keck NIRSPEC) emission line fluxes. Broad lines are identified by “br.”

Line	Wavelength Å	Flux 10^{-17} erg cm $^{-2}$ s $^{-1}$
Pa α	18756	35.90 ± 1.73
br. Pa α	18756	96.72 ± 5.78
Br δ	19451	5.60 ± 1.85
H $_2$	19576	3.86 ± 1.28
[Si VI]	19628	5.69 ± 1.75

(Figure 4.4). As Si VI has an ionization potential of 167 eV, even the hottest, most massive stars do not produce enough high energy ionizing radiation required to produce this ion (Satyapal et al. 2020, in prep).

The SDSS optical spectrum is shown in Figure 4.5. Coronal lines were observed in both the SDSS and Keck observations. The SDSS observations showed [Fe VII] λ 5722 and [Fe VII] λ 6085 emission lines, and [Ne V] λ 3425 and [Ne V] λ 3345 lines. These are the most ubiquitous optical coronal lines, which have been widely seen in AGN [e.g. Appenzeller and Wagner, 1991, Vergani et al., 2018, Yan et al., 2019]. Note that the ionization potentials of Fe VII and Ne V are 99 eV and 97 eV, respectively, significantly less than the ionization potential of Si VI. Fluxes for these lines can be found in Table 4.1 for the [Si VI] and Table 4.2 for the optical lines. Note that the luminosity of the [Si VI] line is 3.18×10^{39} erg s $^{-1}$, well within the range of luminosities of the well-studied AGN from Müller-Sánchez et al. [2018], Lamperti et al. [2017], which range from $5.9 \times 10^{36} - 3.9 \times 10^{41}$ erg s $^{-1}$. The [Fe VII] and [Ne V] lines in J1056+3138 have luminosities of $\approx 10^{40}$ erg s $^{-1}$, comparable to those observed in other AGN samples, with luminosities ranging from $10^{39} - 10^{42}$ erg s $^{-1}$ [Malkan, 1986, Morris and Ward, 1988, Storchi-Bergmann et al., 1995].

As can be seen in Figure 4.3, the spectra also contains a broad Pa α line with a flux of $(35.90 \pm 1.73) \times 10^{-17}$ erg cm $^{-2}$ s $^{-1}$ and a width of 850 ± 25 km s $^{-1}$. A Br δ and H $_2$ line were also detected. Fluxes for all infrared lines can be found in Table 4.1. While its optical narrow emission lines placed the object in the “star-forming” region of the BPT diagram

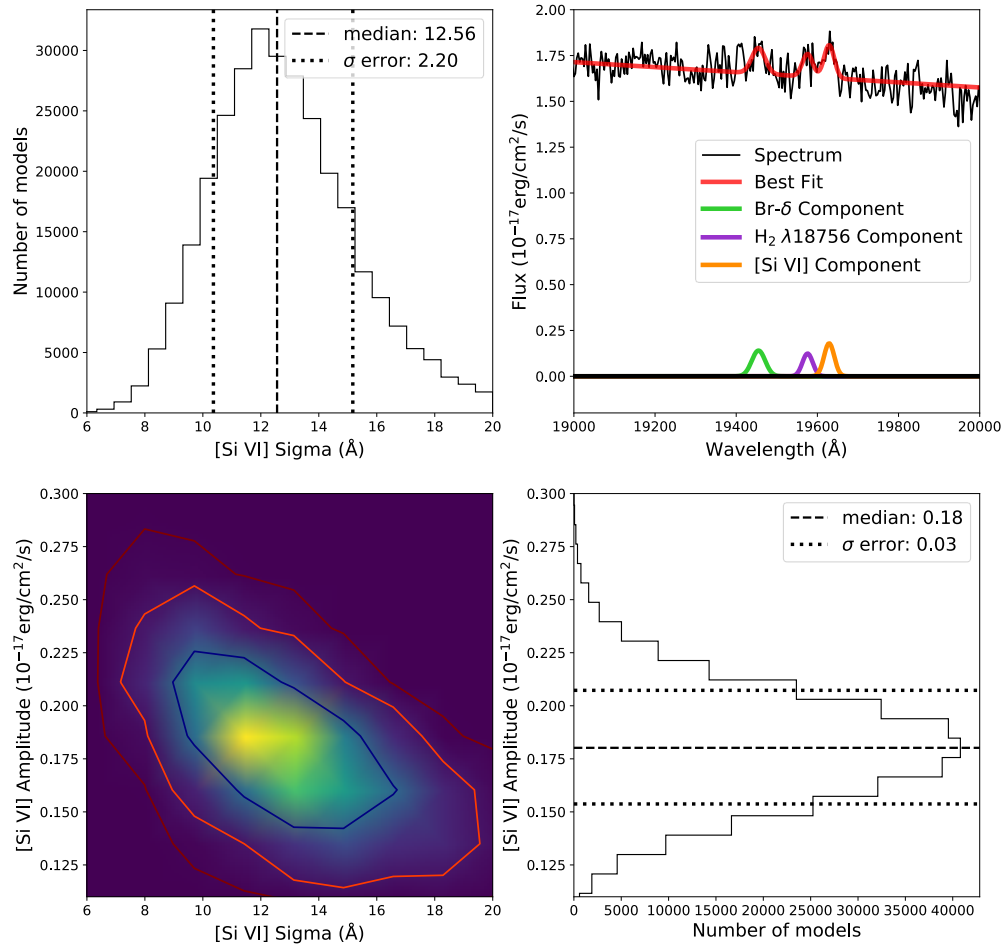


Figure 4.4: Upper Right: The detected [Si VI] emission line, as well as nearby Br δ and H $_2$ lines. Lower Left: A heat map showing the output of the *emcee* fits for the amplitude and width of the Gaussian for the [Si VI] detection in J1056+3138. The contour levels show the σ intervals up to 3σ , and the histograms (upper left and lower right) show the distribution of potential fits for the width (upper left) and amplitude (lower right) of the Gaussian. As can be seen, the solution converged very well, proving a robust detection.

(see Figure 4.1), J1056+3138 showed a broad H α line, as well as [Fe VII] λ 5722, 6085 and [Ne V] λ 3425, 3345 coronal lines, as can be seen in Figure 4.5. While broad lines and coronal lines can be indicative of an AGN, their presence in a BPT star-forming galaxy can often be due to supernova activity, which fades over time [Baldassare et al., 2016]. The first observation of J1056+3138 was taken on 2004 May 12, and our Keck observations took place on 2018 Mar 5. There is a 14 year baseline between these two observations, so we can explore if there is any fading of the broad lines, which would be indicative of a stellar origin to the broad line rather than an AGN. We compared the extinction corrected optical broad line flux to the broad Pa α flux. The theoretical H α /Pa α ratio, assuming Case B recombination, is 8.5 [Osterbrock and Ferland, 2006]. The observed value is 6.0 ± 0.1 , implying negligible extinction toward the ionized gas, and demonstrating that there is no fading of the recombination line flux over a 14 year baseline, ruling out the possibility that the broad lines are due to supernova activity. Since we have multiple recombination lines, we also estimated the extinction using the Pa α and Br δ lines. Using the observed ratio of these fluxes, we find an $A_V < 1$, assuming a Milky Way-like extinction curve ($R_V=3.1$), again implying that there is no fading in recombination line fluxes between the SDSS and near-infrared observations.

4.2.2 X-ray Results

We detected an X-ray point source coincident with the SDSS optical source with an apparent luminosity, uncorrected for intrinsic absorption, of $L_{X, 2-10 \text{ keV}} = (2.3 \pm 0.9) \times 10^{41}$ erg s $^{-1}$, with six counts combined in both hard and soft bands. Due to the low number of counts, we explored the binomial no-source probability of the detection, P_B , which is proportional to the probability that the measured counts are due to spurious background activity (see Weisskopf et al., 2007, Lansbury et al., 2014 for the mathematical expression for this statistic). Adopting the requirement that real sources (not due to background activity) satisfy a threshold of $P_B < 0.002$ [Satyapal et al., 2017], and noting that the X-ray source yields a no-source probability of $\log(P_B) \sim -6.4$, we conclude that the X-ray source is

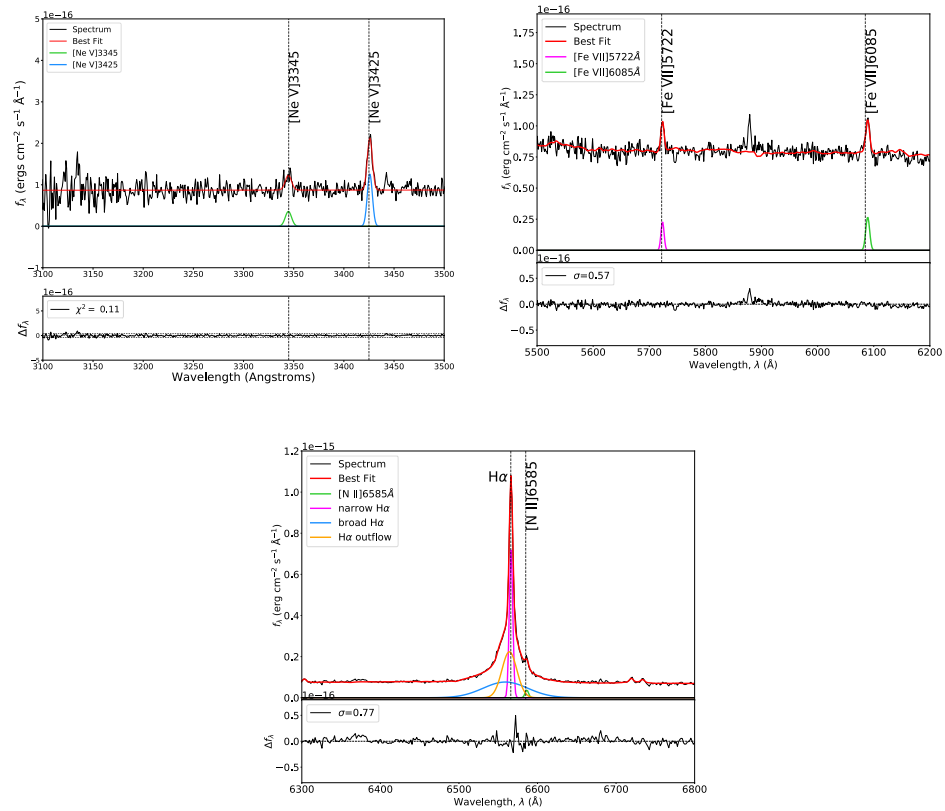


Figure 4.5: Optical spectra from SDSS of J1056+3138. The top panel displays the fits for the [Ne V] λ 3345, 3425 coronal lines. The center panel displays the fit for the [Fe VII] λ 5722, 6085 coronal lines. The bottom panel displays the fit for the broad H α .

Table 4.2: Optical SDSS emission line fluxes. Broad lines are identified by “br.”

Line	Wavelength Å	Flux 10^{-17} erg cm $^{-2}$ s $^{-1}$
[Ne V]	3345	28.2 ± 11.4
[Ne V]	3426	79.2 ± 9.9
[O III]	4363	65.2 ± 2.8
H β	4861	82.7 ± 3.4
br. H β	4861	281.6 ± 9.0
[O III]	4959	135.0 ± 4.9
[O III]	5007	407.4 ± 14.7
[Fe VII]	5722	16.0 ± 1.8
[Fe VII]	6085	23.9 ± 2.3
[O I]	6300	10.3 ± 3.0
[N II]	6549	7.0 ± 0.7
H α	6563	404.5 ± 10.8
br. H α	6563	578.3 ± 13.1
[N II]	6583	20.5 ± 2.1
[S II]	6717	10.8 ± 1.8
[S II]	6730	7.6 ± 1.4

unlikely to be due to spurious background activity. The typical $L_{2-10\text{keV}}$ threshold generally adopted by the community to unambiguously identify an AGN is 10^{42} erg s $^{-1}$ [Zezas et al., 2001, Ranalli et al., 2003, Wang et al., 2013]. While the X-ray luminosity for J1056+3138 is somewhat higher than seen in star forming galaxies, Brorby et al. [2014] find that the X-ray emission produced for a given SFR is approximately an order of magnitude larger than that found in near solar metallicity galaxies (see also Kaaret et al. [2011]). Further, Prestwich et al. [2013] also show that ULXs are more common in low metallicity systems, adding further to the ambiguity of the origin of the X-ray emission in J1056+3138 and making an AGN identification by this observed X-ray luminosity alone tentative.

The observed luminosity is two orders of magnitude lower than what is expected from the $L_X - L_{12\mu\text{m}}$ relation ($\approx 10^{43}$ erg s $^{-1}$) [Secret et al., 2015]. Taking the relation between [Si VI] and L_X from Lamperti et al. [2017], an estimate of $L_X \approx 10^{43}$ is calculated, also two

orders of magnitude above the detected luminosity. These discrepancies strongly suggest that the source is heavily obscured along the line of sight. An estimate for N_H was calculated based on the relation determined in Pfeifle et al. 2020 (in prep) using $12\mu\text{m}$ luminosity data from *WISE* and X-ray data from the *BASS* Survey, which provides $N_H \approx (7\pm 2)\times 10^{24} \text{ cm}^{-2}$.

We compared this discrepancy between the X-ray and mid-IR luminosities to other similar targets in the MPA-JHU catalog in Figure 4.6, where we've plotted the L_X/L_{W2} of various mid-IR selected AGNs compared to broad line AGNs with low metallicity and J1056+3138 compared with their $\log([\text{N II}]/\text{H}\alpha)$. Of the low metallicity galaxies with broad line AGNs, J1056+3138 has the lowest X-ray luminosity when compared to its W2 luminosity. This apparent deficit in X-ray radiation is in agreement with other X-ray studies done on low metallicity galaxies, where it is found that X-ray luminosities tend to be one to two orders of magnitude below that expected from multi-wavelength diagnostics, due either to obscuration of the X-ray emission or an intrinsic X-ray weakness [Simmonds et al., 2016]. This could possibly be due to the lack of an emitting corona, which may be characteristic of a few broad absorption line (BAL) quasars and ultra-luminous infrared galaxies [Luo et al., 2014, Teng et al., 2015]. In addition for low-mass cases, Dong et al. [2012a] find several AGNs in low mass galaxies that appear to be X-ray weak, possibly due to potential changes in the accretion disk temperature or structure which would impact the fraction of the disk energy that is reprocessed into a corona. This is supported by the low $L_{X,2-10 \text{ keV}}$ vs. $L_{[\text{O III}]}$ ratio of several low mass galaxies in their sample. In J1056+3138, however, the $[\text{O III}]$ emission is dominated by star formation, complicating the interpretation of the relationship between these luminosities in this source. It is also possible that there is a different dust-to-gas ratio in this galaxy, potentially affecting the relationship between X-ray absorption and extinction by dust of the broad line region [Groves et al., 2006]. Further, as the *WISE* and *Chandra* observations were not simultaneous, with a 9 year separation between the observations, it is also possible that variability could play a role in this discrepancy, although based on typical flux changes, it may not be able to account for the anomalous ratio found for J1056+3138 [Maughan and Reiprich, 2019, Sheng et al.,

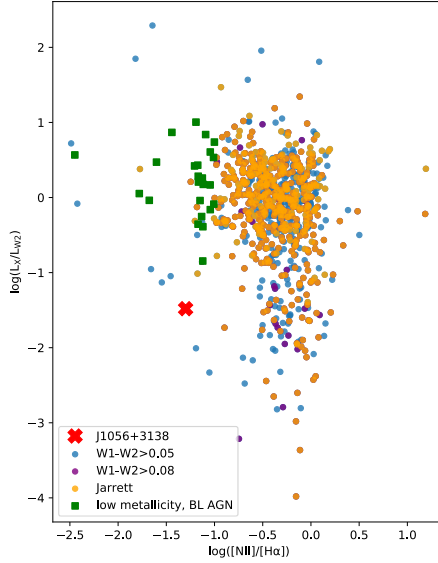


Figure 4.6: L_X/L_{W2} compared with metallicity diagnostic $[\text{N II}]/\text{H}\alpha$ for galaxies in the MPA-JHU catalog (DR8) that show mid-infrared colors suggestive of AGN activity based on three color cuts: $W1-W2 > 0.5$ (blue), $W1-W2 > 0.8$ (purple), and the Jarrett et al. [2011] cut (orange). Galaxies with optical broad lines and $[\text{N II}]/\text{H}\alpha$ ratios that fall below the low metallicity cut-off ($\log([\text{N II}]/\text{H}\alpha) < -1.0$) are shown as green squares, and J1056+3138 is shown as a red ‘X’. Note that J1056+3138 has the lowest L_X/L_{W2} ratio when compared to similar galaxies.

2017]. Due to its low X-ray luminosity, whether due to obscuration, variability, or an inherent X-ray weakness, J1056+3138 would not have been confirmed as an AGN through X-ray follow-up, showing the necessity for multi-wavelength studies when dealing with low mass and low metallicity galaxies. If even a very powerful AGN can be hidden in the X-rays, many more less powerful and low luminosity AGNs may be hiding inside low metallicity dwarf galaxies.

4.2.3 Black Hole Mass and Luminosity Estimates

Black hole masses were calculated using the widths of the broad H α [Woo et al., 2015] and Pa α [Kim et al., 2018] lines. The broad Pa α has a width of $850 \pm 25 \text{ km s}^{-1}$, corresponding to a black hole mass of $(2.2 \pm 1.3) \times 10^6 M_{\odot}$, or $10^{6.4} M_{\odot}$, which was obtained with Equation 10 in Kim et al. [2018]. In this relation, they used the new virial factor $\log f = 0.05 \pm 0.12$ that was derived in Woo et al. [2015]. The broad H α has a width of $1129 \pm 21 \text{ km s}^{-1}$, corresponding to a black hole mass of $(3.4 \pm 1.4) \times 10^6 M_{\odot}$, or $10^{6.5} M_{\odot}$, which was obtained using Equation 5 in Woo et al. [2015].

We estimated the bolometric luminosity of $\approx 10^{44} \text{ erg s}^{-1}$, however there is considerable scatter in the $L_{[\text{Si VI}]}$ vs. $L_{14-195\text{keV}}$ relation reported in Lamperti et al. [2017] with a number of upper limits in their sample. We used a $L_{14-195\text{keV}}/L_{\text{bol}}$ factor as reported in Winter et al. [2012]. We used the [Si VI] to estimate a bolometric luminosity since the [O III] emission is likely dominated by star formation and cannot be used to obtain a bolometric luminosity as is often done in optically identified AGNs. This luminosity, along with the Eddington luminosities calculated from the mass estimates, implies a high Eddington rate, $L/L_{\text{Edd}} \approx 0.3$. These Eddington ratios are similar to those reported in Greene and Ho [2007] and suggest that this is a highly accreting black hole.

4.3 Discussion

4.3.1 Coronal Lines

While coronal lines have often been used as a robust AGN indicator, there is the possibility that these lines arise in star forming regions. In principle, Wolf-Rayet stars and shock excitation in starburst driven winds can generate broad lines and even high ionization lines [Schaerer and Stasińska, 1999, Abel and Satyapal, 2008, Allen et al., 2008]. Since the hardness of the stellar radiation field increases with decreasing metallicity [Campbell et al., 1986], enhanced emission from lines corresponding to higher ionization potentials is

expected for metal deficient galaxies. High ionization lines have indeed been detected in H II regions in blue compact dwarfs and planetary nebulae [Feibelman, 1996, Fricke et al., 2001, Thuan and Izotov, 2005, Izotov et al., 2012] with a detection rate that appears to be correlated with decreasing metallicity [Izotov et al., 2012]. However, the line luminosities are weaker than those found in AGN, by up to four orders of magnitude [Izotov et al., 2012], and the emission line fluxes are weak compared to the recombination line fluxes. For example, Thuan and Izotov [2005] and Izotov et al. [2012] finds [Ne V] emission in ten HII regions in blue compact dwarfs (BCDs), with ratios that range from 0.005 – 0.03 for [Ne V] λ 3345/H β and from 0.003 – 0.005 for [Ne V] λ 3425/H β , 3 orders of magnitude below what is found in J1056+3138. Izotov et al. [2001, 2004] also find [Fe VII] emission in two blue compact dwarf galaxies, with ratios of ≈ 0.001 for [Fe VII] λ 5722/H β and $\approx 0.0002 - 0.002$ for [Fe VII] λ 6085/H β , 2-3 orders of magnitude below what is found in J1056+3138. Note that the [Fe VII] and [Ne V] lines in J1056+3138 have luminosities of $\approx 10^{40}$ erg s $^{-1}$, comparable to those observed in other AGNs, with luminosities ranging from $10^{39} - 10^{42}$ erg s $^{-1}$ [Malkan, 1986, Morris and Ward, 1988, Storchi-Bergmann et al., 1995], as is the case for the [Si VI] line as discussed in Section 4.2. Moreover, while the optical coronal lines have been detected in H II regions and BCDs that may not host AGNs, the ionization potential of Si VI (167 eV) is significantly higher than that of Fe VII or Ne V and is only created in very extreme conditions when not in the presence of an AGN. Note that this line has been seen in planetary nebulae and Galactic supernovae, but its luminosity is eight orders of magnitude lower than that of J1056+3138 and other AGNs [Ashley and Hyland, 1988, Benjamin and Dinerstein, 1990, Greenhouse et al., 1990], making these sources undetectable outside of the Milky Way. Thus far, there is no evidence of any coronal line with ionization potential above ≈ 100 eV in a purely star-forming galaxy, making it highly implausible that star formation is responsible for the coronal lines detected in J1056+3138.

4.3.2 Metallicity Estimates

Current studies of metallicity estimation assume an SED that is either primarily AGN or stellar in origin. As J1056+3138 hosts an AGN, yet displays star-forming colors and has a strong stellar component, determining a precise SED, and thus a precise estimate of abundances is extremely difficult. However, an initial estimate is calculated using the diagnostics determined by photoionization simulations and tested on low metallicity dwarf galaxies, including those with AGNs [Izotov et al., 2006, 2007, Izotov and Thuan, 2008]. This metallicity estimate uses variables t , temperature $T_e(\text{O III})$, C_T , and x as defined by

$$t = \frac{1.432}{\log [\lambda 4959 + \lambda 5007 / \lambda 4363] - \log C_T} \quad (4.1)$$

$$t = 10^{-4} T_e(\text{O III}) \quad (4.2)$$

$$C_T = (8.44 - 1.09t + 0.5t^2 - 0.08t^3) \frac{1 + 0.0004x}{1 + 0.044x} \quad (4.3)$$

$$x = 10^{-4} N_e t^{-0.5} \quad (4.4)$$

where the density, N_e , is 10 [Izotov et al., 2007], as well as emission lines [O III]5007, [O III]4959, [O II]3726, and $\text{H}\beta$. The abundances are then derived using the following:

$$12 + \log \text{O}^+ / \text{H}^+ = \log \frac{\lambda 3727}{\text{H}\beta} + 5.961 + \frac{1.676}{t} - 0.40 \log t - 0.034t + \log(1 + 1.35x) \quad (4.5)$$

$$\begin{aligned}
12 + \log \text{O}^{2+}/\text{H}^+ &= \log \frac{\lambda 4959 + \lambda 5007}{\text{H}\beta} + 6.200 \\
&+ \frac{1.251}{t} - 0.55 \log t - 0.014t
\end{aligned}
\tag{4.6}$$

Considering a value of $12 + \log(\text{O}/\text{H})$ of 8.69 for Solar [Groves et al., 2006, Asplund et al., 2006], these relations provide a metallicity estimate for J1056+3138 of approximately 10% Solar. This is in agreement with our initial $[\text{N II}]/\text{H}\alpha$ cutoff criteria.

4.3.3 Implications

The multi-wavelength study of J1056+3138 has broad astrophysical implications for our understanding of the origins of supermassive black holes. J1056+3138 is in one of the lowest metallicity galaxies known to contain an AGN, and it is one of the lowest metallicity, low mass galaxies to show a high ionization infrared coronal line. While it is a broad line AGN with strong coronal lines in the optical, its BPT line ratios suggest the dominant emission is stellar in origin. While mid-infrared color selection picks it out as a dominant AGN, with a bright $\text{Pa}\alpha$ and strong $[\text{Si VI}]$ coronal line in its K band spectrum, it is barely visible when searching for an X-ray point source, and it would easily be mistaken for X-ray binaries, if it was detected at all. The results presented here strongly support that low mass accreting black holes exist in galaxies that show no evidence for AGNs using traditional diagnostics, such as X-ray detections and BPT line ratios, calling into question the current occupation of fraction of AGNs in the low mass and low metallicity regime and highlighting the importance of multi-wavelength studies to obtain a complete census of AGNs in the low mass, low metallicity regime.

Using SDSS and the *WISE* survey, there are ~ 1500 low mass ($M_* < 10^{10.5} M_\odot$), low metallicity ($\log(\text{N II}/\text{H}\alpha)$) galaxies with infrared colors suggestive of AGN, many of which have stellar masses as low as $10^6 M_\odot$. These are prime candidates for follow-up with the

James Webb Space Telescope (JWST) to search for accreting intermediate mass black holes. None of these galaxies show optical emission line ratios indicative of AGNs, underscoring the limitations of optical studies in the search for accreting black holes in galaxies that may be truly more representative of the local analogs of early galaxies. Currently, there is no direct evidence for black holes with masses anywhere between $\approx 100 - 10,000 M_{\odot}$. This technique can be a powerful avenue in which black holes in this “mass desert” can finally be discovered using future high sensitivity *JWST* observations [Cann et al., 2018]. While coronal lines were also seen in the SDSS spectrum of J1056+3138, the predicted fluxes of optical coronal lines are a factor of at least 5 times less than the infrared coronal lines even in the absence of any extinction (Cann et al. 2020, in prep). The infrared coronal line fluxes are also enhanced when the black hole mass decreases, highlighting the need for infrared spectroscopic observations in the hunt for intermediate-mass black holes [Cann et al., 2018].

4.4 Conclusions

We present a multi-wavelength study of J1056+3138, a low metallicity, broad line AGN, including observations from *Chandra*, *Keck/NIRSPEC*, *WISE* and *SDSS*. Our main results can be summarized as follows:

1. In its *SDSS* spectrum, J1056+3138 displays optical emission line ratios suggestive of a purely star-forming galaxy, despite strong optical broad lines and four optical coronal lines, [Ne V]3345,3425 and [Fe VII]5722,6085.
2. Observations with *WISE* show J1056+3138 to have mid-infrared colors suggestive of a strong AGN, despite only $\approx 0.7\%$ of similarly low metallicity galaxies residing in the same color-color space.
3. K-band observations with *Keck/NIRSPEC* revealed a broad Pa α line that, when its width and luminosity are compared to that of the broad H α , implies negligible extinction. These observations also showed a [Si VI] coronal line, making J1056+3138 the lowest metallicity galaxy to show this line.

4. *Chandra* observations detected an X-ray point source coincident with the SDSS optical source, but at an observed luminosity of only $\approx 10^{41}$ erg s $^{-1}$, two orders of magnitude below that expected based on its mid-infrared luminosity. This discrepancy implies the source is either heavily obscured, with an $N_H \approx (7 \pm 2) \times 10^{24}$ cm $^{-2}$, or inherently X-ray weak. While the presence of optical and infrared broad lines implies a lack of obscuration, a clumpy torus could obscure the X-ray radiation while still showing broad lines.
5. Black hole mass estimates were calculated using the widths of the broad H α and Pa α lines. Estimates ranged from $2.2 - 3.4 \times 10^6 M_\odot$, implying this AGN is fairly massive despite its low metallicity.

Our results highlight the need for a multi-wavelength approach to truly characterize the source of ionization in this population.

Chapter 5: Future Work

5.1 Chapter Overview

This chapter will provide an overview of the next set of projects to further the research presented here.

5.2 Model Validation using Gemini

While the power of infrared coronal lines in estimating the mass of an AGN has been theoretically shown in our CLOUDY models, there has been no dedicated NIR spectroscopic study of AGNs with masses below $\approx 10^6 M_\odot$. As this is the region where the coronal line emission is expected to change dramatically, this is a necessary study to validate the model predictions reported in Chapter 3.

To address this deficiency, we select targets from the Greene and Ho [2007] and Reines et al. [2013] catalogs to observe with the Gemini Near-InfraRed Spectrometer (GNIRS). These are broad line AGNs with robust mass determinations with $M_{BH} < 2 \times 10^6$. For this pilot study, we set an upper mass limit of $10^{5.5} M_\odot$, and selected sources that display BPT line ratios that fall into the “composite” or “star-forming” region of the BPT diagram. We have also included RGG 118, which at $50,000 M_\odot$ is the lowest mass black hole known to date [Baldassare et al., 2015]. As all of these targets fall out of the traditional AGN region on the BPT diagram, they are precisely the targets expected to display a dramatic transition in coronal line ratios as predicted by our models for this mass range. Note that because these are confirmed AGNs with broad lines, the absence of coronal lines itself would be interesting and very unexpected, given that at lower black hole masses, the coronal lines are expected to be enhanced.

GNIRS is the ideal instrument for this study, as the cross-dispersed mode will provide access to several coronal lines from $0.8 - 2.5\mu\text{m}$ at high sensitivity, allowing for an in-depth study of many different coronal line ratios reported as potentially diagnostic in Cann et al. [2018]. These observations will require the ability to detect the [Si VI] line at a sensitivity of $\approx 1e - 16 \text{ erg cm}^{-2} \text{ s}^{-2}$ at a S/N of 20 when compared to the relationship between [Si Roman6] detections and W2 fluxes in the literature [Riffel et al., 2006, Rodríguez-Ardila et al., 2011, Lamperti et al., 2017, Müller-Sánchez et al., 2018]. As these black holes are at a lower mass, and the coronal lines are expected to be enhanced, this is a conservative estimate for predicted flux. The results of this study will provide valuable insight on the results from Chapter 3 and will be necessary groundwork for planning observations with *JWST*.

5.3 The Hunt for Intermediate Mass Black Holes in Low Metallicity Dwarf Galaxies

5.3.1 Ground-based

Since SMBHs in massive bulge-dominated galaxies have undergone significant accretion through multiple dynamical interactions over cosmic history, any information on the original seed population will be erased. While optical emission lines have been used to search for AGNs in dwarf galaxies [e.g., Reines et al., 2013], most may be dominated by star formation regions, severely limiting the diagnostic power of optical surveys in determining the true fraction of dwarf galaxies hosting SMBHs. This is a severe limitation, since the premise behind the use of dwarf galaxies to probe seed black holes rests on the assumption that they have had a quiescent cosmic history, free of external factors such as merging or tidal stirring, which would drive gas to the center, fueling star formation, enriching the gas, increasing the Sérsic index, and potentially fueling the SMBH.

To address this, I have begun a pilot study using *Keck*, *Gemini*, and *LBT* to search for near-infrared coronal lines in low metallicity dwarf galaxies with mid-infrared photometric

colors indicative of either AGN activity or extreme star formation. My diagnostic for low metallicity is the optical emission line ratio $\log([\text{N II}]/\text{H}\alpha) < -1.0$ using values reported in the MPA-JHU catalog from the *Sloan Digital Sky Survey (SDSS)*, which corresponds to when the gas phase metallicity is less than approximately 10% Solar regardless of ionization parameter [Groves et al., 2006]. This results in a sample of 20 galaxies which are bright enough to be detected using existing ground-based facilities, with ≈ 1500 more available by space-based instrumentation, such as the future *James Webb Space Telescope (JWST)*. Through collaborators Barry Rothberg at *LBT* and Gabriela Canalizo at University of California - Riverside, I have access to guaranteed time at *LBT* and *Keck* for this project, along with time already awarded through proposals at *Gemini* and *Keck* through NOAO and NASA, respectively. A paper on a pilot study object has been accepted to ApJ to test coronal line visibility in a low mass, low metallicity galaxy, and observations have already begun for our full sample, expected to be completed in Spring 2021. Targets that show coronal line emission suggestive of an IMBH of mass $< 10^{5.5}M_{\odot}$ will be prime targets for multi-wavelength study to understand their accretion and host galaxy properties in more detail, with observatories such as *Hubble Space Telescope*, *Chandra*, *NuSTAR*, and the *Very Large Array (VLA)*.

5.3.2 JWST

While observations from ground-based telescopes as highlighted above can detect signs of an accreting IMBH in nearby galaxies, the launch of the *James Webb Space Telescope* will offer unprecedented sensitivity and the ability to observe wavelengths that are hidden by atmospheric emission and absorption on the ground. Without the limitations from the ground, we will be able to observe even fainter sources, and a window will be opened into the mid-infrared, where models suggest the coronal lines will be brighter by several orders of magnitude than in the near-infrared, even without counting effects from extinction (Satyapal et al. 2020, in prep). With these advantages, *JWST* will prove pivotally important in unearthing the most elusive IMBHs hidden in low metallicity dwarf galaxies.

5.4 XMM

With the advent of *eROSITA*, the scientific community will have an all-sky X-ray survey expected to be $20\times$ more sensitive than current instruments in the 0.5-2 keV (“soft”) band, and for the first time ever in the 2-10 keV (“hard”) band. This will allow for massive statistical studies of dimmer and more distant X-ray sources than ever before. This could potentially unearth a population of low metallicity and low mass AGNs heretofore unknown, however the X-ray luminosities of AGNs in this regime are often low and indistinguishable from stellar sources (e.g. Fragos et al 2013). An in-depth, multi-wavelength study of this regime, such as the one I did on J1056+3138 in Cann et al. (2020), is needed to truly constrain the occupation fraction of low mass, low metallicity AGNs with the upcoming data.

As *XMM-Newton* has been taking observations across the sky for over 20 years with a field of view of $30'$, it has a vast archive of observations. I have compiled a sample of low metallicity galaxies as defined in the previous section, with masses less than $M_* < 10^{10.5}M_\odot$ at redshifts $z < 0.1$. Of those observed by *XMM*, whether targeted or serendipitous, 11 have mid-infrared colors suggestive of an AGN using the Jarrett et al. (2011) *WISE* color cut, and 14 and 56 galaxies fit the AGN mid-infrared color cuts of $W1 - W2 > 0.8$ and 0.5 respectively. We find a total of 139 observations overlapping with our sample of 56 galaxies. Through a specially developed pipeline (Secret, et al. 2020) that reduces and optimally stacks the images based on statistical calculations of signal-to-noise ratio, I will place constraints on the X-ray luminosity function of this sample.

Regardless of the ability to constrain the presence of an AGN in low metallicity galaxies, an X-ray study of this population will provide critical information about the X-ray luminosity dependence on other physical parameters. Using *SDSS* emission line measurements and the *WISE* colors for each galaxy, I will constrain estimates for metallicity (Z), column density (N_H), ionization parameter (U), and gas density (n) using Cloudy simulations ran over a vast parameter space (Table 5.1). With these constrained properties for each galaxy,

Table 5.1: CLOUDY Parameters

Parameter	Symbol	Range Probed	Step Size
Column Density	$\log(N_H)$	19-24	0.25
Metallicity	Z	$0.1 - 1Z_\odot$	0.1
Gas Density	$\log(n)$	1.5 - 3.5	0.5
Ionization Parameter	$\log(U)$	-1 - -4	0.25

I will look for trends in X-ray luminosity with respect to the parameters probed. The results of this study will be critical to addressing the diagnostic potential of *eROSITA* in tandem with published multi-wavelength data in uncovering low mass AGNs in low metallicity dwarf galaxies.

Bibliography

- Abel, N. P., Dudley, C., Fischer, J., Satyapal, S., and van Hoof, P. A. M. (2009). Dust-Bounded Ultraluminous Infrared Galaxies: Model Predictions for Infrared Spectroscopic Surveys. *ApJ*, 701:1147–1160.
- Abel, N. P. and Satyapal, S. (2008). [Ne V] Emission in Optically Classified Starbursts. *ApJ*, 678:686–692.
- Agarwal, B., Davis, A. J., Khochfar, S., Natarajan, P., and Dunlop, J. S. (2013). Unravelling obese black holes in the first galaxies. *MNRAS*, 432(4):3438–3444.
- Agostino, C. J. and Salim, S. (2019). Crossing the Line: Active Galactic Nuclei in the Star-forming Region of the BPT Diagram. *ApJ*, 876(1):12.
- Allen, M. G., Groves, B. A., Dopita, M. A., Sutherland, R. S., and Kewley, L. J. (2008). The MAPPINGS III Library of Fast Radiative Shock Models. *ApJS*, 178:20–55.
- Alonso-Herrero, A., Rieke, M. J., Rieke, G. H., and Shields, J. C. (2000). The Nature of LINERS. *ApJ*, 530:688–703.
- Alvarez, M. A., Wise, J. H., and Abel, T. (2009). Accretion onto the First Stellar-Mass Black Holes. *ApJL*, 701(2):L133–L137.
- Amaro-Seoane, P., Aoudia, S., Babak, S., Binétruy, P., Berti, E., Bohé, A., Caprini, C., Colpi, M., Cornish, N. J., Danzmann, K., Dufaux, J.-F., Gair, J., Hinder, I., Jennrich, O., Jetzer, P., Klein, A., Lang, R. N., Lobo, A., Littenberg, T., McWilliams, S. T., Nelemans, G., Petiteau, A., Porter, E. K., Schutz, B. F., Sesana, A., Stebbins, R., Sumner, T., Vallisneri, M., Vitale, S., Volonteri, M., Ward, H., and Wardell, B. (2013). eLISA:

- Astrophysics and cosmology in the millihertz regime. *GW Notes, Vol. 6, p. 4-110*, 6:4–110.
- Annun, A., Alexander, D. M., Gandhi, P., Lansbury, G. B., Asmus, D., Ballantyne, D. R., Bauer, F. E., Boggs, S. E., Boorman, P. G., Brandt, W. N., Brightman, M., Christensen, F. E., Craig, W. W., Farrah, D., Goulding, A. D., Hailey, C. J., Harrison, F. A., Koss, M. J., LaMassa, S. M., Murray, S. S., Ricci, C., Rosario, D. J., Stanley, F., Stern, D., and Zhang, W. (2017). A New Compton-thick AGN in our Cosmic Backyard: Unveiling the Buried Nucleus in NGC 1448 with NuSTAR. *ApJ*, 836:165.
- Annun, A., Gandhi, P., Alexander, D. M., Lansbury, G. B., Arévalo, P., Ballantyne, D. R., Baloković, M., Bauer, F. E., Boggs, S. E., Brandt, W. N., Brightman, M., Christensen, F. E., Craig, W. W., Del Moro, A., Hailey, C. J., Harrison, F. A., Hickox, R. C., Matt, G., Puccetti, S., Ricci, C., Rigby, J. R., Stern, D., Walton, D. J., Zappacosta, L., and Zhang, W. (2015). NuSTAR Observations of the Compton-thick Active Galactic Nucleus and Ultraluminous X-Ray Source Candidate in NGC 5643. *ApJ*, 815:36.
- Appenzeller, I. and Wagner, S. J. (1991). Forbidden high-ionization lines in QSO spectra. *A&A*, 250:57.
- Araya Salvo, C., Mathur, S., Ghosh, H., Fiore, F., and Ferrarese, L. (2012). Discovery of an Active Supermassive Black Hole in the Bulgeless Galaxy NGC 4561. *ApJ*, 757:179.
- Arnaud, K. A. (1996). XSPEC: The First Ten Years. In Jacoby, G. H. and Barnes, J., editors, *Astronomical Data Analysis Software and Systems V*, volume 101 of *Astronomical Society of the Pacific Conference Series*, page 17.
- Ashley, M. C. B. and Hyland, A. R. (1988). Detection of Highly Ionized Silicon in the Planetary Nebulae NGC 6302 and NGC 6537. *ApJ*, 331:532.
- Asplund, M., Grevesse, N., and Sauval, A. J. (2006). The new solar abundances - Part I: the observations. *Communications in Asteroseismology*, 147:76–79.

- Assef, R. J., Stern, D., Kochanek, C. S., Blain, A. W., Brodwin, M., Brown, M. J. I., Donoso, E., Eisenhardt, P. R. M., Jannuzi, B. T., Jarrett, T. H., Stanford, S. A., Tsai, C.-W., Wu, J., and Yan, L. (2013). Mid-infrared Selection of Active Galactic Nuclei with the Wide-field Infrared Survey Explorer. II. Properties of WISE-selected Active Galactic Nuclei in the NDWFS Boötes Field. *ApJ*, 772:26.
- Bañados, E., Venemans, B. P., Decarli, R., Farina, E. P., Mazzucchelli, C., Walter, F., Fan, X., Stern, D., Schlafly, E., Chambers, K. C., Rix, H. W., Jiang, L., McGreer, I., Simcoe, R., Wang, F., Yang, J., Morganson, E., De Rosa, G., Greiner, J., Baloković, M., Burgett, W. S., Cooper, T., Draper, P. W., Flewelling, H., Hodapp, K. W., Jun, H. D., Kaiser, N., Kudritzki, R. P., Magnier, E. A., Metcalfe, N., Miller, D., Schindler, J. T., Tonry, J. L., Wainscoat, R. J., Waters, C., and Yang, Q. (2016). The Pan-STARRS1 Distant $z > 5.6$ Quasar Survey: More than 100 Quasars within the First Gyr of the Universe. *ApJS*, 227(1):11.
- Baldassare, V. F., Geha, M., and Greene, J. (2018). Identifying AGNs in Low-mass Galaxies via Long-term Optical Variability. *ApJ*, 868(2):152.
- Baldassare, V. F., Geha, M., and Greene, J. (2020). A Search for Optical AGN Variability in 35,000 Low-mass Galaxies with the Palomar Transient Factory. *ApJ*, 896(1):10.
- Baldassare, V. F., Reines, A. E., Gallo, E., and Greene, J. E. (2015). A $\approx 50,000 M_{\odot}$ Solar Mass Black Hole in the Nucleus of RGG 118. *ApJL*, 809:L14.
- Baldassare, V. F., Reines, A. E., Gallo, E., and Greene, J. E. (2017). X-ray and Ultraviolet Properties of AGNs in Nearby Dwarf Galaxies. *ApJ*, 836:20.
- Baldassare, V. F., Reines, A. E., Gallo, E., Greene, J. E., Graur, O., Geha, M., Hainline, K., Carroll, C. M., and Hickox, R. C. (2016). Multi-epoch Spectroscopy of Dwarf Galaxies with AGN Signatures: Identifying Sources with Persistent Broad $H\alpha$ Emission. *ApJ*, 829:57.

- Baldwin, J. A., Phillips, M. M., and Terlevich, R. (1981). Classification parameters for the emission-line spectra of extragalactic objects. *PASP*, 93:5–19.
- Barth, A. J., Greene, J. E., and Ho, L. C. (2008). Low-Mass Seyfert 2 Galaxies in the Sloan Digital Sky Survey. *AJ*, 136(3):1179–1200.
- Barth, A. J., Ho, L. C., Rutledge, R. E., and Sargent, W. L. W. (2004). POX 52: A Dwarf Seyfert 1 Galaxy with an Intermediate-Mass Black Hole. *ApJ*, 607:90–102.
- Baumgartner, W. H., Tueller, J., Markwardt, C. B., Skinner, G. K., Barthelmy, S., Mushotzky, R. F., Evans, P. A., and Gehrels, N. (2013). The 70 Month Swift-BAT All-sky Hard X-Ray Survey. *ApJS*, 207(2):19.
- Begelman, M. C. and Rees, M. J. (1978). The fate of dense stellar systems. *MNRAS*, 185:847–860.
- Benjamin, R. A. and Dinerstein, H. L. (1990). Near-Infrared Spectroscopy of Classical Novae in the Coronal Phase. *AJ*, 100:1588.
- Bianchi, S., Guainazzi, M., Matt, G., Fonseca Bonilla, N., and Ponti, G. (2009). CAIXA: a catalogue of AGN in the XMM-Newton archive. I. Spectral analysis. *A&A*, 495:421–430.
- Birchall, K. L., Watson, M. G., and Aird, J. (2020). X-ray detected AGN in SDSS dwarf galaxies. *MNRAS*, 492(2):2268–2284.
- Bizzocchi, L., Filho, M. E., Leonardo, E., Grossi, M., Griffith, R. L., Afonso, J., Fernandes, C., Retrê, J., Anton, S., Bell, E. F., Brinchmann, J., Henriques, B., Lobo, C., and Messias, H. (2014). Bulgeless Galaxies at Intermediate Redshift: Sample Selection, Color Properties, and the Existence of Powerful Active Galactic Nuclei. *ApJ*, 782:22.
- Boissay, R., Ricci, C., and Paltani, S. (2016). A hard X-ray view of the soft excess in AGN. *A&A*, 588:A70.

- Brinchmann, J., Pettini, M., and Charlot, S. (2008). New insights into the stellar content and physical conditions of star-forming galaxies at $z = 2-3$ from spectral modelling. *MNRAS*, 385:769–782.
- Bromm, V. and Loeb, A. (2003). Formation of the First Supermassive Black Holes. *ApJ*, 596(1):34–46.
- Brorby, M., Kaaret, P., and Prestwich, A. (2014). X-ray binary formation in low-metallicity blue compact dwarf galaxies. *MNRAS*, 441(3):2346–2353.
- Campbell, A., Terlevich, R., and Melnick, J. (1986). The stellar populations and evolution of H II galaxies - I. High signal-to-noise optical spectroscopy. *MNRAS*, 223:811–825.
- Cann, J. M., Satyapal, S., Abel, N. P., Ricci, C., Secretst, N. J., Blecha, L., and Gliozzi, M. (2018). The Hunt for Intermediate-mass Black Holes in the JWST Era. *ApJ*, 861(2):142.
- Chakravorty, S., Elvis, M., and Ferland, G. (2014). A transition mass for black holes to show broad emission lines. *MNRAS*, 437:740–747.
- Chakravorty, S., Misra, R., Elvis, M., Kembhavi, A. K., and Ferland, G. (2012). The influence of soft spectral components on the structure and stability of warm absorbers in active galactic nuclei. *MNRAS*, 422:637–651.
- Chen, C.-T. J., Brandt, W. N., Reines, A. E., Lansbury, G., Stern, D., Alexander, D. M., Bauer, F., Del Moro, A., Gandhi, P., Harrison, F. A., Hickox, R. C., Koss, M. J., Lanz, L., Luo, B., Mullaney, J. R., Ricci, C., and Trump, J. R. (2017). Hard X-Ray-selected AGNs in Low-mass Galaxies from the NuSTAR Serendipitous Survey. *ApJ*, 837:48.
- Chilingarian, I. V., Katkov, I. Y., Zolotukhin, I. Y., Grishin, K. A., Beletsky, Y., Boutsia, K., and Osip, D. J. (2018). A Population of Bona Fide Intermediate-mass Black Holes Identified as Low-luminosity Active Galactic Nuclei. *ApJ*, 863(1):1.
- Coelho, B., Antón, S., Lobo, C., and Ribeiro, B. (2013). Red bulgeless galaxies in SDSS DR7. Are there any AGN hosts? *MNRAS*, 436:2426–2434.

- Condon, J. J., Huang, Z.-P., Yin, Q. F., and Thuan, T. X. (1991). Compact starbursts in ultraluminous infrared galaxies. *ApJ*, 378:65–76.
- Crummy, J., Fabian, A. C., Gallo, L., and Ross, R. R. (2006). An explanation for the soft X-ray excess in active galactic nuclei. *MNRAS*, 365:1067–1081.
- Czerny, B. and Elvis, M. (1987). Constraints on quasar accretion disks from the optical/ultraviolet/soft X-ray big bump. *ApJ*, 321:305–320.
- D’Abrusco, R., Longo, G., and Walton, N. A. (2009). Quasar candidates selection in the Virtual Observatory era. *MNRAS*, 396(1):223–262.
- Dawson, K. S., Schlegel, D. J., Ahn, C. P., Anderson, S. F., Aubourg, É., Bailey, S., Barkhouser, R. H., Bautista, J. E., Beifiori, A. r., Berlind, A. A., Bhardwaj, V., Bizyaev, D., Blake, C. H., Blanton, M. R., Blomqvist, M., Bolton, A. S., Borde, A., Bovy, J., Brandt, W. N., Brewington, H., Brinkmann, J., Brown, P. J., Brownstein, J. R., Bundy, K., Busca, N. G., Carithers, W., Carnero, A. R., Carr, M. A., Chen, Y., Comparat, J., Connolly, N., Cope, F., Croft, R. A. C., Cuesta, A. J., da Costa, L. N., Davenport, J. R. A., Delubac, T., de Putter, R., Dhital, S., Ealet, A., Ebelke, G. L., Eisenstein, D. J., Escoffier, S., Fan, X., Filiz Ak, N., Finley, H., Font-Ribera, A., Génova-Santos, R., Gunn, J. E., Guo, H., Haggard, D., Hall, P. B., Hamilton, J.-C., Harris, B., Harris, D. W., Ho, S., Hogg, D. W., Holder, D., Honscheid, K., Huehnerhoff, J., Jordan, B., Jordan, W. P., Kauffmann, G., Kazin, E. A., Kirkby, D., Klaene, M. A., Kneib, J.-P., Le Goff, J.-M., Lee, K.-G., Long, D. C., Loomis, C. P., Lundgren, B., Lupton, R. H., Maia, M. A. G., Makler, M., Malanushenko, E., Malanushenko, V., Mandelbaum, R., Manera, M., Maraston, C., Margala, D., Masters, K. L., McBride, C. K., McDonald, P., McGreer, I. D., McMahon, R. G., Mena, O., Miralda-Escudé, J., Montero-Dorta, A. D., Montesano, F., Muna, D., Myers, A. D., Naugle, T., Nichol, R. C., Noterdaeme, P., Nuza, S. E., Olmstead, M. D., Oravetz, A., Oravetz, D. J., Owen, R., Padmanabhan, N., Palanque-Delabrouille, N., Pan, K., Parejko, J. K., Pâris, I., Percival, W. J., Pérez-Fournon, I., Pérez-Ràfols, I., Petitjean, P., Pfaffenberger, R., Pforr, J., Pieri, M. M., Prada, F., Price-Whelan, A. M.,

- Raddick, M. J., Rebolo, R., Rich, J., Richards, G. T., Rockosi, C. M., Roe, N. A., Ross, A. J., Ross, N. P., Rossi, G., Rubiño-Martín, J. A., Samushia, L., Sánchez, A. G., Sayres, C., Schmidt, S. J., Schneider, D. P., Scóccola, C. G., Seo, H.-J., Shelden, A., Sheldon, E., Shen, Y., Shu, Y., Slosar, A., Smee, S. A., Snedden, S. A., Stauffer, F., Steele, O., Strauss, M. A., Streblyanska, A., Suzuki, N., Swanson, M. E. C., Tal, T., Tanaka, M., Thomas, D., Tinker, J. L., Tojeiro, R., Tremonti, C. A., Vargas Magaña, M., Verde, L., Viel, M., Wake, D. A., Watson, M., Weaver, B. A., Weinberg, D. H., Weiner, B. J., West, A. A., White, M., Wood-Vasey, W. M., Yeche, C., Zehavi, I., Zhao, G.-B., and Zheng, Z. (2013). The Baryon Oscillation Spectroscopic Survey of SDSS-III. *AJ*, 145(1):10.
- Desroches, L.-B. and Ho, L. C. (2009). Candidate Active Nuclei in Late-Type Spiral Galaxies. *ApJ*, 690:267–278.
- Dewangan, G. C., Mathur, S., Griffiths, R. E., and Rao, A. R. (2008). X-Ray Emission from Active Galactic Nuclei with Intermediate-Mass Black Holes. *ApJ*, 689:762–774.
- Dietrich, M. and Hamann, F. (2004). Implications of Quasar Black Hole Masses at High Redshifts. *ApJ*, 611(2):761–769.
- Done, C., Davis, S. W., Jin, C., Blaes, O., and Ward, M. (2012). Intrinsic disc emission and the soft X-ray excess in active galactic nuclei. *MNRAS*, 420:1848–1860.
- Dong, R., Greene, J. E., and Ho, L. C. (2012a). X-Ray Properties of Intermediate-mass Black Holes in Active Galaxies. III. Spectral Energy Distribution and Possible Evidence for Intrinsically X-Ray-weak Active Galactic Nuclei. *ApJ*, 761(1):73.
- Dong, X.-B., Ho, L. C., Yuan, W., Wang, T.-G., Fan, X., Zhou, H., and Jiang, N. (2012b). A Uniformly Selected Sample of Low-mass Black Holes in Seyfert 1 Galaxies. *ApJ*, 755:167.
- Donley, J. L., Koekemoer, A. M., Brusa, M., Capak, P., Cardamone, C. N., Civano, F., Ilbert, O., Impey, C. D., Kartaltepe, J. S., Miyaji, T., Salvato, M., Sanders, D. B., Trump, J. R., and Zamorani, G. (2012). Identifying Luminous Active Galactic Nuclei in Deep Surveys: Revised IRAC Selection Criteria. *ApJ*, 748:142.

- Dopita, M. A., Kewley, L. J., Heisler, C. A., and Sutherland, R. S. (2000). A Theoretical Recalibration of the Extragalactic H II Region Sequence. *ApJ*, 542:224–234.
- Ebisuzaki, T., Makino, J., Tsuru, T. G., Funato, Y., Portegies Zwart, S., Hut, P., McMillan, S., Matsushita, S., Matsumoto, H., and Kawabe, R. (2001). Missing Link Found? The “Runaway” Path to Supermassive Black Holes. *ApJL*, 562(1):L19–L22.
- Elitzur, M. and Ho, L. C. (2009). On the Disappearance of the Broad-Line Region in Low-Luminosity Active Galactic Nuclei. *ApJL*, 701:L91–L94.
- Elvis, M., Green, R. F., Bechtold, J., Schmidt, M., Neugebauer, G., Soifer, B. T., Matthews, K., and Fabbiano, G. (1986). X-ray spectra of PG quasars. I - The continuum from X-rays to infrared. *ApJ*, 310:291–316.
- Erb, D. K., Pettini, M., Shapley, A. E., Steidel, C. C., Law, D. R., and Reddy, N. A. (2010). Physical Conditions in a Young, Unreddened, Low-metallicity Galaxy at High Redshift. *ApJ*, 719:1168–1190.
- Fabian, A. C., Miniutti, G., Iwasawa, K., and Ross, R. R. (2005). X-ray reflection in the Seyfert galaxy 1H 0419-577 revealing strong relativistic effects in the vicinity of a Kerr black hole. *MNRAS*, 361:795–802.
- Fan, X., Strauss, M. A., Richards, G. T., Hennawi, J. F., Becker, R. H., White, R. L., Diamond-Stanic, A. M., Donley, J. L., Jiang, L., Kim, J. S., Vestergaard, M., Young, J. E., Gunn, J. E., Lupton, R. H., Knapp, G. R., Schneider, D. P., Brandt, W. N., Bahcall, N. A., Barentine, J. C., Brinkmann, J., Brewington, H. J., Fukugita, M., Harvanek, M., Kleinman, S. J., Krzesinski, J., Long, D., Neilsen, Eric H., J., Nitta, A., Snedden, S. A., and Voges, W. (2006). A Survey of $z \gtrsim 5.7$ Quasars in the Sloan Digital Sky Survey. IV. Discovery of Seven Additional Quasars. *AJ*, 131(3):1203–1209.
- Feibelman, W. A. (1996). The IUE Spectrum of the Planetary Nebula NGC 6905. *ApJ*, 472:294.

- Ferland, G. J., Chatzikos, M., Guzmán, F., Lykins, M. L., van Hoof, P. A. M., Williams, R. J. R., Abel, N. P., Badnell, N. R., Keenan, F. P., Porter, R. L., and Stancil, P. C. (2017). The 2017 Release Cloudy. *RMxAA*, 53:385–438.
- Filippenko, A. V. and Ho, L. C. (2003). A Low-Mass Central Black Hole in the Bulgeless Seyfert 1 Galaxy NGC 4395. *ApJL*, 588:L13–L16.
- Foreman-Mackey, D., Hogg, D. W., Lang, D., and Goodman, J. (2013). emcee: The MCMC Hammer. *PASP*, 125(925):306.
- Fragos, T., Lehmer, B. D., Naoz, S., Zezas, A., and Basu-Zych, A. (2013). Energy Feedback from X-Ray Binaries in the Early Universe. *ApJL*, 776:L31.
- Frank, J., King, A., and Raine, D. J. (2002). *Accretion Power in Astrophysics: Third Edition*.
- Freitag, M., Gürkan, M. A., and Rasio, F. A. (2006). Runaway collisions in young star clusters - II. Numerical results. *MNRAS*, 368(1):141–161.
- Fricke, K. J., Izotov, Y. I., Papaderos, P., Guseva, N. G., and Thuan, T. X. (2001). An Imaging and Spectroscopic Study of the Very Metal-deficient Blue Compact Dwarf Galaxy Tol 1214-277. *AJ*, 121(1):169–181.
- Geballe, T. R., Mason, R. E., Rodríguez-Ardila, A., and Axon, D. J. (2009). The 3-5 μm Spectrum of NGC 1068 at High Angular Resolution: Distribution of Emission and Absorption Features Across the Nuclear Continuum Source. *ApJ*, 701:1710–1720.
- Gebhardt, K., Bender, R., Bower, G., Dressler, A., Faber, S. M., Filippenko, A. V., Green, R., Grillmair, C., Ho, L. C., Kormendy, J., Lauer, T. R., Magorrian, J., Pinkney, J., Richstone, D., and Tremaine, S. (2000). A Relationship between Nuclear Black Hole Mass and Galaxy Velocity Dispersion. *ApJL*, 539:L13–L16.
- Geha, M., Blanton, M. R., Masjedi, M., and West, A. A. (2006). The Baryon Content of Extremely Low Mass Dwarf Galaxies. *ApJ*, 653:240–254.

- Gehrels, N. (1986). Confidence Limits for Small Numbers of Events in Astrophysical Data. *ApJ*, 303:336.
- Genzel, R., Lutz, D., Sturm, E., Egami, E., Kunze, D., Moorwood, A. F. M., Rigopoulou, D., Spoon, H. W. W., Sternberg, A., Tacconi-Garman, L. E., Tacconi, L., and Thatte, N. (1998). What Powers Ultraluminous IRAS Galaxies? *ApJ*, 498:579–605.
- Ghosh, H., Mathur, S., Fiore, F., and Ferrarese, L. (2008). Detecting Low-Mass Supermassive Black Holes. In Chakrabarti, S. K. and Majumdar, A. S., editors, *American Institute of Physics Conference Series*, volume 1053 of *American Institute of Physics Conference Series*, pages 39–42.
- Gierliński, M. and Done, C. (2004). Is the soft excess in active galactic nuclei real? *MNRAS*, 349:L7–L11.
- Glozzi, M., Satyapal, S., Eracleous, M., Titarchuk, L., and Cheung, C. C. (2009). A Chandra View of NGC 3621: A Bulgeless Galaxy Hosting an AGN in Its Early Phase? *ApJ*, 700:1759–1767.
- Glozzi, M. and Williams, J. K. (2020). The soft X-ray excess: NLS1s versus BLS1s. *MNRAS*, 491(1):532–543.
- Goulding, A. D. and Alexander, D. M. (2009). Towards a complete census of AGN in nearby Galaxies: a large population of optically unidentified AGN. *MNRAS*, 398:1165–1193.
- Grandi, S. A. (1978). /Fe XI/ lambda 7892 emission in Seyfert galaxies. *ApJ*, 221:501–506.
- Greene, J. E. (2012). Low-mass black holes as the remnants of primordial black hole formation. *Nature Communications*, 3:1304.
- Greene, J. E. and Ho, L. C. (2004). Active Galactic Nuclei with Candidate Intermediate-Mass Black Holes. *ApJ*, 610:722–736.
- Greene, J. E. and Ho, L. C. (2007). The Mass Function of Active Black Holes in the Local Universe. *ApJ*, 667:131–148.

- Greene, J. E., Peng, C. Y., Kim, M., Kuo, C.-Y., Braatz, J. A., Impellizzeri, C. M. V., Condon, J. J., Lo, K. Y., Henkel, C., and Reid, M. J. (2010). Precise Black Hole Masses from Megamaser Disks: Black Hole-Bulge Relations at Low Mass. *ApJ*, 721:26–45.
- Greenhouse, M. A., Grasdalen, G. L., Woodward, C. E., Benson, J., Gehrz, R. D., Rosenthal, E., and Skrutskie, M. F. (1990). The Infrared Coronal Lines of Recent Novae. *ApJ*, 352:307.
- Griffith, R. L., Tsai, C.-W., Stern, D., Blain, A., Eisenhardt, P. R. M., Harrison, F., Jarrett, T. H., Madsen, K., Stanford, S. A., Wright, E. L., Wu, J., Wu, Y., and Yan, L. (2011). WISE Discovery of Low-metallicity Blue Compact Dwarf Galaxies. *ApJL*, 736(1):L22.
- Groves, B. A., Heckman, T. M., and Kauffmann, G. (2006). Emission-line diagnostics of low-metallicity active galactic nuclei. *MNRAS*, 371(4):1559–1569.
- Grupe, D., Mathur, S., Wilkes, B., and Osmer, P. (2006). XMM-Newton Observations of High-Redshift Quasars. *AJ*, 131:55–69.
- Gültekin, K., Richstone, D. O., Gebhardt, K., Lauer, T. R., Tremaine, S., Aller, M. C., Bender, R., Dressler, A., Faber, S. M., Filippenko, A. V., Green, R., Ho, L. C., Kormendy, J., Magorrian, J., Pinkney, J., and Siopis, C. (2009). The $M-\sigma$ and $M-L$ Relations in Galactic Bulges, and Determinations of Their Intrinsic Scatter. *ApJ*, 698:198–221.
- Haehnelt, M. G. and Rees, M. J. (1993). The formation of nuclei in newly formed galaxies and the evolution of the quasar population. *MNRAS*, 263(1):168–178.
- Hainline, K. N., Reines, A. E., Greene, J. E., and Stern, D. (2016). Mid-infrared Colors of Dwarf Galaxies: Young Starbursts Mimicking Active Galactic Nuclei. *ApJ*, 832:119.
- Hainline, K. N., Shapley, A. E., Kornei, K. A., Pettini, M., Buckley-Geer, E., Allam, S. S., and Tucker, D. L. (2009). Rest-Frame Optical Spectra of Three Strongly Lensed Galaxies at $z \sim 2$. *ApJ*, 701:52–65.
- Halpern, J. P. (1984). Variable X-ray absorption in the QSO MR 2251 - 178. *ApJ*, 281:90–94.

- Hamann, F., Korista, K. T., Ferland, G. J., Warner, C., and Baldwin, J. (2002). Metallicities and Abundance Ratios from Quasar Broad Emission Lines. *ApJ*, 564(2):592–603.
- Ho, L. C. (2008). Nuclear activity in nearby galaxies. *ARA&A*, 46:475–539.
- Ho, L. C., Kim, M., and Terashima, Y. (2012). The Low-mass, Highly Accreting Black Hole Associated with the Active Galactic Nucleus 2XMM J123103.2+110648. *ApJL*, 759:L16.
- Inayoshi, K., Omukai, K., and Tasker, E. (2014). Formation of an embryonic supermassive star in the first galaxy. *MNRAS*, 445:L109–L113.
- Inayoshi, K., Visbal, E., and Haiman, Z. (2020). The Assembly of the First Massive Black Holes. *ARA&A*, 58:27–97.
- Izotov, Y. I., Guseva, N. G., Fricke, K. J., and Henkel, C. (2011). Star-forming galaxies with hot dust emission in the Sloan Digital Sky Survey discovered by the Wide-field Infrared Survey Explorer (WISE). *A&A*, 536:L7.
- Izotov, Y. I., Guseva, N. G., Fricke, K. J., Stasińska, G., Henkel, C., and Papaderos, P. (2010). Tol 2240-384 - a new low-metallicity AGN candidate. *A&A*, 517:A90.
- Izotov, Y. I., Papaderos, P., Guseva, N. G., Fricke, K. J., and Thuan, T. X. (2004). Deep VLT spectroscopy of the blue compact dwarf galaxies Tol 1214-277 and Tol 65. *A&A*, 421:539–554.
- Izotov, Y. I., Schaerer, D., and Charbonnel, C. (2001). On Ionization Effects and Abundance Ratios in Damped Ly α Systems. *ApJ*, 549(2):878–890.
- Izotov, Y. I., Stasińska, G., Meynet, G., Guseva, N. G., and Thuan, T. X. (2006). The chemical composition of metal-poor emission-line galaxies in the Data Release 3 of the Sloan Digital Sky Survey. *A&A*, 448(3):955–970.
- Izotov, Y. I. and Thuan, T. X. (2008). Active Galactic Nuclei in Four Metal-poor Dwarf Emission-Line Galaxies. *ApJ*, 687:133–140.

- Izotov, Y. I., Thuan, T. X., and Guseva, N. G. (2007). Broad-Line Emission in Low-Metallicity Blue Compact Dwarf Galaxies: Evidence for Stellar Wind, Supernova, and Possible AGN Activity. *ApJ*, 671(2):1297–1320.
- Izotov, Y. I., Thuan, T. X., and Privon, G. (2012). The detection of [Ne V] emission in five blue compact dwarf galaxies. *MNRAS*, 427(2):1229–1237.
- Jarrett, T. H., Cohen, M., Masci, F., Wright, E., Stern, D., Benford, D., Blain, A., Carey, S., Cutri, R. M., Eisenhardt, P., Lonsdale, C., Mainzer, A., Marsh, K., Padgett, D., Petty, S., Ressler, M., Skrutskie, M., Stanford, S., Surace, J., Tsai, C. W., Wheelock, S., and Yan, D. L. (2011). The Spitzer-WISE Survey of the Ecliptic Poles. *ApJ*, 735(2):112.
- Jiang, L., Fan, X., Vestergaard, M., Kurk, J. D., Walter, F., Kelly, B. C., and Strauss, M. A. (2007). Gemini Near-Infrared Spectroscopy of Luminous $z \sim 6$ Quasars: Chemical Abundances, Black Hole Masses, and Mg II Absorption. *AJ*, 134(3):1150.
- Jiang, Y.-F., Greene, J. E., Ho, L. C., Xiao, T., and Barth, A. J. (2011). The Host Galaxies of Low-mass Black Holes. *ApJ*, 742:68.
- Jin, C., Done, C., and Ward, M. (2017). Super-Eddington QSO RX J0439.6-5311 - I. Origin of the soft X-ray excess and structure of the inner accretion flow. *MNRAS*, 468:3663–3681.
- Kaaret, P., Schmitt, J., and Gorski, M. (2011). X-Rays from Blue Compact Dwarf Galaxies. *ApJ*, 741(1):10.
- Kauffmann, G., Heckman, T. M., Tremonti, C., Brinchmann, J., Charlot, S., White, S. D. M., Ridgway, S. E., Brinkmann, J., Fukugita, M., Hall, P. B., Ivezić, Ž., Richards, G. T., and Schneider, D. P. (2003). The host galaxies of active galactic nuclei. *MNRAS*, 346:1055–1077.
- Kewley, L. J., Dopita, M. A., Leitherer, C., Davé, R., Yuan, T., Allen, M., Groves, B., and Sutherland, R. (2013). Theoretical Evolution of Optical Strong Lines across Cosmic Time. *ApJ*, 774:100.

- Kewley, L. J., Dopita, M. A., Sutherland, R. S., Heisler, C. A., and Trevena, J. (2001). Theoretical Modeling of Starburst Galaxies. *ApJ*, 556:121–140.
- Kim, D., Im, M., Canalizo, G., Kim, M., Kim, J. H., Woo, J.-H., Taak, Y. C., Kim, J.-W., and Lazarova, M. (2018). Medium-resolution Optical and Near-infrared Spectral Atlas of 16 2MASS-selected NIR-red Active Galactic Nuclei at $z \approx 0.3$. *ApJS*, 238(2):37.
- Kızıltan, B., Baumgardt, H., and Loeb, A. (2017). An intermediate-mass black hole in the centre of the globular cluster 47 Tucanae. *Nature*, 542:203–205.
- Korista, K., Ferland, G., and Baldwin, J. (1997). Do the Broad Emission Line Clouds See the Same Continuum That We See? *ApJ*, 487:555–559.
- Koss, M., Trakhtenbrot, B., Ricci, C., Lamperti, I., Oh, K., Berney, S., Schawinski, K., Baloković, M., Baronchelli, L., Crenshaw, D. M., Fischer, T., Gehrels, N., Harrison, F., Hashimoto, Y., Hogg, D., Ichikawa, K., Masetti, N., Mushotzky, R., Sartori, L., Stern, D., Treister, E., Ueda, Y., Veilleux, S., and Winter, L. (2017). BAT AGN Spectroscopic Survey. I. Spectral Measurements, Derived Quantities, and AGN Demographics. *ApJ*, 850(1):74.
- Kraemer, S. B., Ho, L. C., Crenshaw, D. M., Shields, J. C., and Filippenko, A. V. (1999). Physical Conditions in the Emission-Line Gas in the Extremely Low Luminosity Seyfert Nucleus of NGC 4395. *ApJ*, 520(2):564–573.
- Krolik, J. H. (1999). *Active galactic nuclei : from the central black hole to the galactic environment*.
- Krolik, J. H. and Begelman, M. C. (1988). Molecular tori in Seyfert galaxies - Feeding the monster and hiding it. *ApJ*, 329:702–711.
- Kurk, J. D., Walter, F., Fan, X., Jiang, L., Riechers, D. A., Rix, H.-W., Pentericci, L., Strauss, M. A., Carilli, C., and Wagner, S. (2007). Black Hole Masses and Enrichment of $z \sim 6$ SDSS Quasars. *ApJ*, 669(1):32–44.

- Lacy, M., Storrie-Lombardi, L. J., Sajina, A., Appleton, P. N., Armus, L., Chapman, S. C., Choi, P. I., Fadda, D., Fang, F., Frayer, D. T., Heinrichsen, I., Helou, G., Im, M., Marleau, F. R., Masci, F., Shupe, D. L., Soifer, B. T., Surace, J., Teplitz, H. I., Wilson, G., and Yan, L. (2004). Obscured and Unobscured Active Galactic Nuclei in the Spitzer Space Telescope First Look Survey. *ApJS*, 154:166–169.
- Lamastra, A., Bianchi, S., Matt, G., Perola, G. C., Barcons, X., and Carrera, F. J. (2009). The bolometric luminosity of type 2 AGN from extinction-corrected [OIII]. No evidence of Eddington-limited sources. *A&A*, 504(1):73–79.
- Lamperti, I., Koss, M., Trakhtenbrot, B., Schawinski, K., Ricci, C., Oh, K., Landt, H., Riffel, R., Rodríguez-Ardila, A., Gehrels, N., Harrison, F., Masetti, N., Mushotzky, R., Treister, E., Ueda, Y., and Veilleux, S. (2017). BAT AGN Spectroscopic Survey - IV: Near-Infrared Coronal Lines, Hidden Broad Lines, and Correlation with Hard X-ray Emission. *MNRAS*, 467:540–572.
- Lansbury, G. B., Alexander, D. M., Del Moro, A., Gandhi, P., Assef, R. J., Stern, D., Aird, J., Ballantyne, D. R., Baloković, M., Bauer, F. E., Boggs, S. E., Brandt, W. N., Christensen, F. E., Craig, W. W., Elvis, M., Grefenstette, B. W., Hailey, C. J., Harrison, F. A., Hickox, R. C., Koss, M., LaMassa, S. M., Luo, B., Mullaney, J. R., Teng, S. H., Urry, C. M., and Zhang, W. W. (2014). NuSTAR Observations of Heavily Obscured Quasars at $z \sim 0.5$. *ApJ*, 785(1):17.
- Laor, A. (1990). Massive Thin Accretion Discs - Part Three - Comparison with the Observations. *MNRAS*, 246:369.
- Latif, M. A. and Ferrara, A. (2016). Formation of Supermassive Black Hole Seeds. *PASA*, 33:e051.
- Lemons, S. M., Reines, A. E., Plotkin, R. M., Gallo, E., and Greene, J. E. (2015). An X-Ray Selected Sample of Candidate Black Holes in Dwarf Galaxies. *ApJ*, 805:12.

- Li, J., Wang, R., Riechers, D., Walter, F., Decarli, R., Venamans, B. P., Neri, R., Shao, Y., Fan, X., Gao, Y., Carilli, C. L., Omont, A., Cox, P., Menten, K. M., Wagg, J., Bertoldi, F., and Narayanan, D. (2020). Probing the Full CO Spectral Line Energy Distribution (SLED) in the Nuclear Region of a Quasar-starburst System at $z = 6.003$. *ApJ*, 889(2):162.
- Luo, B., Brandt, W. N., Alexander, D. M., Stern, D., Teng, S. H., Arévalo, P., Bauer, F. E., Boggs, S. E., Christensen, F. E., Comastri, A., Craig, W. W., Farrah, D., Gandhi, P., Hailey, C. J., Harrison, F. A., Koss, M., Ogle, P., Puccetti, S., Saez, C., Scott, A. E., Walton, D. J., and Zhang, W. W. (2014). Weak Hard X-Ray Emission from Broad Absorption Line Quasars: Evidence for Intrinsic X-Ray Weakness. *ApJ*, 794(1):70.
- Lutz, D., Veilleux, S., and Genzel, R. (1999). Mid-Infrared and Optical Spectroscopy of Ultraluminous Infrared Galaxies: A Comparison. *ApJL*, 517:L13–L17.
- Lützgendorf, N., Kissler-Patig, M., Gebhardt, K., Baumgardt, H., Noyola, E., de Zeeuw, P. T., Neumayer, N., Jalali, B., and Feldmeier, A. (2013). Limits on intermediate-mass black holes in six Galactic globular clusters with integral-field spectroscopy. *A&A*, 552:A49.
- Lützgendorf, N., Kissler-Patig, M., Gebhardt, K., Baumgardt, H., Noyola, E., Jalali, B., de Zeeuw, P. T., and Neumayer, N. (2012). Central kinematics of the globular cluster NGC 2808: upper limit on the mass of an intermediate-mass black hole. *A&A*, 542:A129.
- Lynden-Bell, D. (1969). Galactic Nuclei as Collapsed Old Quasars. *Nature*, 223:690–694.
- Maccarone, T. J., Fender, R. P., and Tzioumis, A. K. (2005). Upper limits on central black hole masses of globular clusters from radio emission and a possible black hole detection in the Ursa Minor dwarf galaxy. *MNRAS*, 356:L17–L22.
- Maccarone, T. J., Kundu, A., Zepf, S. E., and Rhode, K. L. (2007). A black hole in a globular cluster. *Nature*, 445:183–185.

- Magorrian, J., Tremaine, S., Richstone, D., Bender, R., Bower, G., Dressler, A., Faber, S. M., Gebhardt, K., Green, R., Grillmair, C., Kormendy, J., and Lauer, T. (1998). The Demography of Massive Dark Objects in Galaxy Centers. *AJ*, 115:2285–2305.
- Maiolino, R., Nagao, T., Grazian, A., Cocchia, F., Marconi, A., Mannucci, F., Cimatti, A., Pipino, A., Ballero, S., Calura, F., Chiappini, C., Fontana, A., Granato, G. L., Matteucci, F., Pastorini, G., Pentericci, L., Risaliti, G., Salvati, M., and Silva, L. (2008). AMAZE. I. The evolution of the mass-metallicity relation at $z > 3$. *A&A*, 488:463–479.
- Maiolino, R., Neri, R., Beelen, A., Bertoldi, F., Carilli, C. L., Caselli, P., Cox, P., Menten, K. M., Nagao, T., Omont, A., Walmsley, C. M., Walter, F., and Weiß, A. (2007). Molecular gas in QSO host galaxies at $z > 5$. *A&A*, 472(2):L33–L37.
- Makishima, K., Maejima, Y., Mitsuda, K., Bradt, H. V., Remillard, R. A., Tuohy, I. R., Hoshi, R., and Nakagawa, M. (1986). Simultaneous X-ray and optical observations of GX 339-4 in an X-ray high state. *ApJ*, 308:635–643.
- Maksym, W. P., Ulmer, M. P., Roth, K. C., Irwin, J. A., Dupke, R., Ho, L. C., Keel, W. C., and Adami, C. (2014). Deep spectroscopy of the $M_V \approx -14.8$ host galaxy of a tidal disruption flare in A1795. *MNRAS*, 444:866–873.
- Malkan, M. A. (1986). Near-Ultraviolet Spectroscopy of Seyfert Nuclei: Reddening and Bowen Fluorescence. *ApJ*, 310:679.
- Mapelli, M., Colpi, M., and Zampieri, L. (2009). Low metallicity and ultra-luminous X-ray sources in the Cartwheel galaxy. *MNRAS*, 395:L71–L75.
- Marconi, A., van der Werf, P. P., Moorwood, A. F. M., and Oliva, E. (1996). Infrared and visible coronal lines in NGC 1068. *A&A*, 315:335–342.
- Martínez-Palomera, J., Lira, P., Bhalla-Ladd, I., Förster, F., and Plotkin, R. M. (2020). Introducing the Search for Intermediate-mass Black Holes in Nearby Galaxies (SIBLING) Survey. *ApJ*, 889(2):113.

- Mason, R. E., Rodríguez-Ardila, A., Martins, L., Riffel, R., González Martín, O., Ramos Almeida, C., Ruschel Dutra, D., Ho, L. C., Thanjavur, K., Flohic, H., Alonso-Herrero, A., Lira, P., McDermid, R., Riffel, R. A., Schiavon, R. P., Winge, C., Hoenig, M. D., and Perlman, E. (2015). The Nuclear Near-Infrared Spectral Properties of Nearby Galaxies. *ApJS*, 217:13.
- Mateos, S., Alonso-Herrero, A., Carrera, F. J., Blain, A., Watson, M. G., Barcons, X., Braitto, V., Severgnini, P., Donley, J. L., and Stern, D. (2012). Using the Bright Ultrahard XMM-Newton survey to define an IR selection of luminous AGN based on WISE colours. *MNRAS*, 426:3271–3281.
- Matsuoka, Y., Strauss, M. A., Kashikawa, N., Onoue, M., Iwasawa, K., Tang, J.-J., Lee, C.-H., Imanishi, M., Nagao, T., Akiyama, M., Asami, N., Bosch, J., Furusawa, H., Goto, T., Gunn, J. E., Harikane, Y., Ikeda, H., Izumi, T., Kawaguchi, T., Kato, N., Kikuta, S., Kohno, K., Komiyama, Y., Lupton, R. H., Minezaki, T., Miyazaki, S., Murayama, H., Niida, M., Nishizawa, A. J., Noboriguchi, A., Oguri, M., Ono, Y., Ouchi, M., Price, P. A., Sameshima, H., Schulze, A., Shirakata, H., Silverman, J. D., Sugiyama, N., Tait, P. J., Takada, M., Takata, T., Tanaka, M., Toba, Y., Utsumi, Y., Wang, S.-Y., and Yamashita, T. (2018). Subaru High- z Exploration of Low-luminosity Quasars (SHELLQs). V. Quasar Luminosity Function and Contribution to Cosmic Reionization at $z = 6$. *ApJ*, 869(2):150.
- Maughan, B. J. and Reiprich, T. H. (2019). The X-ray Variability of AGN and its Implications for Observations of Galaxy Clusters. *The Open Journal of Astrophysics*, 2(1):9.
- Mazzalay, X. and Rodríguez-Ardila, A. (2007). Optical and NIR spectroscopy of Mrk 1210: constraints and physical conditions of the active nucleus. *A&A*, 463:445–454.
- McAlpine, W., Satyapal, S., Gliozzi, M., Cheung, C. C., Sambruna, R. M., and Eracleous, M. (2011). Black Holes in Bulgeless Galaxies: An XMM-Newton Investigation of NGC 3367 and NGC 4536. *ApJ*, 728:25.

- McConnell, N. J. and Ma, C.-P. (2013). Revisiting the Scaling Relations of Black Hole Masses and Host Galaxy Properties. *ApJ*, 764:184.
- McLean, I. S., Becklin, E. E., Bendiksen, O., Brims, G., Canfield, J., Figer, D. F., Graham, J. R., Hare, J., Lacayanga, F., Larkin, J. E., Larson, S. B., Levenson, N., Magnone, N., Teplitz, H., and Wong, W. (1998). Design and development of NIRSPEC: a near-infrared echelle spectrograph for the Keck II telescope. In Fowler, A. M., editor, *Proc. SPIE*, volume 3354 of *Society of Photo-Optical Instrumentation Engineers (SPIE) Conference Series*, pages 566–578.
- Mezcua, M. (2017). Observational evidence for intermediate-mass black holes. *International Journal of Modern Physics D*, 26:1730021.
- Mezcua, M., Civano, F., Fabbiano, G., Miyaji, T., and Marchesi, S. (2016). A Population of Intermediate-mass Black Holes in Dwarf Starburst Galaxies Up to Redshift=1.5. *ApJ*, 817:20.
- Mezcua, M., Civano, F., Marchesi, S., Suh, H., Fabbiano, G., and Volonteri, M. (2018). Intermediate-mass black holes in dwarf galaxies out to redshift ~ 2.4 in the Chandra COSMOS-Legacy Survey. *MNRAS*, 478(2):2576–2591.
- Middleton, M., Done, C., and Gierliński, M. (2007). An absorption origin for the soft excess in Seyfert 1 active galactic nuclei. *MNRAS*, 381:1426–1436.
- Miller, B. P., Gallo, E., Greene, J. E., Kelly, B. C., Treu, T., Woo, J.-H., and Baldassare, V. (2015). X-Ray Constraints on the Local Supermassive Black Hole Occupation Fraction. *ApJ*, 799:98.
- Mitsuda, K., Inoue, H., Koyama, K., Makishima, K., Matsuoka, M., Ogawara, Y., Suzuki, K., Tanaka, Y., Shibazaki, N., and Hirano, T. (1984). Energy spectra of low-mass binary X-ray sources observed from TENMA. *PASJ*, 36:741–759.

- Molina, M., Eracleous, M., Barth, A. J., Maoz, D., Runnoe, J. C., Ho, L. C., Shields, J. C., and Walsh, J. L. (2018). The Shocking Power Sources of LINERs. *ApJ*, 864(1):90.
- Moran, E. C., Shahinyan, K., Sugarman, H. R., Vélez, D. O., and Eracleous, M. (2014). Black Holes At the Centers of Nearby Dwarf Galaxies. *AJ*, 148:136.
- Morris, S. L. and Ward, M. J. (1988). Spectrophotometry of active galaxies - I. The observations. *MNRAS*, 230:639–669.
- Mortlock, D. J., Warren, S. J., Venemans, B. P., Patel, M., Hewett, P. C., McMahon, R. G., Simpson, C., Theuns, T., González-Solares, E. A., Adamson, A., Dye, S., Hambly, N. C., Hirst, P., Irwin, M. J., Kuiper, E., Lawrence, A., and Röttgering, H. J. A. (2011). A luminous quasar at a redshift of $z = 7.085$. *Nature*, 474(7353):616–619.
- Mould, J., Reynolds, T., Readhead, T., Floyd, D., Jannuzi, B., Cotter, G., Ferrarese, L., Matthews, K., Atlee, D., and Brown, M. (2012). Infrared Spectroscopy of Nearby Radio Active Elliptical Galaxies. *ApJS*, 203:14.
- Moustakas, J., Kennicutt, Jr., R. C., Tremonti, C. A., Dale, D. A., Smith, J.-D. T., and Calzetti, D. (2010). Optical Spectroscopy and Nebular Oxygen Abundances of the Spitzer/SINGS Galaxies. *ApJS*, 190:233–266.
- Müller-Sánchez, F., Hicks, E. K. S., Malkan, M., Davies, R., Yu, P. C., Shaver, S., and Davis, B. (2018). The Keck/OSIRIS Nearby AGN Survey (KONA). I. The Nuclear K-band Properties of Nearby AGN. *ApJ*, 858(1):48.
- Müller-Sánchez, F., Prieto, M. A., Hicks, E. K. S., Vives-Arias, H., Davies, R. I., Malkan, M., Tacconi, L. J., and Genzel, R. (2011). Outflows from Active Galactic Nuclei: Kinematics of the Narrow-line and Coronal-line Regions in Seyfert Galaxies. *ApJ*, 739:69.
- Narayan, R., Mahadevan, R., Grindlay, J. E., Popham, R. G., and Gammie, C. (1998). *ApJ*, 492(2):554–568.

- Natarajan, P. (2011). The formation and evolution of massive black hole seeds in the early Universe. *Bulletin of the Astronomical Society of India*, 39:145–161.
- Natarajan, P. (2014). Seeds to monsters: tracing the growth of black holes in the universe. *General Relativity and Gravitation*, 46:1702.
- Natarajan, P. (2021). A new channel to form IMBHs throughout cosmic time. *MNRAS*, 501(1):1413–1425.
- Netzer, H. (1985). Quasar discs. I - The Baldwin effect. *MNRAS*, 216:63–78.
- Netzer, H. (1993). Ionized absorbers, ionized emitters, and the X-ray spectrum of active galactic nuclei. *ApJ*, 411:594–601.
- Oliva, E., Salvati, M., Moorwood, A. F. M., and Marconi, A. (1994). Size and physical conditions of the coronal line region in a nearby Seyfert 2: the Circinus galaxy. *A&A*, 288:457–465.
- Osterbrock, D. E. and Ferland, G. J. (2006). *Astrophysics of gaseous nebulae and active galactic nuclei*. University Science Books.
- Pardo, K., Goulding, A. D., Greene, J. E., Somerville, R. S., Gallo, E., Hickox, R. C., Miller, B. P., Reines, A. E., and Silverman, J. D. (2016). X-Ray Detected Active Galactic Nuclei in Dwarf Galaxies at $0 < z < 1$. *ApJ*, 831:203.
- Perera, B. B. P., Stappers, B. W., Lyne, A. G., Bassa, C. G., Cognard, I., Guillemot, L., Kramer, M., Theureau, G., and Desvignes, G. (2017). Evidence for an intermediate-mass black hole in the globular cluster NGC 6624. *MNRAS*, 468:2114–2127.
- Peterson, B. M. (1997). *An Introduction to Active Galactic Nuclei*.
- Pettini, M., Shapley, A. E., Steidel, C. C., Cuby, J.-G., Dickinson, M., Moorwood, A. F. M., Adelberger, K. L., and Giavalisco, M. (2001). The Rest-Frame Optical Spectra of Lyman Break Galaxies: Star Formation, Extinction, Abundances, and Kinematics. *ApJ*, 554:981–1000.

- Piconcelli, E., Jimenez-Bailón, E., Guainazzi, M., Schartel, N., Rodríguez-Pascual, P. M., and Santos-Lleó, M. (2005). The XMM-Newton view of PG quasars. I. X-ray continuum and absorption. *A&A*, 432:15–30.
- Prestwich, A. H., Tsantaki, M., Zezas, A., Jackson, F., Roberts, T. P., Foltz, R., Linden, T., and Kalogera, V. (2013). Ultra-luminous X-Ray Sources in the Most Metal Poor Galaxies. *ApJ*, 769(2):92.
- Quataert, E. and Gruzinov, A. (2000). Convection-dominated Accretion Flows. *ApJ*, 539(2):809–814.
- Rakshit, S., Stalin, C. S., Chand, H., and Zhang, X.-G. (2017). A Catalog of Narrow Line Seyfert 1 Galaxies from the Sloan Digital Sky Survey Data Release 12. *ApJS*, 229(2):39.
- Ranalli, P., Comastri, A., and Setti, G. (2003). The 2-10 keV luminosity as a Star Formation Rate indicator. *A&A*, 399:39–50.
- Regan, J. A., Visbal, E., Wise, J. H., Haiman, Z., Johansson, P. H., and Bryan, G. L. (2017). Rapid formation of massive black holes in close proximity to embryonic protogalaxies. *Nature Astronomy*, 1:0075.
- Reines, A. E. and Comastri, A. (2016). Observational Signatures of High-Redshift Quasars and Local Relics of Black Hole Seeds. *PASA*, 33:e054.
- Reines, A. E., Greene, J. E., and Geha, M. (2013). Dwarf Galaxies with Optical Signatures of Active Massive Black Holes. *ApJ*, 775:116.
- Reines, A. E., Plotkin, R. M., Russell, T. D., Mezcua, M., Condon, J. J., Sivakoff, G. R., and Johnson, K. E. (2014). A Candidate Massive Black Hole in the Low-metallicity Dwarf Galaxy Pair Mrk 709. *ApJL*, 787:L30.
- Reines, A. E., Sivakoff, G. R., Johnson, K. E., and Brogan, C. L. (2011). An actively accreting massive black hole in the dwarf starburst galaxy Henize2-10. *Nature*, 470:66–68.

- Rhee, J. H. and Larkin, J. E. (2005). Probing the Dust Obscuration in Seyfert Galaxies using Infrared Spectroscopy. II. Implication for the Unification of Seyfert Galaxies. *ApJ*, 620:151–164.
- Ricci, C., Bauer, F. E., Arevalo, P., Boggs, S., Brandt, W. N., Christensen, F. E., Craig, W. W., Gandhi, P., Hailey, C. J., Harrison, F. A., Koss, M., Markwardt, C. B., Stern, D., Treister, E., and Zhang, W. W. (2016). IC 751: A New Changing Look AGN Discovered by NuSTAR. *ApJ*, 820:5.
- Ricci, C., Trakhtenbrot, B., Koss, M. J., Ueda, Y., Del Vecchio, I., Treister, E., Schawinski, K., Paltani, S., Oh, K., Lamperti, I., Berney, S., Gandhi, P., Ichikawa, K., Bauer, F. E., Ho, L. C., Asmus, D., Beckmann, V., Soldi, S., Baloković, M., Gehrels, N., and Markwardt, C. B. (2017). BAT AGN Spectroscopic Survey. V. X-Ray Properties of the Swift/BAT 70-month AGN Catalog. *ApJS*, 233:17.
- Richards, G. T., Myers, A. D., Gray, A. G., Riegel, R. N., Nichol, R. C., Brunner, R. J., Szalay, A. S., Schneider, D. P., and Anderson, S. F. (2009). Efficient Photometric Selection of Quasars from the Sloan Digital Sky Survey. II. ~1,000,000 Quasars from Data Release 6. *ApJS*, 180(1):67–83.
- Richards, G. T., Myers, A. D., Peters, C. M., Krawczyk, C. M., Chase, G., Ross, N. P., Fan, X., Jiang, L., Lacy, M., McGreer, I. D., Trump, J. R., and Riegel, R. N. (2015). Bayesian High-redshift Quasar Classification from Optical and Mid-IR Photometry. *ApJS*, 219(2):39.
- Riechers, D. A., Walter, F., Bertoldi, F., Carilli, C. L., Aravena, M., Neri, R., Cox, P., Weiß, A., and Menten, K. M. (2009). Imaging Atomic and Highly Excited Molecular Gas in a $z = 6.42$ Quasar Host Galaxy: Copious Fuel for an Eddington-limited Starburst at the End of Cosmic Reionization. *ApJ*, 703(2):1338–1345.
- Riffel, R., Rodríguez-Ardila, A., and Pastoriza, M. G. (2006). A 0.8-2.4 μm spectral atlas of active galactic nuclei. *A&A*, 457:61–70.

- Rodríguez-Ardila, A., Prieto, M. A., Portilla, J. G., and Tejeiro, J. M. (2011). The Near-infrared Coronal Line Spectrum of 54 nearby Active Galactic Nuclei. *ApJ*, 743:100.
- Rodríguez-Ardila, A., Prieto, M. A., Portilla, J. G., and Tejeiro, J. M. (2011). The Near-infrared Coronal Line Spectrum of 54 nearby Active Galactic Nuclei. *ApJ*, 743(2):100.
- Rodríguez-Ardila, A., Prieto, M. A., Viegas, S., and Gruenwald, R. (2006). Outflows of Very Ionized Gas in the Centers of Seyfert Galaxies: Kinematics and Physical Conditions. *ApJ*, 653:1098–1114.
- Ryu, T., Tanaka, T. L., Perna, R., and Haiman, Z. (2016). Intermediate-mass black holes from Population III remnants in the first galactic nuclei. *MNRAS*, 460(4):4122–4134.
- Satyapal, S., Abel, N. P., and Secret, N. J. (2018). Star-forming Galaxies as AGN Imposters? A Theoretical Investigation of the Mid-infrared Colors of AGNs and Extreme Starbursts. *ApJ*, 858(1):38.
- Satyapal, S., Böker, T., Mcalpine, W., Gliozzi, M., Abel, N. P., and Heckman, T. (2009). The Incidence of Active Galactic Nuclei in Pure Disk Galaxies: The Spitzer View. *ApJ*, 704:439–452.
- Satyapal, S., Kamal, L., Cann, J. M., Secret, N. J., and Abel, N. P. (2021). The Diagnostic Potential of JWST in Characterizing Elusive AGNs. *ApJ*, 906(1):35.
- Satyapal, S., Sambruna, R. M., and Dudik, R. P. (2004). A joint mid-infrared spectroscopic and X-ray imaging investigation of LINER galaxies. *A&A*, 414:825–838.
- Satyapal, S., Secret, N. J., Ricci, C., Ellison, S. L., Rothberg, B., Blecha, L., Constantin, A., Gliozzi, M., McNulty, P., and Ferguson, J. (2017). Buried AGNs in Advanced Mergers: Mid-infrared Color Selection as a Dual AGN Candidate Finder. *ApJ*, 848(2):126.
- Satyapal, S., Vega, D., Dudik, R. P., Abel, N. P., and Heckman, T. (2008). Spitzer Uncovers Active Galactic Nuclei Missed by Optical Surveys in Seven Late-Type Galaxies. *ApJ*, 677:926–942.

- Satyapal, S., Vega, D., Heckman, T., O'Halloran, B., and Dudik, R. (2007). The Discovery of an Active Galactic Nucleus in the Late-Type Galaxy NGC 3621: Spitzer Spectroscopic Observations. *ApJL*, 663:L9–L12.
- Schaerer, D. and Stasińska, G. (1999). On the origin of [O iv] emission in Wolf-Rayet galaxies. *A&A*, 345:L17–L21.
- Schramm, M., Silverman, J. D., Greene, J. E., Brandt, W. N., Luo, B., Xue, Y. Q., Capak, P., Kakazu, Y., Kartaltepe, J., and Mainieri, V. (2013). Unveiling a Population of Galaxies Harboring Low-mass Black Holes with X-Rays. *ApJ*, 773:150.
- Scott, A. E., Stewart, G. C., and Mateos, S. (2012). Detectability of low-energy X-ray spectral components in type 1 active galactic nuclei. *MNRAS*, 423:2633–2641.
- Secrest, N. J., Satyapal, S., Gliozzi, M., Cheung, C. C., Seth, A. C., and Böker, T. (2012). The Chandra View of NGC 4178: The Lowest Mass Black Hole in a Bulgeless Disk Galaxy? *ApJ*, 753:38.
- Secrest, N. J., Satyapal, S., Gliozzi, M., Rothberg, B., Ellison, S. L., Mowry, W. S., Rosenberg, J. L., Fischer, J., and Schmitt, H. (2015). An Optically Obscured AGN in a Low Mass, Irregular Dwarf Galaxy: A Multi-Wavelength Analysis of J1329+3234. *ApJ*, 798:38.
- Secrest, N. J., Satyapal, S., Moran, S. M., Cheung, C. C., Giroletti, M., Gliozzi, M., Bergmann, M. P., and Seth, A. C. (2013). A Multi-wavelength Analysis of NGC 4178: A Bulgeless Galaxy with an Active Galactic Nucleus. *ApJ*, 777:139.
- Sexton, R. O., Canalizo, G., Hiner, K. D., Komossa, S., Woo, J.-H., Treister, E., and Hiner Dimassimo, S. L. (2019). Stronger Constraints on the Evolution of the $M_{BH}-\sigma_*$ Relation up to $z \approx 0.6$. *ApJ*, 878(2):101.
- Shakura, N. I. and Sunyaev, R. A. (1973). Black holes in binary systems. Observational appearance. *A&A*, 24:337–355.

- Sheng, Z., Wang, T., Jiang, N., Yang, C., Yan, L., Dou, L., and Peng, B. (2017). Mid-infrared Variability of Changing-look AGNs. *ApJL*, 846(1):L7.
- Shields, G. A. (1978). Thermal continuum from accretion disks in quasars. *Nature*, 272:706–708.
- Shields, J. C., Walcher, C. J., Böker, T., Ho, L. C., Rix, H.-W., and van der Marel, R. P. (2008). An Accreting Black Hole in the Nuclear Star Cluster of the Bulgeless Galaxy NGC 1042. *ApJ*, 682:104–109.
- Simmonds, C., Bauer, F. E., Thuan, T. X., Izotov, Y. I., Stern, D., and Harrison, F. A. (2016). Do some AGN lack X-ray emission? *A&A*, 596:A64.
- Simmons, B. D., Lintott, C., Schawinski, K., Moran, E. C., Han, A., Kaviraj, S., Masters, K. L., Urry, C. M., Willett, K. W., Bamford, S. P., and Nichol, R. C. (2013). Galaxy Zoo: bulgeless galaxies with growing black holes. *MNRAS*, 429:2199–2211.
- Singh, P., Refregier, A., Majumdar, S., and Nath, B. B. (2017). Constraining the X-ray AGN halo occupation distribution: implications for eROSITA. *MNRAS*, 466(4):3961–3972.
- Souchay, J., Andrei, A. H., Barache, C., Bouquillon, S., Suchet, D., Taris, F., and Peralta, R. (2012). The second release of the Large Quasar Astrometric Catalog (LQAC-2). *A&A*, 537:A99.
- Souchay, J., Andrei, A. H., Barache, C., Kalewicz, T., Gattano, C., Coelho, B., Taris, F., Bouquillon, S., and Becker, O. (2015). The third release of the Large Quasar Astrometric Catalog (LQAC-3): a compilation of 321 957 objects. *A&A*, 583:A75.
- Stern, D., Assef, R. J., Benford, D. J., Blain, A., Cutri, R., Dey, A., Eisenhardt, P., Griffith, R. L., Jarrett, T. H., Lake, S., Masci, F., Petty, S., Stanford, S. A., Tsai, C.-W., Wright, E. L., Yan, L., Harrison, F., and Madsen, K. (2012). Mid-infrared Selection of

- Active Galactic Nuclei with the Wide-Field Infrared Survey Explorer. I. Characterizing WISE-selected Active Galactic Nuclei in COSMOS. *ApJ*, 753:30.
- Stern, D., Eisenhardt, P., Gorjian, V., Kochanek, C. S., Caldwell, N., Eisenstein, D., Brodwin, M., Brown, M. J. I., Cool, R., Dey, A., Green, P., Jannuzi, B. T., Murray, S. S., Pahre, M. A., and Willner, S. P. (2005). Mid-Infrared Selection of Active Galaxies. *ApJ*, 631:163–168.
- Stern, J. and Laor, A. (2013). Type 1 AGN at low z - III. The optical narrow-line ratios. *MNRAS*, 431(1):836–857.
- Stone, N. C., Küpper, A. H. W., and Ostriker, J. P. (2017). Formation of massive black holes in galactic nuclei: runaway tidal encounters. *MNRAS*, 467(4):4180–4199.
- Storchi-Bergmann, T., Kinney, A. L., and Challis, P. (1995). Ultraviolet to Near-Infrared Spectral Distributions of Star-forming and Seyfert 2 Galaxies. *ApJS*, 98:103.
- Storchi-Bergmann, T., Schmitt, H. R., Calzetti, D., and Kinney, A. L. (1998). Chemical Abundance Calibrations for the Narrow-Line Region of Active Galaxies. *AJ*, 115(3):909–914.
- Strader, J., Chomiuk, L., Maccarone, T. J., Miller-Jones, J. C. A., Seth, A. C., Heinke, C. O., and Sivakoff, G. R. (2012). No Evidence for Intermediate-mass Black Holes in Globular Clusters: Strong Constraints from the JVLA. *ApJL*, 750:L27.
- Sturm, E., Lutz, D., Verma, A., Netzer, H., Sternberg, A., Moorwood, A. F. M., Oliva, E., and Genzel, R. (2002). Mid-Infrared line diagnostics of active galaxies. A spectroscopic AGN survey with ISO-SWS. *A&A*, 393:821–841.
- Svensson, R. (1999). Thermalization Mechanisms in Compact Sources. In Poutanen, J. and Svensson, R., editors, *High Energy Processes in Accreting Black Holes*, volume 161 of *Astronomical Society of the Pacific Conference Series*, page 361.

- Tagawa, H., Umemura, M., and Gouda, N. (2016). Mergers of accreting stellar-mass black holes. *MNRAS*, 462(4):3812–3822.
- Teng, S. H., Rigby, J. R., Stern, D., Ptak, A., Alexander, D. M., Bauer, F. E., Boggs, S. E., Brandt, W. N., Christensen, F. E., Comastri, A., Craig, W. W., Farrah, D., Gandhi, P., Hailey, C. J., Harrison, F. A., Hickox, R. C., Koss, M., Luo, B., Treister, E., and Zhang, W. W. (2015). A NuSTAR Survey of Nearby Ultraluminous Infrared Galaxies. *ApJ*, 814(1):56.
- Thuan, T. X. and Izotov, Y. I. (2005). High-Ionization Emission in Metal-deficient Blue Compact Dwarf Galaxies. *ApJS*, 161(2):240–270.
- Toba, Y., Oyabu, S., Matsuhara, H., Malkan, M. A., Gandhi, P., Nakagawa, T., Isobe, N., Shirahata, M., Oi, N., Ohyama, Y., Takita, S., Yamauchi, C., and Yano, K. (2014). Luminosity and Redshift Dependence of the Covering Factor of Active Galactic Nuclei viewed with WISE and Sloan Digital Sky Survey. *ApJ*, 788(1):45.
- Trump, J. R., Sun, M., Zeimann, G. R., Luck, C., Bridge, J. S., Grier, C. J., Hagen, A., Juneau, S., Montero-Dorta, A., Rosario, D. J., Brandt, W. N., Ciardullo, R., and Schneider, D. P. (2015). The Biases of Optical Line-Ratio Selection for Active Galactic Nuclei and the Intrinsic Relationship between Black Hole Accretion and Galaxy Star Formation. *ApJ*, 811:26.
- Turner, T. J. and Pounds, K. A. (1989). The EXOSAT spectral survey of AGN. *MNRAS*, 240:833–880.
- Van Borm, C., Bovino, S., Latif, M. A., Schleicher, D. R. G., Spaans, M., and Grassi, T. (2014). Effects of turbulence and rotation on protostar formation as a precursor of massive black holes. *A&A*, 572:A22.
- van Wassenhove, S., Volonteri, M., Walker, M. G., and Gair, J. R. (2010). Massive black holes lurking in Milky Way satellites. *MNRAS*, 408:1139–1146.

- Veilleux, S. and Osterbrock, D. E. (1987). Spectral Classification of Emission-Line Galaxies. *ApJS*, 63:295.
- Vergani, D., Garilli, B., Polletta, M., Franzetti, P., Scodeggio, M., Zamorani, G., Haines, C. P., Bolzonella, M., Guzzo, L., Granett, B. R., de la Torre, S., Abbas, U., Adami, C., Bottini, D., Cappi, A., Cucciati, O., Davidzon, I., De Lucia, G., Fritz, A., Gargiulo, A., Hawken, A. J., Iovino, A., Krywult, J., Le Brun, V., Le Fèvre, O., Maccagni, D., Małek, K., Marulli, F., Pollo, A., Tasca, L. A. M., Tojeiro, R., Zanichelli, A., Arnouts, S., Bel, J., Branchini, E., Coupon, J., Ilbert, O., Moutard, T., and Moscardini, L. (2018). The VIMOS Public Extragalactic Redshift Survey (VIPERS). AGN feedback in [NeV] emitters. *A&A*, 620:A193.
- Vignali, C., Brandt, W. N., Boller, T., Fabian, A. C., and Vaughan, S. (2004). Arakelian 564: an XMM-Newton view. *MNRAS*, 347:854–860.
- Volonteri, M. (2010). Formation of supermassive black holes. *AAPR*, 18(3):279–315.
- Volonteri, M. and Begelman, M. C. (2010). Quasi-stars and the cosmic evolution of massive black holes. *MNRAS*, 409:1022–1032.
- Volonteri, M. and Natarajan, P. (2009). Journey to the $M_{BH}-\sigma$ relation: the fate of low-mass black holes in the Universe. *MNRAS*, 400:1911–1918.
- Volonteri, M. and Rees, M. J. (2005). Rapid Growth of High-Redshift Black Holes. *ApJ*, 633(2):624–629.
- Wang, F., Yang, J., Fan, X., Yue, M., Wu, X.-B., Schindler, J.-T., Bian, F., Li, J.-T., Farina, E. P., Bañados, E., Davies, F. B., Decarli, R., Green, R., Jiang, L., Hennawi, J. F., Huang, Y.-H., Mazzucchelli, C., McGreer, I. D., Venemans, B., Walter, F., and Beletsky, Y. (2018). The Discovery of a Luminous Broad Absorption Line Quasar at a Redshift of 7.02. *ApJL*, 869(1):L9.

- Wang, R., Carilli, C. L., Neri, R., Riechers, D. A., Wagg, J., Walter, F., Bertoldi, F., Menten, K. M., Omont, A., Cox, P., and Fan, X. (2010). Molecular Gas in $z \sim 6$ Quasar Host Galaxies. *ApJ*, 714(1):699–712.
- Wang, S. X., Brandt, W. N., Luo, B., Smail, I., Alexander, D. M., Danielson, A. L. R., Hodge, J. A., Karim, A., Lehmer, B. D., Simpson, J. M., Swinbank, A. M., Walter, F., Wardlow, J. L., Xue, Y. Q., Chapman, S. C., Coppin, K. E. K., Dannerbauer, H., De Breuck, C., Menten, K. M., and van der Werf, P. (2013). An ALMA Survey of Submillimeter Galaxies in the Extended Chandra Deep Field-South: The AGN Fraction and X-Ray Properties of Submillimeter Galaxies. *ApJ*, 778(2):179.
- Weisskopf, M. C., Wu, K., Trimble, V., O’Dell, S. L., Elsner, R. F., Zavlin, V. E., and Kouveliotou, C. (2007). A Chandra Search for Coronal X-Rays from the Cool White Dwarf GD 356. *ApJ*, 657(2):1026–1036.
- Wilkes, B. J. and Elvis, M. (1987). Quasar energy distributions. I - Soft X-ray spectra of quasars. *ApJ*, 323:243–262.
- Wilson, A. S., Binette, L., and Storchi-Bergmann, T. (1997). The Temperature of Extended Gas in Active Galaxies: Evidence for Matter-bounded Clouds. *ApJL*, 482:L131–L134.
- Winter, L. M., Veilleux, S., McKernan, B., and Kallman, T. R. (2012). The Swift Burst Alert Telescope Detected Seyfert 1 Galaxies: X-Ray Broadband Properties and Warm Absorbers. *ApJ*, 745(2):107.
- Wolcott-Green, J., Haiman, Z., and Bryan, G. L. (2017). Beyond J_{crit} : a critical curve for suppression of H_2 -cooling in protogalaxies. *MNRAS*, 469(3):3329–3336.
- Woo, J.-H., Yoon, Y., Park, S., Park, D., and Kim, S. C. (2015). The Black Hole Mass-Stellar Velocity Dispersion Relation of Narrow-line Seyfert 1 Galaxies. *ApJ*, 801(1):38.
- Woods, T. E., Agarwal, B., Bromm, V., Bunker, A., Chen, K.-J., Chon, S., Ferrara, A., Glover, S. C. O., Haemmerlé, L., Haiman, Z., Hartwig, T., Heger, A., Hirano, S.,

- Hosokawa, T., Inayoshi, K., Klessen, R. S., Kobayashi, C., Koliopanos, F., Latif, M. A., Li, Y., Mayer, L., Mezcua, M., Natarajan, P., Pacucci, F., Rees, M. J., Regan, J. A., Sakurai, Y., Salvadori, S., Schneider, R., Surace, M., Tanaka, T. L., Whalen, D. J., and Yoshida, N. (2019). Titans of the early Universe: The Prato statement on the origin of the first supermassive black holes. *PASA*, 36:e027.
- Wrobel, J. M., Miller-Jones, J. C. A., and Middleton, M. J. (2016). A Very Large Array Search for Intermediate-mass Black Holes in Globular Clusters in M81. *AJ*, 152:22.
- Wu, X.-B., Wang, F., Fan, X., Yi, W., Zuo, W., Bian, F., Jiang, L., McGreer, I. D., Wang, R., Yang, J., Yang, Q., Thompson, D., and Beletsky, Y. (2015). An ultraluminous quasar with a twelve-billion-solar-mass black hole at redshift 6.30. *Nature*, 518(7540):512–515.
- Xiao, T., Barth, A. J., Greene, J. E., Ho, L. C., Bentz, M. C., Ludwig, R. R., and Jiang, Y. (2011). Exploring the Low-mass End of the $M_{BH}-\sigma_*$ Relation with Active Galaxies. *ApJ*, 739:28.
- Yan, L., Wang, T., Jiang, N., Stern, D., Dou, L., Fremling, C., Graham, M. J., Drake, A. J., Yang, C., Burdge, K., and Kasliwal, M. M. (2019). Rapid “Turn-on” of Type-1 AGN in a Quiescent Early-type Galaxy SDSS1115+0544. *ApJ*, 874(1):44.
- Yuan, F. and Narayan, R. (2014). Hot Accretion Flows Around Black Holes. *ARA&A*, 52:529–588.
- Yuan, W., Zhou, H., Dou, L., Dong, X.-B., Fan, X., and Wang, T.-G. (2014). Chandra and MMT Observations of Low-mass Black Hole Active Galactic Nuclei Accreting at Low Rates in Dwarf Galaxies. *ApJ*, 782:55.
- Zezas, A., Alonso-Herrero, A., and Ward, M. J. (2001). Searching for X-Ray Luminous Starburst Galaxies. *APSS*, 276:601–607.

Curriculum Vitae

Jenna M. Cann graduated from W.T. Woodson High School, Fairfax, VA in 2011. She received her Associate's of Science in Mathematics from Northern Virginia Community College, Annandale, VA in 2013. From there, she transferred to George Mason University, where she received her Bachelor of Science in Astronomy in 2017. She remained at George Mason University for her graduate studies and completed her PhD in Physics in 2021.